GIA INSTITUTE OF TECHNOLOGY — OFFICE OF CONTRACT ADMINISTRATION

PROJECT ADMINISTRATION DATA SHEET

[X] ORIGINAL [ ] REVISION NO. ____

No. A-3574 GTRI/~~GIT~~ DATE 6 / 28 / 83

Director: J. M. Lefferdo ~~School~~ Lab EMSL/ESD

r: U.S. Dept. of Energy; San Francisco

Agreement: Contract No. DE-AC03-83F11921

Period: From 6/15/83 To 11/15/83 (Performance) _____ (Reports)

r Amount:

	This Change	Total to Date
Estimated:	$ 33,452	$ 33,452
Funded:	$ 33,452	$ 33,452

aring Amount: $ _____ Cost Sharing No: _____

Solar Thermal Research Workshop

ISTRATIVE DATA OCA Contact Frank Huff X4820

sor Technical Contact:

designated

rticle IV of the Schedule

2) Sponsor Admin/Contractual Matters:

Joann P. Littlehales
U. S. Dept. of Energy
San Francisco Operations Office
1333 Broadway
Oakland, CA 94612
(415) 273-4112

Priority Rating: BDSA Reg 2 and/or DMS Reg 1; No rating

Military Security Classification: _____

(or) Company/Industrial Proprietary: _____

CTIONS

ached _____ Supplemental Information Sheet for Additional Requirements.

Foreign travel must have prior approval – Contact OCA in each case. Domestic travel requires sponsor approval where total will exceed greater of $500 or 125% of approved proposal budget category.

ent: Title vests with Government $1,000 and above; less than $1,000 with GIT approval obtained prior to approval.

JUL 1983 RECEIVED Research Reports Office

ENTS:

Funds made available for operating expenses only and not for purchase of capital equipment.

NOTE: Request for one Advanced Project Number was approved 6/17/83. The budget was $3,735.

TO:

Director
Administrative Network
Property Management
ing

Procurement/EES Supply Services
Research Security Services
Reports Coordinator (OCA)
Research Communications (2)

GTRI
Library
Project File
Other I. Newton

RGIA INSTITUTE OF TECHNOLOGY OFFICE OF CONTRACT ADMINISTRATION

SPONSORED PROJECT TERMINATION/CLOSEOUT SHEET

Date November 15, 1983

ct No. A-3574 ~~School~~/Lab EMSL

des Subproject No.(s) _____

ct Director(s) J. M. Lefferdo GTRI/~~GIT~~

sor U.S. Department of Energy; San Francisco, CA

Solar Thermal Research Workshop

tive Completion Date: 11/15/83 (Performance) 11/15/83 (Reports)

/Contract Closeout Actions Remaining:

- [ ] None
- [X] Final Invoice or Final Fiscal Report
- [ ] Closing Documents *
- [X] Final Report of Inventions
- [X] Govt. Property Inventory & Related Certificate
- [ ] Classified Material Certificate
- [ ] Other _____

*(See page 4 of 26; Assignment of Claims is not applicable)

nues Project No. _____

nued by Project No. _____

ES TO:

ct Director
arch Administrative Network
arch Property Management
unting
urement/EES Supply Services
arch Security Services
rts Coordinator (OCA)
l Services

Library
GTRI
Research Communications (2)
Project File
Other _____

OCA ~~52-1001~~

A-3574

ENGINEERING EXPERIMENT STATION
Georgia Institute of Technology
A Unit of the University System of Georgia
Atlanta, Georgia 30332

July 21, 1983

Dr. K. Rose
U. S. Department of Energy
San Francisco Operations Office
1333 Broadway
Oakland, CA 94612

Dear Keith:

Enclosed are deliverables 1 and 2 (Management Plan and Cost Plan) for Contract DE-AC03-83F11921 Solar Thermal Research Workshop in formats per our telephone conversation of 20 July 1983.

Please contact me if there are any questions.

Yours very truly,

J. M. Lefferdo
Head, Thermal Sciences Branch

jw

Enclosure

MANAGEMENT PLAN

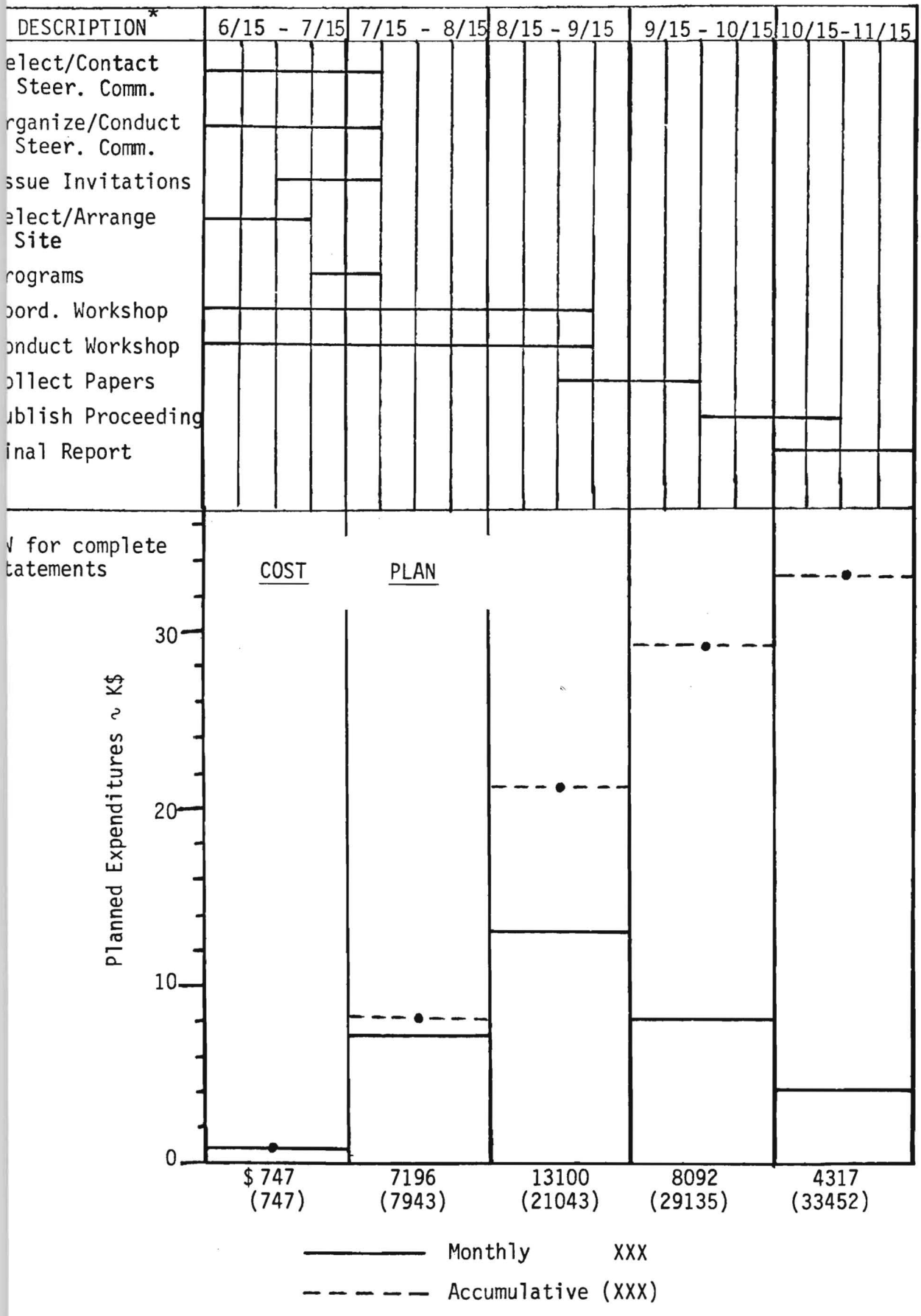

PROJECT STATUS REPORT #1

SOLAR THERMAL RESEARCH WORKSHOP

GEORGIA TECH PROJECT A-3574

J. M. Lefferdo
September 1983

PROJECT STATUS REPORT

6/15 - 8/31/83

A tentative workshop agenda was sent to the steering group. Comments were solicited regarding topics and speakers. Replies were received in writing from two on the committee and verbal comments from two others. The suggestions were incorporated and a revised agenda resulted.

Workshop announcements were mailed to over 600 on July 8. Invitations to present papers were initially made by telephone in early July and followed by written invitations on July 14. At the same time invitation letters to participate were mailed to panel members.

Following the announcement and invitation mailing, activity work centered around firming up the facilites preparation for the workshop. This was completed in early August. Activities during the next reporting period consist of holding the workshop, collecting and publishing the proceedings and issuing a final report summarizing the workshop.

A September 30 date has been established for presenters to mail their 5 page paper to Georgia Tech. It is expected that the proceedings will then be assembled and mailed to registrants of the workshop by November 15.

FINANCIAL REPORT

(ESTIMATE)

COVERING PERIOD

6/15/83 - 8/31/83

PROJECT A-3574

REPORT DATE: 9/6/83

	Reporting Date	Cumulative
Direct Labor	6741	6741
Fringe Benefits	1584	1584
Materials	124	124
Overhead	4174	4174
	12623	12623

FINAL REPORT

CONTRACT NO. DE-AC03-83F 11921

SOLAR THERMAL RESEARCH WORKSHOP

J. M. LEFFERDO

GEORGIA INSTITUTE OF TECHNOLOGY

NOVEMBER 7, 1983

The Solar Thermal Research Workshop was held on the Georgia Tech campus on September 7 - 8, 1983. The two-day, four-session agenda is shown as Appendix A of this report. The speakers and topics were chosen by a workshop steering group in July. The panel session, participants who were also selected by the steering group committee, followed the last formal presentation session. The notes of the panel session are contained as Appendix B to this report.

The workshop was attended by 66 registrants and some unregistered Georgia Tech graduate students. A break-down of the registrants shows the following composition:

- o industry; 18
- o university, national labs; 42
- o utilities; 2
- o non-presenters/session chairman; 31

The workshop proceedings, because of the length of 192 pages, will not be included with this final report. Copies have been mailed to all registrants and per contract reporting requirements, 4 additional copies are included as separate deliverables at the time of this report submission.

Appendix B, the panel session summary provides a succinct assessment of the panel and workshop participant viewpoints of the solar thermal research program. The summary comments are comprised of panel summaries as well as workshop attendee floor statements.

Some comments represent general workshop viewpoints based upon the elaboration of discussion that followed. Three comments have been selected as representative of the panel session. It was generally agreed that this type of peer review was valuable and should occur at least annually; research cannot be effectively focussed on day-by-day industrial needs, but at the same time a stronger link must be established between researchers and industry; more definitive goals must be set to focus the program.

APPENDIX A

ENGINEERING EXPERIMENT STATION
Georgia Institute of Technology
A Unit of the University System of Georgia
Atlanta, Georgia 30332

SOLAR THERMAL RESEARCH WORKSHOP

Space and Sciences Technology Building, Georgia Tech

AGENDA

Wednesday, September 7, 1983

7:30-8:30 am Registration
8:30-9:00 am Introduction
J. M. Lefferdo, Workshop Chairman & Head, Thermal Sciences Branch, Georgia Tech Engineering Experiment Station
Welcome,
Dr. D. J. Grace, Director of Georgia Tech Engineering Experiment Station

DOE Opening Comments,
F. Wilkins, DOE Headquarters

SESSION I

FUELS AND CHEMICALS SESSION

Chairman: Gerry Katz - DOE/San

9:00-9:25 Technical Summary - Ram Manvi - Jet Propulsion Lab

9:25-9:50 Chemical vs Thermal Energy Storage - John Norman - G. A. Technologies

9:50-10:15 Reactor Design for Decomposition of Sulphuric Acid - Larry Van Bibber - Westinghouse Electric Corp.

10:15-10:30 Break

10:30-10:55 Solar Field/Chemical Process Interface - Charles Pitman - U. Houston

10:55-11:20 Direct Flux Reactor Design Fundamentals - Bernie Yudow - Institute of Gas Technology

11:20-11:45 Entrainment Reactor Fundamentals - Doug Neale - Georgia Tech

11:45-12:10 High Flux Photoconversion Research - Dave Johnson - Solar Energy Research Institute

12:30-2:00 Lunch, Alumni House
Luncheon address: "Industry View of R&D in Area of Solar Thermal," Tom Springer, Rockwell International & Chairman, Solar Thermal Division of Solar Energy Industry Assoc.

SESSION II

OPTICAL AND THERMAL MATERIALS AND CONCEPTS

Chairman: Gordon Gross - Solar Energy Research Institute

2:15-2:40 pm Polymer Research - Paul Schissel - Solar Energy Research Institute

2:40-3:05 Advanced Concentrator Research - Marty Murphy - Solar Energy Research Institute

3:05-3:30 U. Houston Materials Research - Alex Ignatiev - U. Houston

3:30-3:45 Break

3:45-4:10 Georgia Tech Ceramic Activities - Steve Bomar - Georgia Tech

4:10-4:35 Direct Absorption High Temperature Receiver - Bob Copeland - Solar Energy Research Inst

4:35-5:00 Small Particle Heat Exchanger Receiver - Arlon Hunt - Lawrence Berkeley Labs

5:00- Tour of U. S. DOE Advanced Components Test Facility (ACTF)

Thursday, September 8, 1983

SESSION III

HIGH TEMPERATURE EXPERIMENTAL FACILITIES - RECENT ACTIVITIES

Chairman: Tom Brown - Georgia Tech

8:30-8:55 am Advanced Solar Thermal Experimental Diagnostic Techniques - Paul Mackie - Georgia Tech

8:55-9:20 CRTF Activities - Cheryl Maxwell - Sandia National Lab Albuquerque

9:20-9:45 JPL/PDTS Activities - Darrell Ross - Jet Propulsion Lab

9:45-10:10 CRNS 1000 kW Solar Furnace Activities - Claude Royere - CNRS

10:10-10:25 Break

SESSION V

INNOVATIVE SOLAR THERMAL RESEARCH

Chairman: Keith Rose - DOE/SAN

10:25-10:50 am	Direct Contact Solar Thermal Storage - R. Petri - Institute of Gas Technology
10:50-11:15	Novel Trough and Dish Collector Receiver Designs - T. Kuehn - U. Minn.
11:15-11:40	Photosynthetic Production of Ammonia - W. Mallow - Southwest Research Institute
11:40-12:05	Polymeric Domes and Mirrors Production Process - R. Liang - Jet Propulsion Laboratory
12:20-1:30	Lunch, Alumini House
1:45-2:30 pm	Summary of Additional Innovative Solar Thermal Research Topics - K. Rose - DOE/SAN

2:30-4:00 Panel Discussion

Chairman: Alvin F. Hildebrandt - U. Houston

Panel:

Bob Cassanova - Georgia Tech
Bim Gupta - Solar Energy Research Institute
Carlo La Porta - Solar Energy Industry Association
Ram Manvi - Jet Propulsion Lab
Jim Wright - Sandia National Lab Livermore

APPENDIX B

PANEL DISCUSSION SUMMARY

Directly following the last workshop session a panel of six solar thermal experts was convened to summarize views of the workshop and the solar thermal research program. Following this, workshop attendees participated in an open floor discussion with the panel in which specific and general aspects of the solar thermal program were addressed.

The summary which follows is a compilation of both the panel comments as well as the floor participation:

- a general sense of continuity and direction in the program is evolving including a positive thrust even though budgets are diminishing - probably partially due to large demonstration projects coming on line

- direction of research program should be for new markets and new technology rather than solving problems in a retrospective mode

- general perception is that industrial view of research and development is very near term

- engineering design problems have in some instances become confused with research

- recommend a more open approach to selection and performance of research topics rather than establishment of artificial criteria

- this workshop is based on peer review - this type of review process should continue on an annual basis

- there is a danger in looking at too many diverse studies and trying to define future needs too far in future
- recognize important work being done in materials and heat and mass transfer but sharp focus lacking in both
- recommend getting industry acceptance of R&D approach then work to commonly accepted goal with all resources available
- recommend focus on controls, storage, materials, heat and mass transfer as research topics
- recommend narrowing field of view and concentrating effort to show industry real progress
- emphasis of research program should be to reduce cost of current systems by introducing innovative ideas, improve performance to reduce cost and widen application potential
- recommend a fixed 25-30 percent level of solar thermal budget for research
- research cannot be effectively focussed on industrial needs
- it is important to understand and make transition from research to engineering development
- some activities even if not strictly defined as research are as important as research in the end result
- a diminishing budget has caused introspective questioning of relevancy of heretofore reasonable research thrusts

- industry has to make known their concerns through better communications with research community
- critical to amassing large amounts of capital for energy research is national energy policy including tax credit policies - high focus in this area now
- must strive towards strengthened co-operative link between research community and industry
- more industry participation is needed directly with universities and national laboratories
- recommend diminishing the programmatic issues in favor of the philosophical and directional issues
- need to publish more in refereed journals
- need to be more quantitative as our efforts reach maturity
- recommend smaller research group meetings/reviews to scope out receivers and reactors in fuels/chemicals area since this technology will be critical to success
- better liason between industry/universities/labs can be achieved through workshops and jury or advisory board activities with overview functions for solar thermal program
- need for a clear-cut goal is evident as opposed to extended option sorting activities

- appears that there is a missing emphasis of solar thermal research for fossil fuel displacement in favor of solar uniqueness - while displacement is not as attractive as uniqueness, goal of program should be to convert solar energy into a more useful form of available resource to which displacement addresses.
- need to set a common goal or define a large project to strive toward (and one which is attainable) similar to Barstow project since so many diverse interests abound.

Proceedings of the

SOLAR THERMAL RESEARCH WORKSHOP

Held at Georgia Institute of Technology

September 7–8, 1983

GEORGIA INSTITUTE OF TECHNOLOGY
A Unit of the University System of Georgia
Engineering Experiment Station
Atlanta, Georgia 30332

GT EES

1983

Proceedings of the

SOLAR THERMAL RESEARCH WORKSHOP

Held at Georgia Institute of Technology

September 7-8, 1983

FOREWORD

A two day workshop was held at Georgia Tech on September 7 and 8, 1983 for researchers in solar thermal technology. It was sponsored by the U. S. Department of Energy and coordinated by the Engineering Experiment Station of Georgia Tech.

The purpose of the workshop is to review current efforts in solar thermal research so that an understanding may be gained of the various approaches being pursued to achieve solar thermal feasibility.

Current solar thermal research is being pursued by several investigators in a wide variety of scientific disciplines. Categories of investigation include solar fuels and chemicals, optical and solar thermal materials and concepts, high temperature facilities activities, and innovative solar thermal research. The common thrust of the research is to advance the technological readiness of the solar thermal concept as a practical application of solar energy.

The workshop was conducted under the following schedule:

Wednesday, September 7

SESSION I: Fuels and Chemicals

Recent experimental activities including an overall perspective of the thrust of solar thermal produced fuels and chemicals research.

SESSION II: Optical and Thermal Concepts and Materials

Current progress in materials research for optical as well as containment applications; advanced low-cost configuration concepts.

Thursday, September 8

SESSION III: High Temperature Experimental Facilities - Recent Activities

Experimental support considerations including advanced diagnos techniques.

SESSION IV: Innovative Solar Thermal Research

New research approaches to solar thermal applications with potential substantial performance and cost improvements.

Following the last session a panel discussion was held in which a pa of experts summarized their views of the two day workshop, commented on direction of the research program and chaired open floor discussion of top from the workshop attendees. The objective of the panel discussion was provide post-workshop focus.

Papers were presented by invitation and are contained in these proce ings in order of presentation.

J. M. Lefferdo, Workshop Chairman

T. B. Elfe, Workshop Coordinator

J. N. Harris, Workshop Coordinator

ENGINEERING EXPERIMENT STATION
Georgia Institute of Technology
A Unit of the University System of Georgia
Atlanta, Georgia 30332

SOLAR THERMAL RESEARCH WORKSHOP

Space and Sciences Technology Building, Georgia Tech

AGENDA

Wednesday, September 7, 1983

7:30-8:30 am Registration
8:30-9:00 am Introduction
J. M. Lefferdo, Workshop Chairman & Head, Thermal Sciences Branch, Georgia Tech Engineering Experiment Station
Welcome,
Dr. D. J. Grace, Director of Georgia Tech Engineering Experiment Station

DOE Opening Comments,
F. Wilkins, DOE Headquarters

SESSION I

FUELS AND CHEMICALS SESSION

Chairman: Gerry Katz - DOE/San

9:00-9:25	Technical Summary - Ram Manvi - Jet Propulsion Lab
9:25-9:50	Chemical vs Thermal Energy Storage - John Norman - G. A. Technologies
9:50-10:15	Reactor Design for Decomposition of Sulphuric Acid - Larry Van Bibber - Westinghouse Electric Corp.
10:15-10:30	Break
10:30-10:55	Solar Field/Chemical Process Interface - Charles Pitman - U. Houston
10:55-11:20	Direct Flux Reactor Design Fundamentals - Bernie Yudow - Institute of Gas Technology
11:20-11:45	Entrainment Reactor Fundamentals - Doug Neale - Georgia Tech
11:45-12:10	High Flux Photoconversion Research - Dave Johnson - Solar Energy Research Institute

12:30-2:00 Lunch, Alumni House
Luncheon address: "Industry View of R&D in Area of Solar Thermal," Tom Springer, Rockwell International & Chairman, Solar Thermal Division of Solar Energy Industry Assoc

SESSION II

OPTICAL AND THERMAL MATERIALS AND CONCEPTS

Chairman: Gordon Gross - Solar Energy Research Institute

2:15-2:40 pm Polymer Research - Paul Schissel - Solar Energy Research Institute

2:40-3:05 Advanced Concentrator Research - Marty Murphy - Solar Energy Research Institute

3:05-3:30 U. Houston Materials Research - Alex Ignatiev - U. Houston

3:30-3:45 Break

3:45-4:10 Georgia Tech Ceramic Activities - Steve Bomar - Georgia Tech

4:10-4:35 Direct Absorption High Temperature Receiver - Bob Copeland - Solar Energy Research Ir

4:35-5:00 Small Particle Heat Exchanger Receiver - Arlon Hunt - Lawrence Berkeley Labs

5:00- Tour of U. S. DOE Advanced Components Test Facility (ACTF)

Thursday, September 8, 1983

SESSION III

HIGH TEMPERATURE EXPERIMENTAL FACILITIES - RECENT ACTIVITIES

Chairman: Tom Brown - Georgia Tech

8:30-8:55 am Advanced Solar Thermal Experimental Diagnostic Techniques Paul Mackie - Georgia Tech

8:55-9:20 CRTF Activities - Cheryl Maxwell - Sandia National Lab Albuquerque

9:20-9:45 JPL/PDTS Activities - Darrell Ross - Jet Propulsion Lab

9:45-10:10 CRNS 1000 kW Solar Furnace Activities - Claude Royere - CNRS

10:10-10:25 Break

SESSION V

INNOVATIVE SOLAR THERMAL RESEARCH

Chairman: Keith Rose - DOE/SAN

10:25-10:50 am	Direct Contact Solar Thermal Storage - R. Petri - Institute of Gas Technology
10:50-11:15	Novel Trough and Dish Collector Receiver Designs - T. Kuehn - U. Minn.
11:15-11:40	Photosynthetic Production of Ammonia - W. Mallow - Southwest Research Institute
11:40-12:05	Polymeric Domes and Mirrors Production Process - R. Liang - Jet Propulsion Laboratory
12:20-1:30	Lunch, Alumini House
1:45-2:30 pm	Summary of Additional Innovative Solar Thermal Research Topics - K. Rose - DOE/SAN

2:30-4:00 Panel Discussion

Chairman: Alvin F. Hildebrandt - U. Houston

Panel:

Bob Cassanova - Georgia Tech
Bim Gupta - Solar Energy Research Institute
Carlo La Porta - Solar Energy Industry Association
Ram Manvi - Jet Propulsion Lab
Jim Wright - Sandia National Lab Livermore

SOLAR FUELS AND CHEMICALS

Ram Manvi
Jet Propulsion Laboratory

1. Introduction

The Solar Fuels and Chemicals program adapts solar technology to drive chemical processes and develops chemical technology to uniquely utilize the solar heat source. This paper describes research and technology needs related to developing solar chemical technology for central receiver applications.

Central receiver technology provides some unique opportunities for driving chemical processes efficiently. This is because the advanced central receiver systems can supply heat at the rate and temperature level required by the chemical process. This can reduce both heat requirements and costs by eliminating much of the need for internal heat recovery. The use of solar technology, however, introduces some critical problems into the chemical process. These are related to unsteady heat production which makes the operation of reactors and other process equipment difficult. To address these problems, a program has been established by DOE with the purpose of establishing the engineering feasibility of solar chemical technology.

2. Program Goals and Objectives

Past efforts have been devoted to determining the utility and applicability of solar thermal energy to primary fuel and chemical processes. Results of exploratory studies demonstrated that this energy resource could be used to drive all major fuel and chemical conversion processes, including reduction, gasification, pyrolysis, and liquifaction. In addition, it was clear that intermittent, high-flux, high-temperature inputs could be accommmodated within a broad range of processes. Other work with windowed reactors and moving beds demonstrated ease of control over heat and mass transfer using direct radiant heat transfer to solids.

Building upon this exploratory research base, the program activities focus on analytical and experimental tasks that would provide:

(1) Insight and understanding into whether the solar thermal resource contained unique or advantageous elements that could be beneficial to the fuel and chemical industry.

(2) Identification and definition of the technical barriers that would limit or prevent utilization of the resources.

(3) Development of a program and management structure that would result in assessing the technical and economic feasibility for production of fuels and chemicals from renewable resources.

3. Program Structure (Figure 1)

An assessment was performed to identify the technical barriers that prevented industry from capitalizing on the potential for fuels and chemicals. It was learned that, in essence, while specific solar capability exists (i.e.,

high-temperature capability), the technical base to make use of it has not been developed. This area requires a new understanding of materials, reactor design and catalyst behavior under conditions of multiple, deep thermal cycles. It also requires new methods to control reaction time under conditions of variable heat input. The assessment also indicated that process control and stability are unknown for integrated solar plants; this requires knowledge of how to adapt chemical operations to large thermal transients and understanding the dynamics of processes with variable heat and product stream flows. New methods will have to be developed for rapid start-up, shutdown, and plant operation.

In performing the assessment, several major fuel and chemical processes were examined in great detail. What was learned is that there is a great deal of commonality in terms of missing technologies among the processes. These have been identified as "core technologies". A program structure has been developed to focus on these technologies since an appraisal of the technical feasibility of the core technologies will permit applications to a range of fuel and chemical processes. The goal is to provide the basic fuel elements (H_2 and CO). The selected mechanism or process to focus the effort is thermochemical hydrogen.

4. Technology Program Elements

The Solar Fuels and Chemicals Program has been reorganized from its previous loosely-knit, diverse, task-oriented effort which largely concentrated on proof-of-principle experiments to a project-oriented program stressing engineering fundamentals. The various technology elements are delineated in Table 1. These technology elements address some of the following research and development needs of interest to Solar Fuels and Chemicals:

Material Related

- Corrosion and thermal cycling of metal alloy process equipment
- Surface coatings for heat transfer augmentation, minimize radiation damage, increase erosion and abrasion resistance
- Fabrication techniques, thermal stress-relieving designs, and modular replacements of metal alloy reactors
- Catalyst supports to minimize break-up and poisoning
- Window materials, enclosures, seals and support
- Low-cost ceramics, ceramic-coated metal surfaces for process equipment applications
- Physical and thermal properties measurement of ceramic and ceramic-coated surfaces
- Transparent ceramics for direct flux reactors
- Fabrication, forming and assembly of ceramic components, ceramic-ceramic and ceramic-metal

- Measurements and characterization of abrasion and erosion of ceramic and ceramic-coated surfaces in chemical equipment

- Corrosion of ceramic and ceramic-coated surfaces in high temperature chemical environment

- Aging, characterization and measurements of thermal and physical changes in high flux insolation of metal, ceramic and ceramic-coated surfaces

- Reinforcement of ceramic components, composites and glassy metal structures

- Materials for thermal energy storage of 1500^{o}F and above

Thermal Science Related

- Measurement and characterization of the optical properties of reactant materials, metal alloy surfaces, ceramics, window materials, and ceramic-coated solid surfaces

- Heat transfer models of chemical catalytic reactors. Computer analyses, bench scale experiments to simulate transient and steady-state operations for heating and boiling

- Mass transfer models. Computer analyses, bench scale experimentation, correlations. Transient and steady state operations

- Optimized control strategies of solar chemical reactors. Computer models, bench scale experiments to simulate operating conditions

- Flux mapping and temperature distributions in windowed and unwindowed chemical reactors. Flux leveling, heat transfer augmentation and window protection

Solar Thermal Fuels and Chemicals

Figure 1.

PROGRAM STRUCTURE

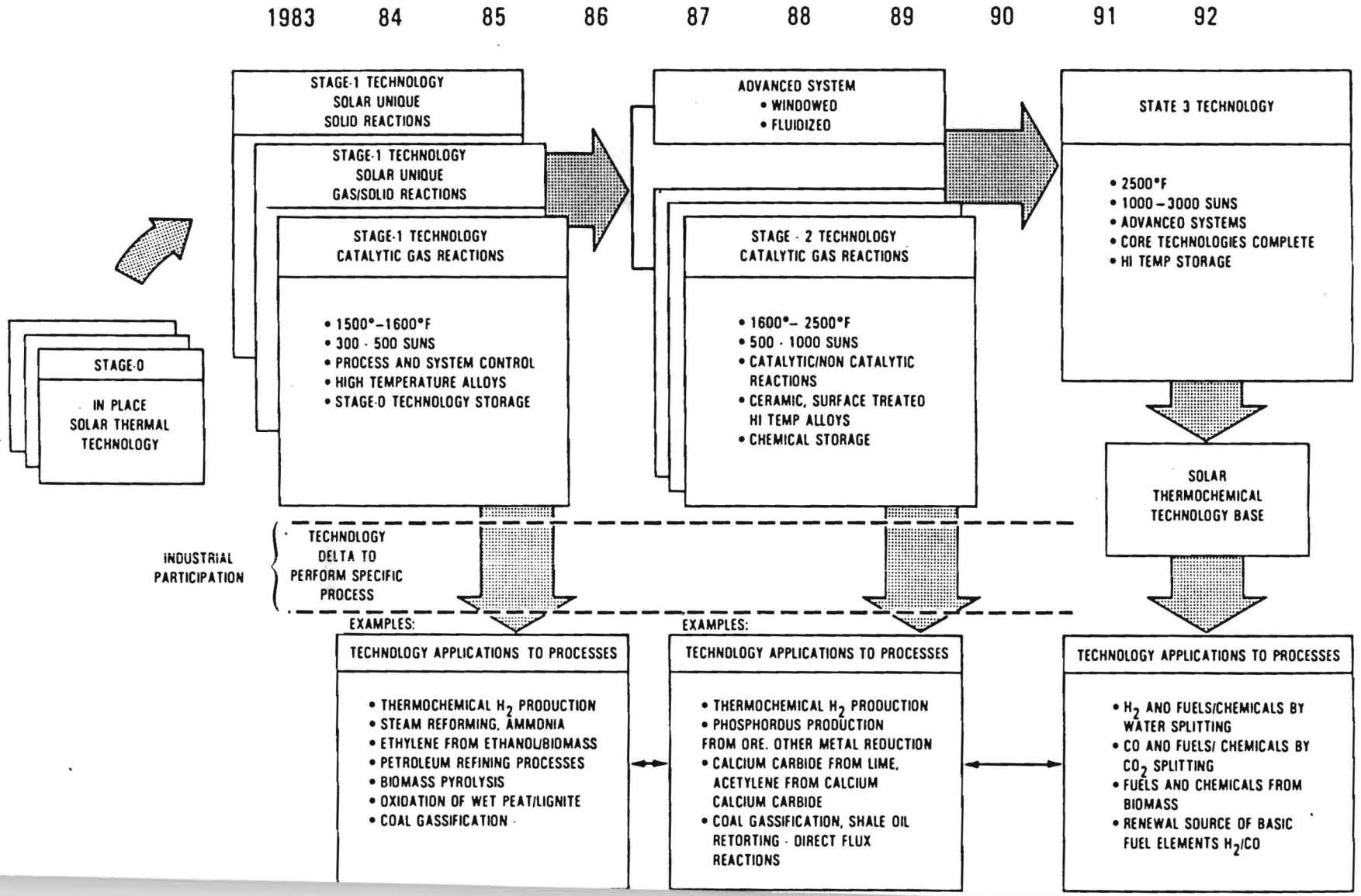

Table 1. SOLAR FUELS AND CHEMICALS
TECHNOLOGY PROGRAM ELEMENTS

ELEMENT	WHAT?	WHO?	WHEN?	COMMENTS
1. CHEMICAL KINETICS	$ZnSo_4$ DECOMPOSITION	UNIV. OF HAWAII	FY 1984	SPOUTED BED, DIFFERENT FROM LLL, SOLIDS DECOMPOSITION IN RADIATION FIELD
2. HEAT TRANSFER	PARTICIAL HEAT EXCHANGER	LAWRENCE BERKELEY	FY 1982 & 1983	NOT DIRECTLY RELATED TO FUELS AND CHEMICALS. WORK DISCONTINUED DUE TO LACK OF FUNDS
3. MASS TRANSFER	TRANSIENT EFFECTS	?	FY 1985	NO PRESENT WORK, ANALYSES ONLY
4. CONTROLS	TRANSIENT OPERATIONS	?	FY 1984	ANALYSES ONLY
5. SOLAR INTERFACES	HARDWARE CONFIGURATIONS	WESTINGHOUSE/FUNK	FY 1983	DESIGN OPTIONS, SULFURIC ACID DECOMPOSITION EVALUATION
6. SUPPORTING HARDWARE	PUMPS, METERS	GENERAL ATOMIC	FY 1984	LIMITED TO IODINE PROCESS
7. CONTAINMENT	METAL ALLOYS	GENERAL ATOMIC	FY 1982-1985	SUITABILITY, CORROSION AND METALLOGRAPHY
	CERAMIC	GARRET	FY 1984	SEALING AND JOINING OF CERAMIC COMPONENTS

Table 1. SOLAR FUELS AND CHEMICALS TECHNOLOGY PROGRAM ELEMENTS (CONTINUED)

ELEMENT	WHAT?	WHO?	WHEN?	COMMENTS
8. PHYSICAL PROPERTIES	RADIATION PARAMETERS	LAWRENCE BERKELEY	FY 1984	MEASURE OPTICAL PROPERTIES FOR SOLIDS DECOMPOSITION
9. PROCESS DESIGN	SULFURIC ACID DECOMPOSITION SUBSYSTEM	FOSTER WHEELER	FY 1984	SPECIFIC DETAILED DESIGN, SOLAR FIELD LAYOUT
10. REACTOR DESIGN	CATAYLTIC METAL REACTORS	GENERAL ATOMIC	FY 1982-1985	STRESS, FABRICATION, AND PERFORMANCE
	DIRECT FLUX	IGT/SANDERS	FY 1983	ROTARY KILN & CONVEYOR FOR $CaCo_3$ DECOMPOSITION
	DIRECT FLUX	IGT/BADGER	FY 1983	TRANSPARENT RECTOR FOR NATURAL GAS REFORMER
11. PHOTO-CHEMICAL	ENGINEERING	JPL	FY 1983	ECONOMICS OF FLAT PLATE AND LINE FOCUS REACTORS
	FUNDAMENTALS	SERI	FY 1983	RESEARCH PLAN

THE THERMOCHEMICAL SULFUR THERMAL ENERGY STORAGE SYSTEM *

J.H. Norman, G.E. Besenbruch, L.C. Brown, and K.H. McCorckle
GA Technologies
San Diego, CA 92138

INTRODUCTION

Many energy consuming systems exhibit a relatively level energy demand day and night, season to season. This is particularly true of the chemical industry where plant investment and start-up and shut-down difficulties nearly make constant energy supply a requirement.

Solar systems, having an inherent periodic nature, are considerably improved by coupling with a thermal energy storage system (TES).

Thermal Energy Storage has been categorized in one of three categories - sensible heat, latent heat, and thermochemical heat. DOE[1] has developed a method of evaluating these processes which divides the economic evaluation into two parts: power cost and capacity cost. They have set economic goals for processes in these terms. In these goals DOE clearly labels sensible heat sources as near term but expensive technology which it hopes will be bettered by the other two technologies. Their goals indicate that the longest range, least developed, highest potential area is in thermochemical. At the present time the hopes for the high potential thermochemical system has not been realized and it is unclear whether total cost goals of one third the cost of sensible heat and one half the cost of latent heat will be realized.

This study has as its subject a highly promising thermochemical system where the capacitive cost clearly are an order of magnitude lower than other sensible, latent, and thermochemical thermal storage systems that the authors have encountered. The sulfur storage system has an unusual feature which leads to the extremely low capacitive costs and extreme thermal capability but only at a cost of system complication. It remains to be learned whether the costs associated with these added complications will exceed the values of the cycle which promises economic seasonal storage if it can deliver economic diurnal storage. This cycle, which is based on sulfur chemistry is fully capable as a stand alone TES system. However, the sulfur system is particularly useful with a H_2SO_4 based thermochemical water splitting cycle since it stores energy in sulfur which is burned to SO_2 to release this energy. In doing so the basic chemical for H_2SO_4 water splitting is created. This cycle obviates the need for storing SO_2 for chemical uses by replacing SO_2 storage with S storage. Also the energy released in S burning per mole of S is a good fit to the thermochemical requirements of water splitting per mole of SO_2.

The capacitive benefits of the sulfur storage system are demonstrated in Figs. 1 and 2 where respectively the inventory costs of storage media per 1000 kcal energy storage and the volume occupied by the media per unit of stored energy are compared with other TES materials. This later term combined with the storage conditions (e.g. hot tanks for stored sensible heat and latent heat) can be used to define tankage costs for the

stored energy. This table shows that many storage media can be generally classified as inexpensive yet sulfur storage is generally an order of magnitude better in inventory and tankage costs than other commonly proposed storage media. Note that of the media listed only coal looks better.

The power costs of storage will clearly be higher in the case of the sulfur storage system than for most of the other media listed. Nevertheless, "power-related costs are a function of the special application... Only in detailed analyses of specific systems applications can these power-related costs be determined."(1). It remains to evaluate the proposed sulfur storage system from a power cost standpoint. As demonstrated in Fig. 3 describing the DOE TES goals, sulfur storage will clearly meet the stringent thermochemical capacitive goals. One should note that the power cost goals are less demanding on thermochemical systems than they are on sensible and latent heat systems due to projected longer projected hours of storage service.

The Sulfur Energy Storage System

In most thermal storage systems the energy releasing process is the reverse of the storage process. This is a requirement of a two-step process. Thermochemical cycles need not be confined to two-step cycles. In fact, three-step cycles have some enhanced energetic properties not found in two-step cycles. For instance, temperatures to operate a two-step thermochemical water splitting process are extreme while three-step

processes can reduce this temperature to ~1000K. Thermochemical water splitting is a thermal energy storage process.

Similarly there can be energetic advantages to three-step TES thermochemical systems. This is illustrated well by the sulfur TES system, which accepts heat at decomposition temperatures of SO_2 (and below by concentrating and boiling H_2SO_4), rejects a portion of the stored heat at relatively low temperature in the form of low quality heat, and by this low temperature reaction is activated to be able to produce considerably higher quality heat than was initially utilized in the process. The process is illustrated by the following three reactions:

$$2H_2SO_4 \rightarrow 2SO_2 + O_2 + 2H_2O \quad (1)$$

$$2H_2O + 3SO_2 \rightarrow 2H_2SO_4 + S(\ell) \quad (2)$$

$$S(\ell) + O_2 \rightarrow SO_2 \quad (3)$$

The first reaction is solar driven and takes 134.0 kcal/2 moles H_2SO_4 of solar energy from ~200 to 900°C to charge the reactants. The second reaction disproportionates the SO_2 product of the first reaction releasing 62.2 kcal per three moles of SO_2 at ~150 - 250°C. The third reaction releases the bulk of the stored energy capability of 71.8 kcal/moles of very high quality heat. This heat can be of higher quality than can be easily utilized if burned in oxygen. Thus, burning superstoichiometrically air is projected. The excess air can be used to control temperatures to below 1500 K. This hot fluid is a candidate for use in a Brayton cycle. The product of this reaction is redirected to reaction two to create more S in the TES version of this storage cycle but in concert with thermo-

chemical hydrogen energy cycles is redirected to the process as a feedstock for hydrogen production.[2,3]

The merits of the heat delivery system can be compared to draw salt energy storage where a Carnot efficiency capability of the stored energy is about 50%. If one calculates the stored energy Carnot efficiency of the sulfur storage cycle, both for the low temperature and the high temperature reactions combined, one exceeds 50%. Thus, it would appear that energy losses will not invalidate the candidacy of this system.

This system does require at least three different energy subsystems and thus is clearly more complicated than a draw salt TES system. Nevertheless, the promises of low capacitive costs (high energy density and inexpensive chemicals) and the produced high temperature fluids of Brayton cycle capability are the important assets of the cycle.

Cycle Development

Neither chemical development nor engineering flowsheeting and costing are sufficiently advanced to fully define the potential of this cycle.

The chemical development is aided by thermochemical hydrogen efforts on the decomposition of H_2SO_4. Thus reaction (1) can be considered well characterized. Reaction (2) data can be found in the literature[4] and these kinetic data have been cursorily confirmed in our laboratory[3]. Little is known about catalytic potential in speeding up reaction (2). With presently available kinetics reaction (2) is feasible as a

storage system reaction but is relatively slow. Reaction (3) has been studied in the H_2SO_4 manufacturing industry but certainly has not been approached from the point of view of an efficient energy delivery reaction. The reaction proceeds swiftly but needs to be studied in an energy engineering sense.

Engineering development is characterized by its absence and, before this cycle can be considered viable, a considerable evaluation effort will be required. Of course this evaluation effort will need to be based on some preliminary development information. With the high potential, including seasonal storage, that the sulfur TES system offers the proposed efforts appear warranted.

REFERENCES

1. Thermal Energy Storage Technology, Development for Solar Thermal Power Systems, Multiyear Program Plan, (DRAFT) U.S. Dept. of Energy, Divisions or Energy Storage Systems and Central Solar Technology, March 13, 1979.
2. G.E. Besenbruch and K.H. McCorckle, "Thermochemical Water Splitting with Solar Thermal Energy: Final Report," General Atomic Report GA-A16022, Feb. 1981.
3. J.H. Norman, G. Besenbruch, and L. Brown, "Solar Production of Hydrogen Using the Sulfur-Iodine Thermochemical Water Spiltting Cycle," General Atomic Report GA-A16493, Sept. 1981.
4. A.F. Ryabinina and V.A. Oshman, "Thermal Decomposition of Aqueous Sulfur Dioxide Solutions," Tr. Ural. Lesotekh. Inst. 1972, No. 28, 182 (Russ), Chem. Abstracts 79, 58115 p, 1973.

FIG. 1: THERMAL ENERGY STORAGE INVENTORY COSTS

CHEMICAL	DENSITY (G/CM^3)	STORAGE CONDITION	VOLUME (CM^3/KCAL)	
			CHARGED	DISCHARGED
NaCl	2.165	HOT	1.80	
KCl	1.984	HOT	2.56	
$MgCl_2$	2.316	HOT	1.89	
NaF	2.79	HOT	0.95	
KF	2.48	HOT	1.61	
NaOH	2.13	HOT	1.15	
Na_2CO_3	2.509	HOT	1.59	
K_2CO_3	2.428	HOT	2.17	
$NaNO_3$	2.261	HOT	1.69	
KNO_3	2.109	HOT	2.70	
CaO	3.37	AMB	0.73	
$Ca(OH)_2$	2.343	AMB		1.39
H_2O	1.00	AMB	0.79	
SO_2	1.434	COLD	1.92	
SO_3	1.925	AMB		2.14
O_2	0.065 50ATM	AMB PRESS.	10.6	
S	1.957	AMB (WARM)	0.12	
H_2SO_4	1.834	AMB		0.39
H_2O	1.00	AMB	0.13	
H_2	0.0041 50ATM	AMB PRESS.	7.27	

FIG. 2: THERMAL ENERGY STORAGE DENSITY

STORAGE SUBSYSTEM	Cp/h GOAL ($/kWeh)	HOURS OF STORAGE	Cs GOAL ($/kWeh)	Ce COMPONENTS ($/kWeh)		
				INITIAL* INVENTORY	CONTAINMENT	LITERATURE CONTAINMENT
SENSIBLE HEAT –DRAW SALT	30	6	30	3.50	X	($12 COPELAND)
ADVANCED SENSIBLE AND LATENT –MIXED HALIDES	20	6	20	0.86	X	($17 COPELAND)
THERMOCHEMICAL –GA SULFUR STORAGE SYSTEM	15	16	5	0.022	$\frac{X}{7^{S}F_{C}}$**	

*LOWEST PRICE IN AUG 1, 1983 CHEMICAL MARKETING REPORTER CONVERTED FOR ELECTRICAL CONVERSION EFFICIENCY:
0.25–SENSIBLE HEAT
0.4 –ADVANCED SENSIBLE AND LATENT
0.5 –THERMOCHEMICAL

**F_C IS FACTOR ALLOWING FOR AMBIENT STORAGE (>1)
S IS A SIZE CORRECTION FACTOR (~ 0.7)
$7^{S}F_{C}$ PROBABLY EXCEEDS 10

FIG. 3: CAPACITY COST BREAKDOWN INVENTORY AND CONTAINMENT COMPARED TO GOALS

CHEMICAL	TYPE	ΔH (KCAL/MOL)	$\int_{400}^{1000} C_p dT$ (KCAL/MOL)	COST* ($/TON)	ENERGY STORAGE COST ($/1000 KCAL - ONE CYCLE)	LITERATURE ($/1000 KCAL - ONE CYCLE)
NaCl	LATENT	6.73	8.28	50	0.21	0.59[1]
KCl	LATENT	6.282	8.42	105	0.59	
$MgCl_2$	LATENT	10.3	11.8	255	1.22	
NaF	LATENT	7.97	7.79	1200	3.60	1.30[1] ($NaFMgF_2$)
KF	LATENT	6.50	8.02	1340	5.90	
NaOH	LATENT	3.04	13.36	657	1.76	1.40[2]
Na_2CO_3	LATENT	7.09	23.92	427	1.90	1.16[1]
K_2CO_3	LATENT	6.6	19.73	650	3.70	
$NaNO_3$	SENSIBLE		22.3	130	0.56	
KNO_3	SENSIBLE		17.7	267	1.70	
CaO	CHEMICAL	22.7		31.25	0.083	
SO_2	CHEMICAL	23.3		50	0.076	
S	CHEMICAL	138.8		50	0.013	
H_2	CHEMICAL	67.7		1280	0.042	
C	CHEMICAL	94.3		35	0.0049	

1 COPELAND, ULLMAN AND LEACH '81
2 COPELAND, 82
* LOW PRICE IN CHEMICAL MARKETING REPORTER AUGUST 1, 1983

* Work performed under USDOE Contract No. DE-AC03-83SF11929

REACTOR DESIGN STATUS FOR THE SULFUR CYCLE HYDROGEN PRODUCTION PROCESS

L. E. VANBIBBER
WESTINGHOUSE ELECTRIC CORPORATION
ADVANCED ENERGY SYSTEMS DIVISION

INTRODUCTION

Westinghouse has been developing the Sulfur Cycle, a hybrid thermochemical-electrochemical process for the production of hydrogen and oxygen from water, with sponsorship from the United States Department of Energy. The process, in its most general form, consists of two chemical reactions. The production of oxygen occurs via the thermal reduction of sulfuric acid into sulfur dioxide, water and oxygen. The process is completed by using the sulfur dioxide from the thermal reduction step to depolarize the anode of an electrolyser using dilute sulfuric acid electrolyte to produce hydrogen and more sulfuric acid. The net result of the two reactions is the decomposition of water into hydrogen and oxygen with the sulfur dioxide and sulfuric acid involved solely as recycling intermediates.

The energy needs of the process are thermal energy for the acid vaporization and thermal reduction steps, and electrical energy for the electrolysis and auxiliary power (e.g. pumps, circulators, etc.). The temperature levels required for the thermal inputs are compatible with advanced high temperature solar receivers. The electrical power (which is much smaller than conventional water electrolysis), can also be provided by solar electric sources.

A major milestone in the development program was the definition of a Pressurized Test Unit (PTU) which would provide a prototypical demonstration of the coupling of the hybrid sulfur cycle with the distributed solar collector technology. This paper describes the PTU, the designs of critical solar interface equipment such as the acid vaporizer and the decomposition reactor and experimental studies leading to the selection of critical temperature materials.

PRESSURIZED TEST UNIT

The PTU was designed for a nominal 86 kW(t) rate of hydrogen generation that will permit the coupling of the thermochemical system to a single distributed solar collector of reasonable size. The PTU process flowsheet is shown in Figure 1. Figure 2 shows the solar interface with the sulfur cycle. Helium is used as a heat transport medium to provide the heat for endothermic decomposition of sulfur trioxide, both preheating and decomposing the acid vapor, and to provide the heat for the final stage of acid vaporization. This unit produces 850 SCFH of hydrogen and requires 33 KW_e to the electrolyzer, 85 KW_t to the decomposition reactor and 41 KW_t to the acid vaporizer II. This PTU was selected based on consideration of development risk, information payoff, experimental flexibility, performance, safety considerations, and capital costs.

ACID VAPORIZER DESIGN

Optimization of the PTU design led to a concept with two stages of vaporizatio in which the first stage vaporizer would use energy from the decomposer exit stream and the second stage vaporizer uses solar energy supplied by the interconnecting helium loop. Because of the absence of industrial experience in producing equipment that contains boiling concentrated sulfuric acid at hig pressure, the acid vaporizers are critical components requiring development. The second stage vaporizer which has the most severe environment and which is part of the solar coupling has been given an extensive design evaluation supported by experimental efforts.

A primary consideration in the second stage acid vaporizer design was the selection of a corrosion resistant material. Approximately three dozen candidate materials were selected for corrosion tests. Samples of these materials were exposed to 98 w/o sulfuric acid at 634 K, 379 kPa and 725 K, 2068 kPa for periods up to 1000 hours. Based on weight change measurements th materials that had the best corrosion resistance in both liquid and vapor phases were the chemical vapor deposited (CVD) silicon carbide (SiC) hot pressed silicon nitride ($\dot{S}i_3N_q$) and metallic silicon. The most attractive metals were Durichlor 51 and Duriron. Silicon carbide was selected because of

its desirable characteristics, such as good thermal shock resistance and thermal conductivity coupled with its excellent corrosion resistance.

Evaluation of silicon carbide acid vaporizers led to a design shown in Figure 3. This design is a counterflow shell-and-tube heat exchanger, with 233 kg/hr of helium entering the shell side at 1020 K and exiting at 877 K. The process stream is 220 kg/hr of acid vapor entering at 661 K and exiting at 725 K. Both streams are pressurized to 20 atmospheres so that the differential pressure on the tubes and tube sheets is very small and can be in either direction to control cross-mixing of the streams. The shell and heads must withstand this pressure continuously, and the tubes and tubesheets must survive it during accidental depressurization of either stream and during startup/shutdown transients.

The design of the heat exchanger is based upon elimination of stresses in the SiC tubes due to axial differential thermal expansion by permitting the tubes to slide through mechanical seals in tube sheets used at both ends of the tubes. Instead of being attached to the tube sheets, the tubes are sealed and restrained by an unstressed performed plate to limit motion. The seals chosen for this design are Helicoflex seals, developed by CEA (the French Atomic Energy Commission). Each seal consists of a coil spring made of Inconel X750 wound with initial tension and coiled into a torus. The spring is covered with a thin gold liner. Sealing takes place when the torus is compressed, usually axially but in some cases radially, so that the cross section of the toroidal spring is elastically deformed. Pressure between two flanges (for axial deformation) or between a tube and tube-sheet cavity (for radial deformation) causes the liner to seal against the contacting surfaces. This sealing with proper dimensional control can be helium leaktight. Fabrication limitations of SiC tubes prompted the use of 2.5 cm O.D. tubes not more than 213 cm long. Accordingly, the tube bundle consisted of seven tubes extending 183 cm between tube sheets with baffles spaced 30 cm apart. The seven heat exchanger tubes are arranged in a hexagonal pattern and enclosed in a 10 cm I.D. shell. The shell is flanged at both ends and connected to hemispherical heads. The shell flange, tube sheets and head flanges are clamped together using a split ring wedge type enclosure.

DECOMPOSER REACTOR DESIGN

The decomposition reactor has a dual purpose of preheating the acid vapor and reducing the H_2SO4 first into H_2O and SO_3 and finally into H_2O, SO_2, and O_2. The preheating section is sized based on heat transfer requirements coupled with pressure drop limitations. The reactor section must operate at temperatures around 1170 K under pressurized conditions and needs a suitable catalyst to ensure adequate reaction rates for sulfur trioxide cracking.

To meet these requirements a shell and tube heat exchanger (Figure 4) driven by 1250 K helium on its tube side was selected. The shell side receives acid vapor at 800 K. The acid vapor flows through a packed bed of aluminum spheres and is preheated to 1080 K. It then enters a catalyst bed in which the cracking reaction occurs while being heated further to 1170 K. The catalyst bed uses a commercially available catalyst that has iron oxide deposited on an aluminum substrate. Helium on the tube side ranges from 1250 K to 990 K.

The tube bundle consists of twenty one 2.5 cm tubes in a 5 x 5 square array with the corners replaced by solid bars which separate the tube sheets and restrain them from further separation. In the preheat section the tubes are made of Hastelloy X and are free to expand axially through annular Helicoflex seals at both ends of the tube. The reaction zone tube bundle including the tubes and tube sheets are made of SiC. As in the acid vaporizer, helioflex seals are used to provide a mechanical seal while permiting each tube to slide axially through the tube sheets. The low and high temperature heads, and the shell are made of alonized Hastelloy. The tube sheet flanges are clamped to the high and low temperature heads and sealed using Helioflex face seals. The tube lengths are 282 cm and 183 cm in the preheat and reaction zones respectively. The overall dimensions are 503 cm in length by 25 cm OD.

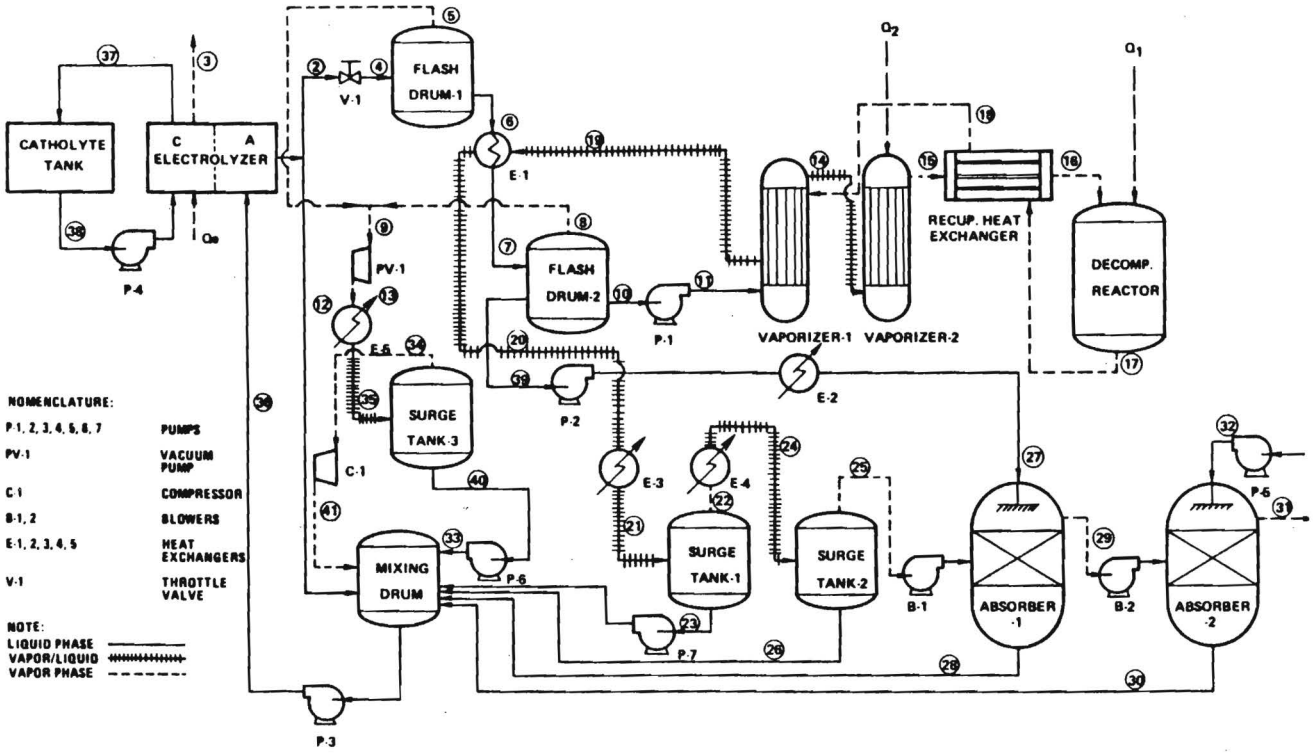

Figure 1. PTU Process Flow Sheet

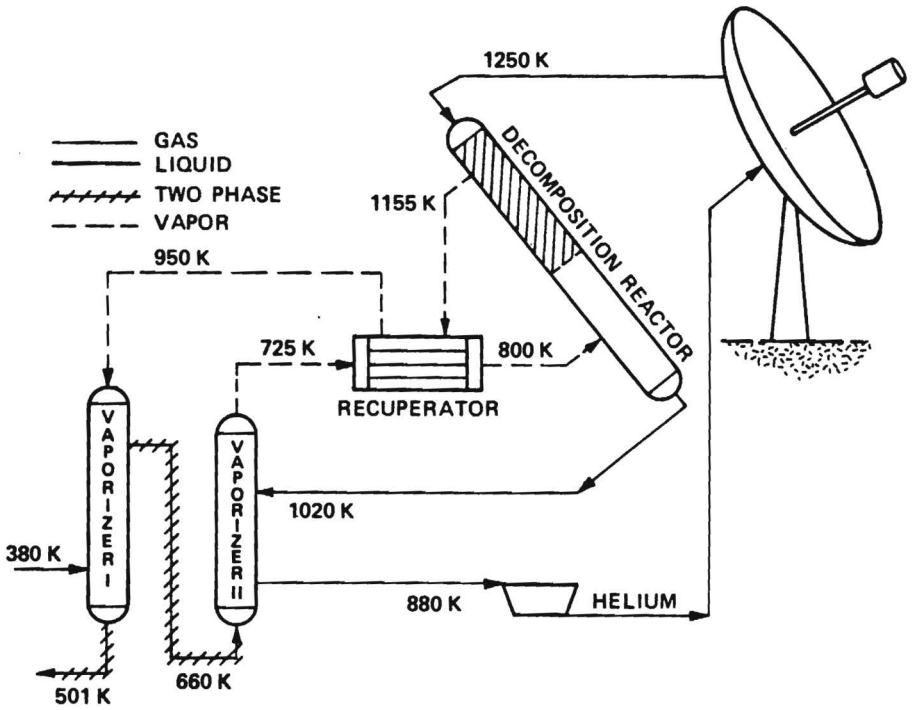

Figure 2. Sulfur Cycle Interfaces with Solar Collector

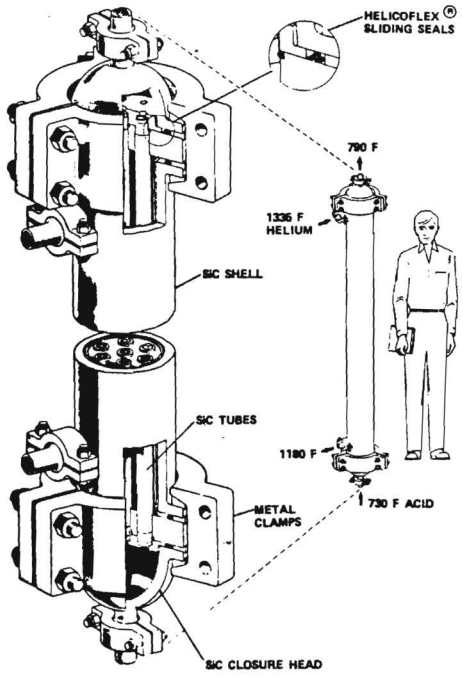

Figure 3. Sulfuric Acid Vaporizer

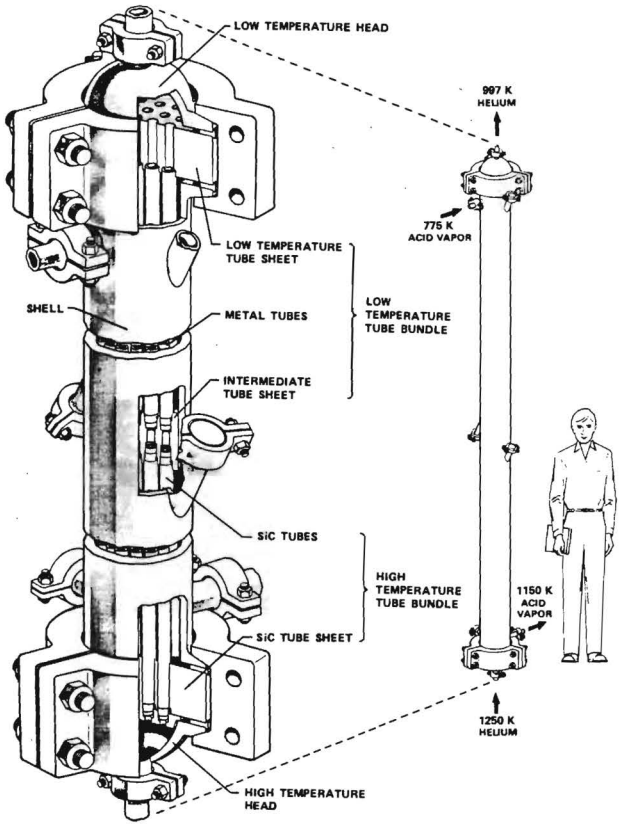

Figure 4. Decomposition Reactor

EFFECT OF HIGH RECEIVER THERMAL LOSS ON THE EFFICIENCY OF CENTRAL RECEIVER SYSTEMS HAVING OPTIMUM HELIOSTAT FIELDS AND OPTIMUM RECEIVER APERTURE AREAS

Charles L. Pitman and Lorin L. Vant-Hull

Solar Thermal Program Division
Energy Laboratory
University of Houston
Houston, Texas 77004

ABSTRACT

Thermal losses through the receiver aperture have a significant impact on the design and performance of optimized central receiver systems. Average aperture losses (from reradiation plus convection) ranging from 0.04 to 0.50 MW m^{-2} were considered, corresponding to working fluid temperatures (at receiver exit) in the range of 650 C to 1650 C. As the thermal loss increases over this range, the receiver thermal efficiency decreases from 0.93 to 0.70, and the interception factor decreases from 0.93 to 0.78. In contrast, the average cos I remains approximately constant at 0.81, and the shading and blocking factor decreases from 0.95 to 0.925. The optimal power level decreases from 310 to 170 MW for a tower focal height of 150 m. The resulting decrease in solar subsystem efficiency from 0.57 to 0.35 is about a factor of 1/2 (or nearly -40%). Unoptimized systems would experience an even greater degradation in performance. The design assumptions given in section 2 influence the above results, and futher study of this problem will indicate the extent of their influence.

1. Introduction

Reradiation and convection cause the loss of significant amounts of thermal energy from the apertures of a high temperature, cavity type central receiver. This thermal loss certainly affects the receiver thermal efficiency (i.e., the fraction of energy absorbed by the cavity which is transferred into the working fluid), but this is not the only effect on optimized central receiver systems. The receiver thermal loss also affects the optimal aperture size and heliostat field layout because of optimization trade-offs which arise in the following way. In order to compensate for an increase in the receiver loss per square meter, the average concentration must be increased. This is achieved by reducing the aperture area and increasing the heliostat field density. As a result, the interception factor for distant heliostats is decreased, and the shading and blocking losses are increased. These responses result in a reduction in the optimal field size and thus the delivered energy. Clearly, a trade between these effects is required to achieve an optimum solar thermal system, i.e., to achieve lowest cost per unit energy delivered.

A detailed study of the effect of high receiver thermal loss per square meter on the performance of central receiver systems having optimum heliostat fields and optimum receiver aperture areas has been initiated. The method of investigation involved assuming an average aperture loss per square meter and a tower focal height and then computing the optimum aperture area and heliostat field layout using the University of Houston computer code RCELL (plus several other small codes used to speed the interpolation and analysis of the numerous RCELL results). Tower focal heights of 150 meters and 180 meters and aperture losses ranging from 0.04 to 0.50 MW m^{-2} were assumed, since these correspond to typical commercial systems operating at very high

For a fixed aperture and an associated optimized field (i.e., a sub-optimum case), the receiver thermal efficiency does not drop off as rapidly because the field has been re-designed for each L in order to increase the average concentration. However, the interception factor also decreases (although it is still better than the fully optimized case), since the field is expanding and thus absorbing more heliostats with poor interception.

The other sub-optimum case of a fixed field and an optimized aperture shows a similar behavior, except that here the interception factor is decreasing because the aperture is shrinking. Note that it is indeed possible for this case to have a better receiver thermal efficiency than the fully optimized case.

Finally, in the optimum design, the aperture area diminishes (decreasing the interception) and the heliostat field becomes more densely packed (increasing the shading and blocking loss) as L increases; the field shrinks. This case of optimized field and aperture has the best solar subsystem efficiency even though it may not have either the best interception factor or receiver thermal efficiency; of course, the solar subsystem efficiency is the efficiency used to determine the figure of merit.

. Efficiency and Other Susbystem Characteristics vs. Aperture Loss

The most significant results of this study are the curves of efficiency s a function of aperture loss per square meter. Figure 2 shows the umulative effect of the various subsystem efficiencies, i.e., each curve is he product of the efficiencies listed above it. The results shown are for a ower focal height of 150 m; the results for a 180 m tower are similar and hus will not be presented here. The heliostat reflectance (including an llowance for dust, outage, and layout slippage) is 0.894, and the receiver

temperatures. For example, an average aperture loss of 0.04 MW m^{-2} is roughly equivalent to a working fluid outlet temperature of 650 C, and 0.50 MW m^{-2} is roughly equivalent to 1650 C. ("Roughly equivalent" is used here because the temperature vs. loss function depends on the precise cavity emittance and the precise ratio of convection to reradiation.)

2. Design Assumptions

McDonnell-Douglas second generation heliostats having 56.84 m^2 of reflective area were used in this study. The heliostats were focused in one axis and canted in both axes; the focusing and canting distances were slant range plus 20%. The hot air receivers used two elliptical apertures, each nodded down by 20 degrees from the vertical position and facing either 60 degrees west or east of due north. Beam degrading was assumed to be Gaussian in character with an rms value of 2.83 milliradians (about 1/6 degree). N-th plant costs were used.

Further study of this problem will indicate the effects which better focusing heliostats, receiver orientation, other tower focal heights, heliostat size, and beam degrading have on the results.

3. Subsystem Efficiencies For Various Levels of Optimization

With increasing aperture loss per square meter (L), unoptimized or sub-optimized heliostat systems undergo an even greater degradation in performance than do optimized systems. Figure 1 is a schematic illustration of the efficiencies of unoptimized, sub-optimized, and optimized systems as a function of L. For the unoptimized case (i.e., a fixed field and a fixed receiver aperture), the receiver thermal efficiency plummets as L increases, although the interception factor remains constant.

bsorptance (i.e., one minus the receiver reflectance) is 0.96. The cos I actor, which is approximately constant at 0.81, accounts for the annual verage losses due to sunlight striking inclined and thus apparently oreshortened heliostats. RCELL handles the shading and blocking problem very deptly and introduces a heliostat density having only the optimum amount of nnual average shading and blocking loss; the shading and blocking factor i.e., the fraction of energy which is unshaded and unblocked) decreases from .95 to 0.925 as L increases from 0.04 to 0.50 MW m^{-2}. The atmospheric ransmittance factor is the average fraction of redirected energy which is not bsorbed by the atmosphere between the heliostats and receiver. Obviously, he interception factor and receiver thermal efficiency undergo the greatest hanges as L increases. The interception factor (including the atmospheric ransmittance factor) decreases from 0.93 to 0.78 and the receiver thermal fficiency decreases from 0.93 to 0.70 as L increases.

The bottom curve in Figure 2 displays the solar subsystem efficiency hich decreases from 0.57 to 0.35 as L increases. This drop is about a factor 3/2 (or nearly -40%) and is a significant effect.

Finally, Figure 3 shows various subsystem characteristics as a function aperture loss per square meter. Results are shown for a tower focal height 150 m. Although the results for a 180 m tower are not shown, it should be ntioned that the absorbed energies and optimum aperture areas are 25 to 30% rger than those for the 150 m tower and FMI and F do not decrease gnificantly. FMI affects the heliostat density and field boundaries and is e of the principal input parameters to RCELL. The figure of merit F is the st of the solar subsystem per annual MWH of thermal energy produced; the tailed behavior of this curve depends heavily on the various cost sumptions and on the fact that air was assumed to be the working fluid (as

may be seen by the minimum in the curve). The other results were not as greatly influenced by these assumptions.

5. Conclusion

The solar subsystem efficiency of central receiver systems having optimum heliostat fields and optimum receiver aperture areas decreases by a factor of 3/2 (or about -40%) as the aperture loss per square meter increases from 0.04 to 0.50 MW m^{-2}.

Further study of this problem will indicate the effect which better focusing heliostats, receiver orientation, tower focal height, heliostat size, and beam degrading have on the results.

6. Acknowledgements

This research was performed with the support of:

(i) U.S. Department of Energy under contract number SNLL-84-1637;

(ii) Shell Companies Foundation under a Graduate Aid Award;

(iii) Energy Laboratory, University of Houston; and

(iv) Olin and Rosalie Pitman.

However, any opinions, findings, conclusions, or recommendations expressed herein are those of the authors and do not necessarily reflect the views of the U. S. Department of Energy.

Figure 1

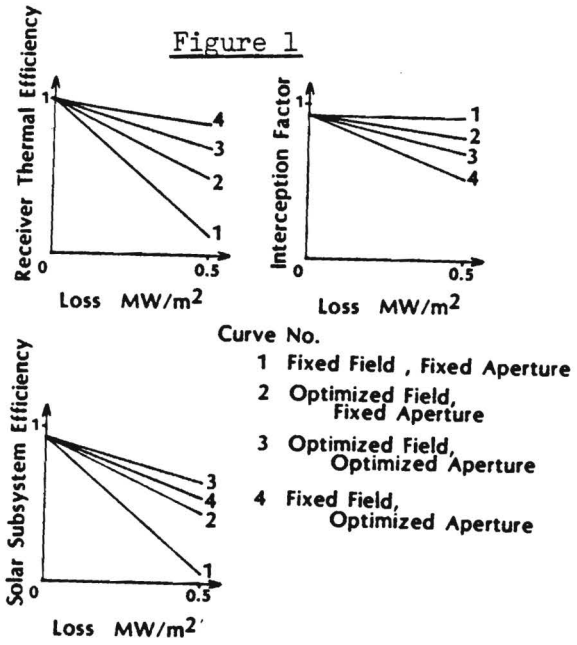

Figure 1. Schematic diagram of efficiencies of unoptimized (1), sub-optimized (2 & 4), and optimized (3) systems as a function of aperture loss per square meter (L). The optimized case (3) has the best solar subsystem efficiency.

Figure 2. Cumulative effect of subsystem efficiencies vs loss per square meter (L) for optimized systems having a tower focal height of 150 m. Each curve is the product of the efficiencies listed above it. The values shown by the lowest curve are called the "solar subsystem efficiencies".

Figure 3. Annual absorbed thermal energy (E), aperture area (A), figure of merit (F), and input parameter (FMI) vs L. The curves show values for optimized systems having a tower focal height of 150 m.

Figure 2

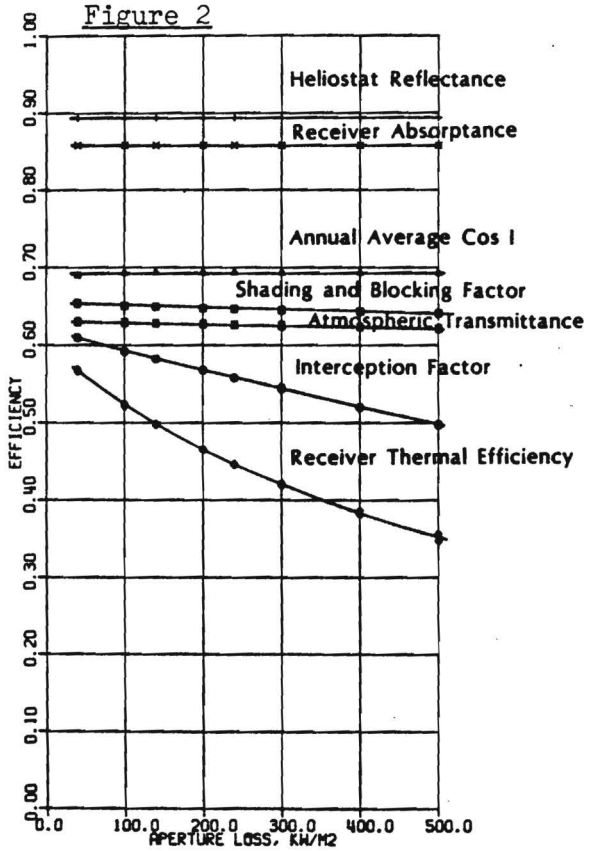

Figure 3

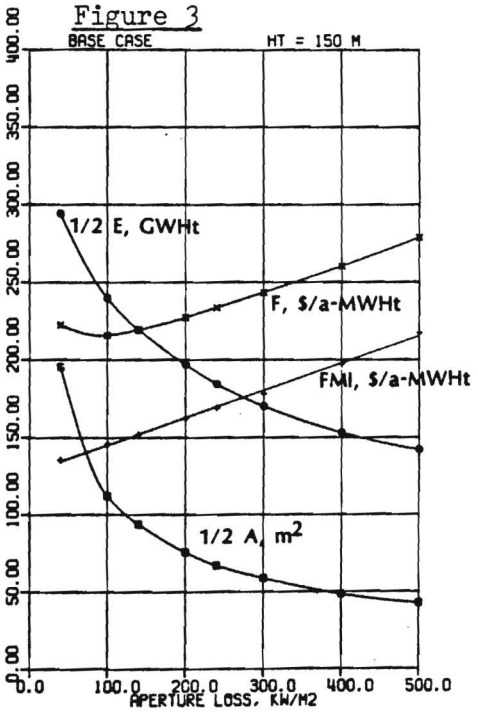

DIRECT FLUX SOLAR CHEMICAL REACTORS

Bernard Yudow
Institute of Gas Technology
3424 S. State Street
Chicago, Illinois 60616

The objective of the direct flux reactor project was to determine the technical feasibility, and practicality of developing commercial-scale direct flux solar chemical reactors. In essence, the issues are whether it is possible to utilize direct flux reactors for chemical processing and, if so, are the benefits compelling enough to justify their development and commercialization?

Important questions include: 1) why the interest in direct flux reactors, and 2) what defines a direct flux reactor? Central receivers are the only heat source considered appropriate for large-scale chemical processing. The tower-mounted reactor must have no opaque heat transfer surfaces. Reaction heat can be supplied by any single source or combination of sources among direct solar radiation, reflected solar radiation, and reradiant solar energy from hot surfaces within the reactor. Potential economic benefits create the interest in direct flux reactors. A potential benefit may be in the form of more compact reactors, because direct flux heating may permit high heat transfer rates through reduction in heat transfer resistances, thus reducing required heat transfer areas. Reduction in heat transfer resistance effectively lowers the reactor temperature required to deliver heat to the reaction. This may increase receiver thermal efficiency resulting in reduced heliostat field size and cost.

The literature on high-temperature receiver/reactor concepts and experiments was reviewed. The review shed very little light on the problems

of commercial-scale direct flux reactor design because experiments and conceptual designs were confined to small scales of 2 to 100 kW. No direct flux work was found pertaining to gas phase reactions. Furthermore, most investigations have been for chemical heat pipe or thermochemical hydrogen applications, not for endothermic reactions of commercial significance. Direct flux work had been done, however, for solid reactions. With the exception of work done in France on the decomposition (calcination) of calcium carbonate in small-windowed rotary kiln and fluid bed reactors,[1] no work had been done on chemical reactions of commercial significance. The main problems that arose in solids experiments were devitrification and/or chemical attack of quartz windows and tubular reactor vessels, and erosion of quartz by reactants or fluidization media. Quartz windows were always less than 1 foot in diameter. No concepts for large windows (>15 feet diameter) have been explored, nor have window materials alternative to quartz been investigated. Research on window materials is under way at Georgia Tech.

Designs of conventional high-temperature reactors were found relevant to direct flux reactor design because the primary heat transfer mechanism is radiation. It was from conventional high-temperature commercial reactor designs that conceptual designs for direct flux solar reactors were developed.

Two reactions were picked — one in the solid phase, one in the gas phase reactor; conceptual designs were developed around these reactions.

The solid phase reaction was the calcination of calcium carbonate:

$$\underset{\text{(Limestone)}}{CaCO_3} \xrightarrow[1100^0F]{\text{Heat}} \underset{\text{(Lime)}}{CaO} + CO_2$$

Calcination is an industrially significant reaction with broad applications. Lime production uses gas or fuel oil at 2000 Btu/lb of lime with an annual energy requirement in 1976 of 9.2×10^{13} Btu. Calcination is a well established process, this stimulates the concentration of R&D dollars on solar reactor development. Limestone calcination is a generic reaction that is broadly representative of a large class of industrial solids reactions. Another important potential application is to iron ore reduction using a commercial process known as the SL/RN process. This is typically done in rotary kilns similar to those used for lime production. This process has excellent potential to displace large quantities of costly metallurgical coke that is burned to provide heat to conventional iron ore reduction processes (i.e. blast furnaces.)[2] Limestone calcination has well-characterized properties. The operating temperature of 900° to 1100°C is a good match for the solar heat source. The atmospheric pressure reactions simplifies design and operation of the reactor vessel. Finally, the use of a solar heat source has been demonstrated by the French.[1]

The gas phase reaction was the steam reforming of methane:

$$CH_4 + H_2O \xrightarrow[790^0C]{\text{nickel catalyst}} CO + 3H_2$$

Steam reforming is of major industrial significance for ammonia production, hydrogenation processes, and for methanol production. At 238 Btu/SCF of hydrogen, steam reforming is an enormously energy intensive industry consuming 6×10^{14} Btu/year.

Since steam reforming is a well established process research, priority can be given to reactor design rather than to overall process development. This reaction is generic and design work can be applied to design of reactors

for catalytic reforming of propane and naphtha, the thermal cracking of ethane, and the catalytic decomposition of sulfuric acid. Properties are well established. The operating temperature of 790°C is a good match for the solar heat source and operating pressures may be varied from 1 atmosphere to 350 psig to suit possible constraints on materials of construction for direct flux reactors. A conceptual design study for a commercial-scale metallic solar steam reformer[3] was used as a basis for design.

The approach taken for reactor selection was conservative with reactor designs derived from reactors used currently used for calcination and steam reforming reactions. The design approach may be viewed as a baseline to which potential benefits of other reactor designs may be compared.

The choices for reactor concepts were a windowless rotary kiln for the calcination of calcium carbonate and a multi-tube packed bed cavity receiver/reactor for the steam reforming of methane. These are essentially the reactor types used industrially for these reactions.

As analysis proceeded on the design of the rotary kiln, a number of problems were identified that led to the selection of an alternative kiln concept: the conveyor kiln. The nearly horizontal rotary kiln has poor coupling of direct solar flux to the reactants. The integration of burners in the rotating kiln, while not impossible, was considered a problem and a drawback to the concept. The motion of the reactant bed, while providing good mixing, leads to dusting, which may impede penetration of solar radiation into the kiln. The greatest problem with the rotary kiln concept was the anticipated periodic heating of the kiln refractory liner. The nearly horizontal kiln leads to flux impinging largely on the top and upper sides of the rotating wall. A simple energy balance suggests these surfaces will be heated

Results were generated using an assumed net flux distribution, as shown in Figure 1. This is the sum of solar and IR flux absorbed by the burden. Later work will use a flux distribution developed by mapping the heliostat field onto the cavity and considering both solar and IR radiant heat transfer. Temperature histories of kiln solids and gases are shown in Figure 2. Kiln length is 35 feet.

The approach taken for the design of the steam reformer was influenced by information on the high cost and moderate performance of candidate transparent or translucent materials for a direct flux reactor (Table 1). All materials are significantly more costly than Inconel. Availability is a problem. Typically reformer tubes are 4-inch diameter and 30 to 40 feet long. While candidate materials can be obtained in the desired diameter, lengths are limited by the size of fabrication equipment to less than 6 feet. With no market there is no incentive to develop fabrication facilities. There is not a market that might serve to bring the cost of transparent materials down.

Will quartz work in a direct flux reactor? Unfortunately, quartz will not work (Table 2). The assumption is that heat transport is from the hot refractory liner. Tubes are inevitably spaced apart to permit more uniform circumferential irradiation. Uniform circumferential temperatures are necessary to avoid hot or cold spots and to avoid stress concentrations. Thus the projected area of the tubes is far less than the area of the refractory wall. Quartz is substantially opaque to IR. The other candidate materials have a lower temperature gradient that leads to improved cavity thermal efficiency. It is doubtful that the economics of solar steam reforming will be good enough to allow recovery of the costs of these materials.

As a result, the steam reformer design was based on the use of nickel alloy tubing. The conceptual design for the reformer is shown in Figure 3. The basic design is derived from the PFR study. The cavity shape gives uniform IR flux irradiation of the centrally located tubes. The shock wall blocks any direct flux. The 40-foot-long tubes are packed with catalyst. Twenty percent of the daytime heat requirement is derived from fossil fuel to ensure uniform circumferential flux distribution and the desired axial flux distribution. Fossil fuel burners are integrated with the solar reactor to provide 100% of the heat requirements at night. Heat recovery equipment is used to recover heat from reaction products and combustion products. A forced draft/induced draft system is employed to minimize daytime aperture convective losses. The aperture will be closed at night. The scale is 15 MWth at the aperture. This scale realistically corresponds to an application for vegetable oil hydrogenation.

The assessment of these designs is currently under way. The kiln appears to be a technically feasible design that should have reasonable thermal efficiency. The kiln should have very broad applicability for solids reactions over a wide range of scales. The technology exists to fabricate a conveyor kiln. Integration of the kiln with conventional means of feeding and discharging materials, including heat recovery appears straightforward. What must be proved out is whether air heated by the hot solids can be injected around the aperture without excessive convective losses.

A hybrid-metallic reformer appears technically and economically feasible. The prohibitive cost of transparent tubes does not offset the minor enhancement possible through direct flux heating of the reaction. There is no incentive for manufacturers to develop the capability of fabricating long

tubes because there is not a large enough market. There are significant uncertainties in the fabricatability of a transparent reactor (i.e., sealing connections, tube support). Elevated pressure operation may be a problem with the transparent materials. The development of a transparent steam reformer would be a very-high-risk program with a payoff that would at best be perhaps a 10% improvement in receiver efficiency, which would permit transparent materials to cost only twice as much as metallic tubes, through heliostat field cost reduction.

Are windows necessary? For most industrially significant solids reactions the answer is no. These reactions tolerate air. The principal issue is that technology must not cause safety and pollution problems. Maintenance of a positive draft and/or a hood to capture escaping gases such as carbon monoxide or sulfur oxide are possible solutions. The use of air windows which blow a gas stream across the aperture show promise and should be examined as a means to isolate the reactor atmosphere. Windows are viewed as the ultimate means to control the atmosphere within the reactor. Because of the high flux levels at reactor apertures, the problems of identifying inexpensive materials, seals, and fabrication methods are many. This suggest that window R&D should be secondary to the investigation of the use of air windows. Window development should be continued so that windows will be technically ready for applications where they are necessary.

One of the objectives of this research effort is to identify R&D needs for the establishment of a direct flux reactor design data base. Modeling efforts need to be undertaken to gain understanding of radiant heat transfer within reactors. This will lead to better understanding of cavity design to achieve desired flux distributions, of the effect of flux distributions on

transient performance, and of the impacts of diurnal and seasonal flux variations on reactor performance. Modeling will point to ways to properly integrate fossil fuel firing into hybrid reactors. The development of transparent gas phase reactors hinges upon the possibility of achieving a major cost reduction in reformer tubes. Tube cost must be brought down by a factor of several hundred. Long tubes must be fabricatable for reformers or design modifications must be developed for length reduction that do not impede catalyst changeout. The lifetime of the transparent materials is very uncertain. Modeling and experiments must be undertaken to establish reactor performance, especially when subject to nonuniform circumferential fluxes that may lead to undesirable side reactions. The conveyor kiln will require further investigation of coupling to the heliostat field through cavity shape variation and tilting of the reactant bed. The conveyor appears technically feasible, but alternative materials with adequate corrosion resistance to sulfates will have to be investigated if the potential versatility of the kiln is to be realized. The use of air windows to isolate the reactor environment should be explored. Window development is a long-term research priority. Economic assessments must be carried out to identify tradeoffs. Pilot scale reactors must be demonstrated. The integration of reactors into a pilot plant must be demonstrated.

Acknowledgements

This work was performed under DOE Contract No. DE-AC03-82SF11662. Assisting IGT were subcontractors Sanders Associates, Incorporated of Nashua, N.H. and Badger Engineers, Inc. of Cambridge, Mass.

References Cited

1. Flamant, G., et al., "Experimental Aspects of the Thermochemical Conversion of Solar Energy; Decarbonization of $CaCO_3$," Solar Energy 24, 385-395, London: Pergamon Press, 1980.

2. Krishnan, G. N., et al., "Design of an Experimental High Temperature Materials Processing System for the Solar Thermal Test Facility," Final Report for SRI International Project No. PYU 8291, prepared for Solar Energy Research Institute under Contract No. EG 77-C-01-4042 (Subcontract No. XJ-9-8017-1), Menlo Park, California, November 1979.

3. PFR Engineering Systems, Inc., "Solar Central Receiver Reformer System for Ammonia Plants," Final Report for U.S. DOE under Contract No. DE-AC03-79SF10735, Marina del Rey, California, July 1980.

Table 1. COST OF VARIOUS MATERIALS FOR A DIRECT FLUX REACTOR

Material	Cost/lb, $	Cost Ratio
Inconel	8.3	1.0
SiC	100.0	12
Quartz	110.0	13
Vistal (polycrystalline alumina)	1630.0	196
Spinel (magnesia aluminate)	4930.0	594
Sapphire	4210.0	507

Table 2. PROPERTIES OF VARIOUS MATERIALS FOR A DIRECT FLUX REACTOR

Property	Material				
	SiC	Inconel	Quartz	Spinel	Sapphire
Conductivity (W/M•K)	7.7	7.7	2.2	8.0	13
Transmitted Flux (W/M^2)	0	0	150	250	225
Conducted Flux (W/M^2)	300	300	150	50	75
Temperature Gradient (°C)	248	248	434	39.8	36.7

Assumptions:

Solar Concentration at Aperture	1500:1
Cavity Ratio	10:1
Reaction Temperature	900°C
Cavity Wall Is Perfectly Insulated	
Tube Wall Thickness	0.25 in.

12/flux/PAE

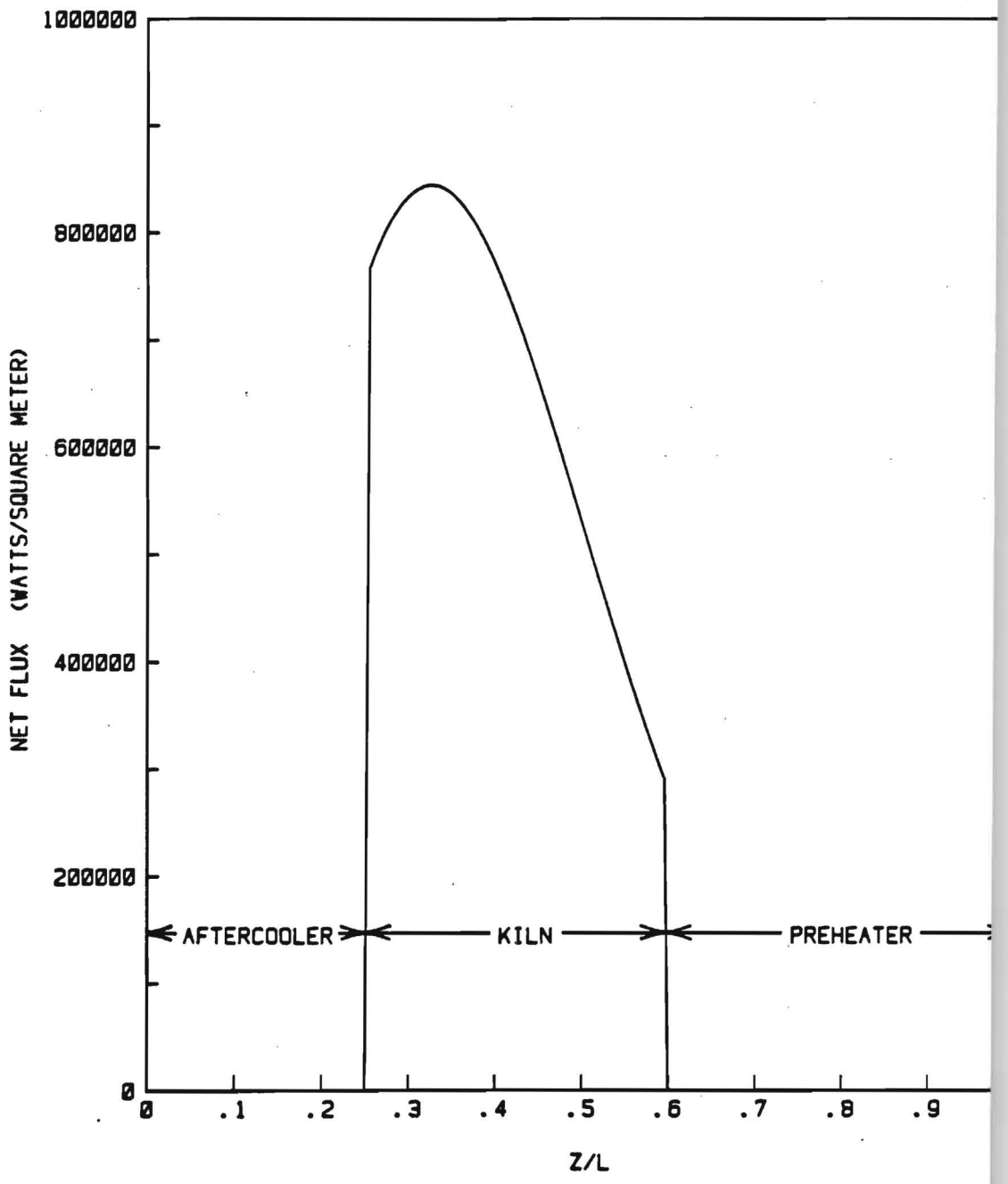

Figure 1. ASSUMED FLUX DISTRIBUTIONS IN SOLAR KILN REACTOR

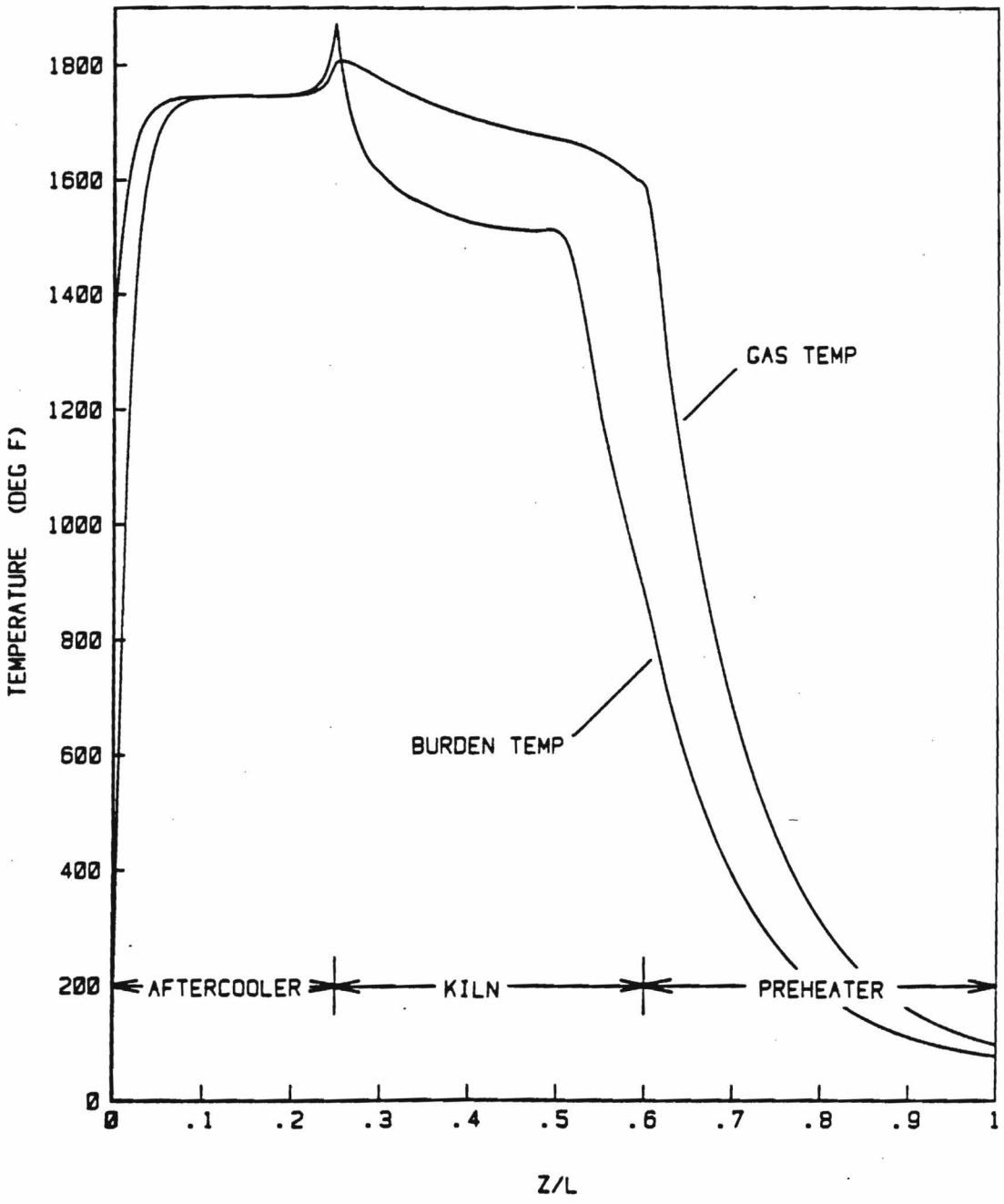

Figure 2. TEMPERATURE DISTRIBUTIONS IN SOLAR KILN REACTOR

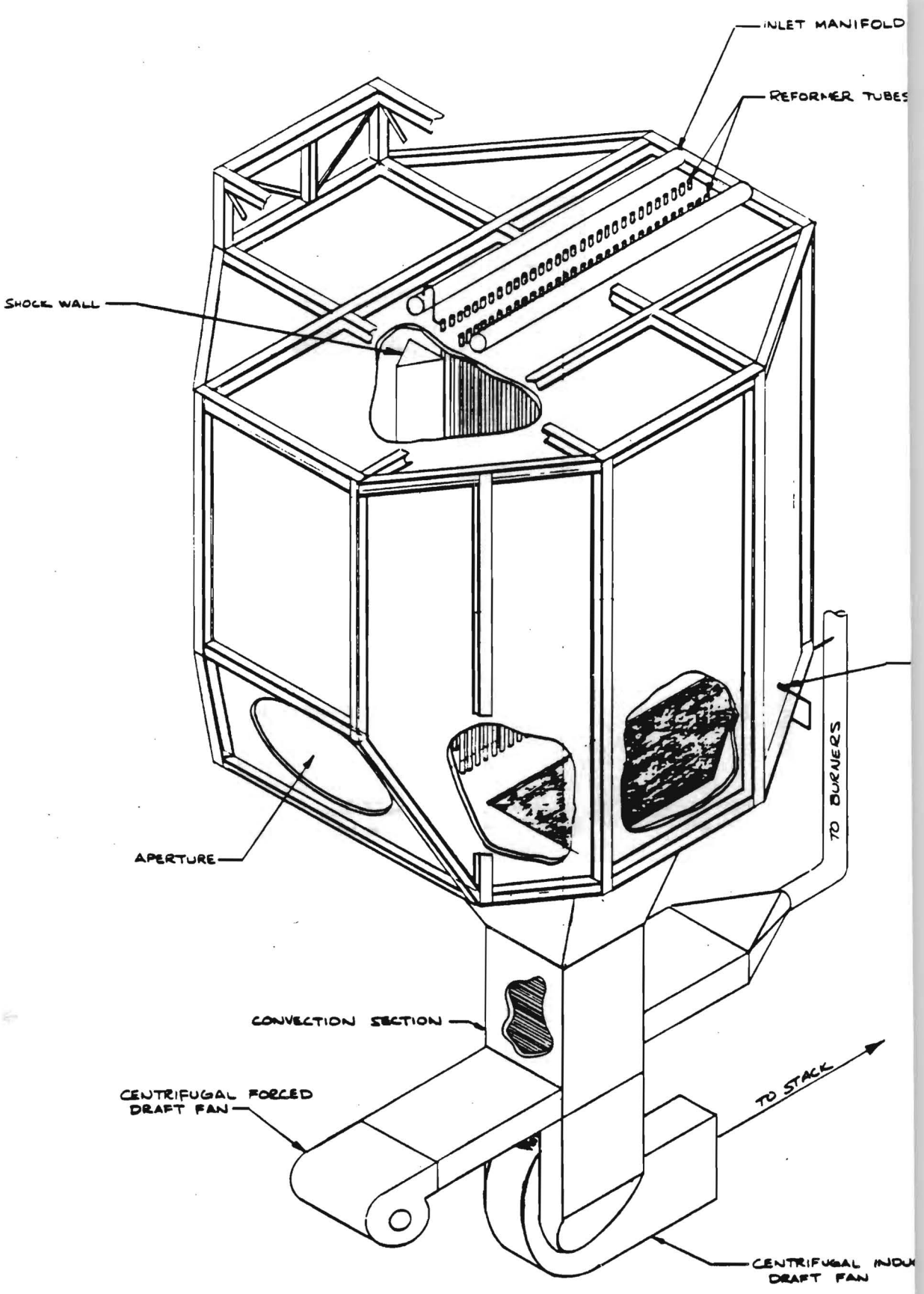

Figure 3. CONCEPTUAL DESIGN OF HYBRID SOLAR STEAM REFORMER

THE GEORGIA TECH DIRECT FLUX SOLAR THERMAL ENTRAINMENT REACTOR

D. H. Neale, R. A. Cassanova

Georgia Institute of Technology
Engineering Experiment Station
Atlanta, Georgia 30332

Georgia Tech is currently performing an experimental program to characterize the generic direct flux absorption particle entrainment reactor shown in Figure 1. Tests of this unit are designed to explore the effects on reactor performance of such parameters as particle size, particle residence time, flux level, flux distribution, reactant mixture ratios and hardware configuration. Ultimately, it is desired to provide sufficient engineering data to establish design criteria for future direct flux reactors. The present hardware was designed for tests at the Advanced Components Test Facility (ACTF) operated by Georgia Tech for the U.S. Department of Energy (U.S. DOE).

As shown in Figure 1, powdered reactant is supplied by a variable speed screw feeder unit with a volumetric feed range of 0.05-25 feet^3/hour. Dry particulate is discharged from the feeder and allowed to fall through a hollow ceramic tube which penetrates the reactor cap and runs concentric with the five-inch diameter quartz reactor tube. The particles are introduced into the reactor approximately eight inches above the base of the quartz tube, fall into the upward counter-flowing stream, become entrained and are carried through the solar beam to the exhaust port in the reactor cap. A small flow of dry nitrogen gas is metered and injected at the feeder outlet to co-flow with the falling particles. The nitrogen serves to prevent steam from migrating into the hopper and acts as the reference gas in the exhaust composition analysis. Four-foot lengths of alumina, silicon carbide and mullite have been used for the feeder tube.

The quartz reactor tube is enclosed by a 40-inch diameter x 2-foot deep cylindrical stainless steel cavity shell. The shell is lined on the inner surface with a nominal two-inch thickness of 2600° F insulation blanket. The cavity is used primarily to shield the process hardware mounted adjacent to the reactor and to reduce convective heat loss from the quartz tube. The lining is optically diffuse and provides no coherent beam redirection for rays missing or reflected from the reactor.

The well-known "water gas" reaction of carbon with steam to produce hydrogen and carbon monoxide was selected for initial study with the Georgia Tech reactor. This strongly endothermic reaction (136 Kjoule/mole, 1000° K) requiring elevated temperatures (1800° F, 1000° C) is an excellent match to the high fluxes existing at the focus of the ACTF beam. The black carbon particulate provides an ideal radiation absorbing medium and the steam is a natural vehicle for entrainment. The reaction yields a clean product whose equilibrium composition is well characterized as a function of pressure and temperature. Finally, the water gas reaction has practical interest as one of the principal reactions in coal gasification.

The Georgia Tech direct flux entrainment reactor was first operated in the Summer of 1982. Saturated steam was supplied by a 34 kW electric boiler with a capacity of 75 lb/hr at 75 psig (320° F). Initial tests were conducted with inert powders of alumina, silicon carbide and quartz to establish solar worthiness of the design, to demonstrate the range and control of steam and particle feeds and to evaluate the effectiveness of particle entrainment. Prior design modeling predicted that particle sizes up to 75μ with densities up to that of iron could be entrained with the current reactor with residence times ranging from 0.5 to 5 seconds (based on bulk inlet steam velocity). Approximately nine hours of inert particle

solar testing was completed using powders with mean particle sizes ranging from 60 to 90μ. Steam flows were varied from 10 to 75 lb/hr (0.6-4.5 ft/sec mean inlet velocity) with particle feed rates ranging from 20-110 lb/hr. The reactor system performed as expected and only minor hardware modifications were required before reaction tests were attempted.

The entrainment reactor system was returned to the ACTF tower in December, 1982 for tests of the solar driven carbon-steam reaction. A commercially available graphitic form of carbon (44μ) was selected for the first tests. As expected, entrainment was excellent with this material and opacity appeared to be higher than for similar particle/steam mass ratios used earlier in the test program with larger, inert particles. Flow opacity, however, was not high even for carbon/steam ratios greater than stoiciometric. As with the inert particle tests, quartz tube devitrification was evident on the inner surface within the first four hours of testing. Tube deterioration and darkening, however, did not appear to significantly reduce exhaust temperatures under similar flux conditions. Approximately 15 hours of solar tests were completed in this series which is summarized in Figure 2.

Exhaust gas composition was determined for each of the data points in Figure 2 and an example is shown in Figure 3. Calculations to evaluate reactor effectiveness revealed that no more than 10% of the input carbon had been converted in any of the runs. The low conversion rate may be attributed to marginal reactor temperatures (exhaust gas typically less than 1700° F), short residence times (gas expansion with heating accelerates particles through the high flux region) and low carbon reactivity (graphite).

Tests are now in progress with the reactor system employing modifications to enhance carbon conversion. The original diffuse cavity has been replaced with a water cooled conical reflector designed to boost thermal input to the reactor by 70% (design). A 40μ activated carbon particulate has been

substituted for the graphite. A quartz feeder tube will be used to increase apparent flow opacity and residence time by exposing carbon particles to the beam during decent as well as during upward entrainment. Both the reflector and the increased opacity should result in higher reaction temperatures. Finally, a de-ionizing unit has been installed in the boiler supply in order to extend quartz reactor tube life.

Future work includes development of an analytical model to explain past reactor performance and to aid in design of future direct flux receivers. Also, alternate reactions will be identified and evaluated with the current experimental apparatus. Finally, as tests continue, hardware configuration will be refined to develop an effective direct flux solar entrainment reactor test bed.

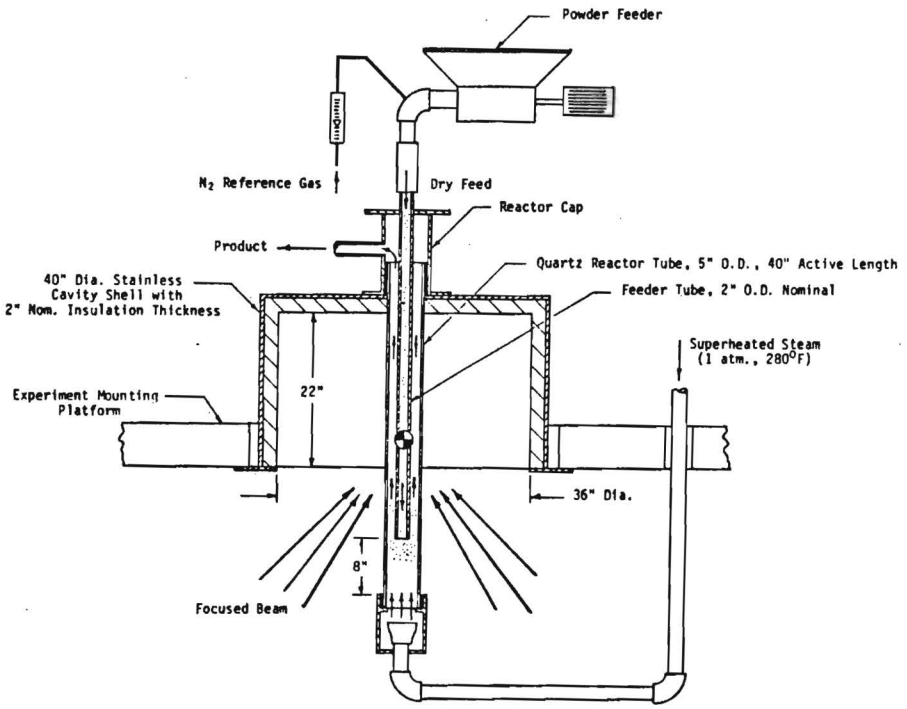

Figure 1. Direct Flux Entrainment Reactor Hardware Schematic.

Date (Sample No.)	Steam Flow (lb/hr)	Carbon Feed (lb/hr)	Carbon/ Steam Stoic. Fraction	Residence Time (τ) (sec.)	Mean Exhaust Temp. (^{o}F)	Mean Insolation (W/m^2)
1/13/83 (3)	10.6	3.2	0.45	5	1450.	800.
1/28/83 (7)	10.6	4.0	0.57	5	1390.	660.
1/26/83 (4)	10.3	4.0	0.58	5	1470.	685.
1/28/83 (8)	10.6	6.5	0.92	5	1340.	685.
1/13/83 (4)	10.5	6.5	0.93	5	1440.	800.
1/26/83 (3)	10.3	6.5	0.95	5	1440.	710.
1/05/83 (3)	<15	1.5	--	>3.5	1630.	770.
1/05/83 (4)	<15	6.5	--	>3.5	1570.	750.
1/06/83 (6)	18.9	3.2	0.25	2.5	1300.	725.
1/26/83 (1)	20.7	4.0	0.29	2.5	1535.	720.
1/26/83 (2)	20.8	6.5	0.47	2.5	1580.	675.
1/06/83 (5)	20.1	6.5	0.49	2.5	1335.	730.
1/28/83 (5)	20.4	7.4	0.54	2.5	1525.	650.
1/13/83 (1)	20.4	12.5	0.89	2.5	1590.	785.
1/28/83 (6)	20.4	14.0	1.03	2.5	1570.	640.
1/14/83 (9)	18.0	18.0	1.50	2.5	1685.	755.
1/05/83 (1)	33.9	6.5	0.29	1.4	1613.	700.
1/05/83 (2)	33.8	12.5	0.55	1.4	1612.	775.
1/13/83 (2)	34.9	24.0	1.02	1.4	1690.	795.
1/13/83 (5)	33.9	23.5	1.04	1.4	1680.	795.
1/14/83 (6)	70.1	12.0	0.26	0.7	1410.	760.
1/14/83 (7)	69.5	23.5	0.51	0.7	1540.	750.
1/14/83 (8)	68.0	46.5	1.01	0.7	1645.	745.

Figure 2. Water gas reaction test summary.

	1/13/83				
Sample No.→ ↓% (Volume)	1	2	3	4	5
O_2	0.97	1.27	5.70	0.80	1.29
N_2	45.88	46.44	52.02	28.27	33.67
CO	2.94	4.35	1.74	3.62	4.52
CO_2	16.76	16.22	11.90	22.48	20.68
H_2	32.5	30.8	28.1	44.25	39.6
CH_4	tr	tr	tr	tr	tr
Total	99.1	99.1	99.5	99.4	99.8

Figure 3. Exhaust gas composition.

Quantum and Thermal Conversion of Solar Energy to Useful Work

D.H. Johnson

SERI

1.0 INTRODUCTION

This talk will summarize the results of a thermodynamic analysis of quantum and thermal processes for converting sunlight into useful work. Quantum and thermal processes acting alone as well as combined quantum thermal processes will be discussed. Two types of combined processes have been analyzed, the thermally coupled process and the thermally decoupled process. These processes were addressed because there is a hope that a combined quantum thermal conversion system will prove to be cheaper than either system acting separately. A first step in determining cost is to determine maximum system efficiency. The analysis also indicates the concept with the greatest potential so that further efforts can focus on it. Previous analysis of the thermodynamics of quantum and thermal conversion have been performed by Haught (Ref. 1), Bolton (Ref. 2), Ross (Ref. 3), and others. This talk will review Haught's analysis and present the results of an extension of this analysis to a thermally decoupled combined quantum thermal system performed at SERI. Only systems using unconcentrated solar flux will be considered in the present analysis.

2.0 THERMAL CONVERSION

Figure 1 is a schematic of a thermal conversion system. Incident radiation is absorbed in a receiver operating at temperature T_T. The receiver is assumed to be perfectly insulated against convective and conductive losses. Some of the absorbed radiation is reradiated to the environment. The rest is converted to heat at temperature T_T. A heat engine converts some of this heat to useful work and rejects the rest to a heat reservoir at the ambient temperature.

We will assume here and in the rest of this talk that the incident radiation is composed of radiation from the sun and from the ambient environment. We will also assume that all sources of radient energy are black bodies characterized by their temperature. Thus, the intensity of photons from the sun $I_{\underset{\sim}{s}}(\nu)$ as a function of frequency ν is

$$I_s(\nu) = \frac{2\pi n^2 \nu^2}{c^2}\left[e^{-\frac{h\nu}{kT_s}} - 1\right]^{-1}\left(\frac{R_s}{R_{EO}}\right)^2 \qquad (1)$$

where n is the index of refraction (I assume n = 1), c is the speed of light

($3.00 \times 10^8 ms^{-1}$), h is Planck's constant (6.63×10^{-30} Js), k is Boltzman's constant (1.38×10^{23} JK^{-1}), R_s is the radius of the sun (6.95×10^8 m), R_{EO} is the radius of the earth's orbit (1.49×10^{11} m), and T_s is the temperature of the sun (6000K). The factor $(R_s/R_{EO})^2$ is the solid angle subtended by the sun and represents the fraction of the radient energy emitted by the sun which is incident on the receiver. Similarly, the intensity of photons from the ambient environment $I_A(\nu)$ is

$$I_A(\nu) = \frac{2\pi n^2 \nu^2}{c^2}\left[e^{-\frac{h\nu}{kT_A}} - 1\right]^{-1}\left[1 - \left(\frac{R_s}{R_{EO}}\right)^2\right] \tag{2}$$

where T_A is the ambient temperature (300K) and the factor $[1 - (R_s/R_{EO})^2]$ accounts for the blocking of the environment by the sun. the intensity of light reradiated from the receiver is

$$I(\nu, T_T) = \frac{2\pi n^2 \nu^2}{c^2}\left[e^{-\frac{h\nu}{kT_T}} - 1\right]^{-1}. \tag{3}$$

We will assume that the heat engine absorbs heat from a reservoir at temperature T_T (the receiver), rejects heat to a reservoir at temperature T_A (the ambient environment) and converts the difference into work with a Carnot efficiency given by $(1-T_A/T_T)$.

The efficiency of the thermal conversion process is then given by

$$\eta_T = \frac{\int_0^\infty \left[I_S(\nu) + I_A(\nu) - I(\nu, T_T)\right] h\nu \left(1 - \frac{T_A}{T_T}\right) \sigma(\nu, T_T)\, d\nu}{\int_0^\infty I_S(\nu)\, h\nu\, d\nu} \tag{4}$$

where the factor in brackets represents the number of photons absorbed per unit area of the receiver, $h\nu$ is the energy per photon of frequency ν, $(1-T_A/T_T)$ is the Carnot efficiency of conversion of thermal energy to work, and $\sigma(\nu, T_T)$ is the absorptivity of the receiver.

According to the principle of detailed balancing the absorptivity equals the emissivity. Since the spectrum of incident photons from the sun is peaked at much higher frequency than the spectrum of the photons emitted from the receiver, conversion efficiency will be improved by choosing an absorptivity that is large at high frequencies and small at low frequencies. We will consider a step function absorptivity such that

$$\sigma(\nu, T_T) = \begin{cases} 0 & \nu < \nu_T(T_T) \\ 1 & \nu > \nu_T(T_T) \end{cases} \tag{5}$$

The conversion efficiency is a function of T_T and ν_T. The temperature

which produces the maximum conversion efficiency for each ν_T is plotted as a function of ν_T in Figure 2. The conversion efficiency produced by using the optimum temperature for each ν_T is also plotted as a function of ν_T in Figure 2. The maximum possible conversion efficiency is 54% and occurs at a temperature of 862K and an absorption cut off of $2.22 \times 10^{14} s^{-1}$ (a wavelength λ of 1.35×10^{-6} m). Notice that the optimum temperature is essentially proportional to the absorption cut-off frequency except near $\nu_T = 0$ where $T_T \approx$ 400K.

3.0 QUANTUM CONVERSION

Figure 3 is a schematic of a quantum conversion system. The entire system is perfectly insulated against conductive and convective heat loss and operates at temperature T_Q. The receiver absorbs incident radiation, some of which is reradiated to the environment. However, the absorption process is different than in the thermal case. Instead of being completely converted to heat, a portion μ of the energy of each absorbed photon is converted to the available energy of an excited state with the remaining energy dissipated as heat at the temperature T_Q. The population of the excited state is not in equilibrium with the receiver at temperature T_Q. It can be thought of as the population which would exist in equilibrium with its surroundings at a higher temperature. The population of the excited state is separated from the surrounding unexcited material (and possibly stored for a time). A quantum engine then converts the population of the excited state to unexcited material, recovering the available energy μ as useful work in the process. Notice that the separation step is unavoidable. If this step were not performed independently, the process of converting the population of the excited state to unexcited material in the presence of material which was never excited would effectively result in separating the population of the excited state from that material.

The intensity of photons incident from the sun and the ambient environment is as discussed in the preceeding section. The requirement that the quantum receiver, which converts $(h\nu - \mu)$ of the energy of each absorbed photon to heat at temperature T_Q, be in equilibrium with the radiation which it emits, leads to the following intensity of light emitted from the receiver.

$$I(\nu,\mu,T_Q) = \frac{2\pi n^2 \nu^2}{c^2}\left[e^{\frac{-(h\nu-\mu)}{kT_Q}} - 1\right]^{-1} \tag{6}$$

We will assume that the quantum engine converts all of the available energy of the excited state into useful work.

The efficiency of the quantum conversion process is then given by

$$\eta_Q = \frac{\int_0^\infty [I_S(\nu) + I_A(\nu) - I(\nu,\mu,T_Q)]\,\mu\,\sigma(\nu,\mu,T_Q)\,d\nu}{\int_0^\infty I_S(\nu)\,h\nu\,d\nu} \tag{7}$$

where, as before, the factor in brackets represents the number of photons absorbed per unit area of the receiver, μ is the portion of the energy of each absorbed photon converted to available energy of the excited state, and $\sigma(\nu,\mu,T_Q)$ is the absorptivity of the receiver. The absorptivity of the quantum receiver is determined by the quantum process. We will assume a single photon excitation process characterized by a threshold frequency below which absorption and excitation of the medium does not occur. In this case,

$$\sigma(\nu,\mu,T_Q) = \begin{cases} 0 & \nu < \nu_Q(\mu,T_Q) \\ 1 & \nu > \nu_Q(\mu,T_Q) \end{cases} \qquad (8)$$

Notice that to have a finite emission spectrum, the threshold for emission must always be less than the threshold for absorption $h\nu_Q$. The difference between $h\nu_Q$ and μ is the heat of mixing, released during separation of the population of the excited state from the unexcited states. The fact that μ is less than $h\nu_Q$ is required by the second law of thermodynamics and in that sense, μ plays the same role as the Carnot efficiency of a heat engine.

The conversion efficiency is a function of μ, T_Q, and ν_Q. By inspection of equation 7, it is obvious that the maximum quantum conversion efficiency occurs at the lowest possible temperature of the receiver, which is the ambient temperature T_A. Henceforth, we will assume that for a pure quantum conversion system $T_Q = T_A$. If we find the available energy which maximizes the conversion efficiency for a given threshold frequency ν_Q and then do this again for a range of ν_Q we get the results shown in Figure 3. The maximum possible conversion efficiency is 31% and occurs at an available energy of 1.5×10^{-12} erg and a threshold frequency of 3.16×10^{14} S^{-1} ($\lambda = 9.5 \times 10^{-7}$ m). Also, notice that the optimum μ is approximately proportional to ν_Q and that at $\nu_Q = 0$, the optimum μ is zero.

4.0 THERMALLY COUPLED QUANTUM - THERMAL CONVERSION

Figure 5 is a schematic of a thermally coupled combined quantum-thermal conversion system. A receiver operating at a temperature T_Q absorbs incident radiation and converts a portion μ of the energy of each absorbed photon to the available energy of an excited state. The remaining energy ($h\nu - \mu$) is rejected as waste heat at the temperature of the quantum converter T_Q. This waste heat is used as the input to a bottoming thermal cycle.

The incident radiation spectrum is the same as previously discussed and the emitted radiation spectrum is the same as for a quantum system. The quantum engine converts all of the available energy μ into useful work while the heat engine converts the remaining energy ($h\nu - \mu$) of each photon into useful work with the Carnot efficiency $(1 - T_A/T_Q)$.

The efficiency of the thermally coupled combined quantum-thermal conversion process is given by

$$\eta_{Q-T} = \frac{\int_0^\infty [I_S(\nu) + I_A(\nu) - I(\nu,\mu,T_Q)]\left[\mu + (h\nu - \mu\chi)\left(1 - \frac{T_A}{T_Q}\right)\right]\sigma(\nu,\mu,T_Q)\,d\nu}{\int_0^\infty I_S(\nu)\, h\nu\, d\nu} \quad (9)$$

where all the symbols have been previously defined and $\sigma(\nu,\mu,T_Q)$ is, as before, the absorptivity of the receiver. We will assume, as previously, that

$$\sigma(\nu,\mu,T_Q) = \begin{cases} 0 & \nu < \nu_Q(\mu,T_Q) \\ 1 & \nu > \nu_Q(\mu,T_Q) \end{cases} \quad (10)$$

where ν_Q is, again, the threshold frequency below which absorption and excitation of the quantum process does not occur.

The conversion efficiency is a function of μ, T_Q, and ν_Q. Because of the appearance of T_Q in the Carnot efficiency factor as well as the emitted radiation spectrum, the maximum efficiency will not in general occur at $T_Q = T_A$. If we find the available energy which maximizes the efficiency for a given ν_Q and T_Q and then plot contours of the efficiency for this value of μ versus ν_Q and T_Q, we get the results shown in Figure 6. The curve which runs from the lower left hand side of the figure to the upper right hand side represents the conditions for which $\mu = 0$. Along this curve, the quantum part of the system produces no useful work and the combined system is equivalent to a pure thermal system. Efficiency and corresponding temperature plotted versus threshold frequency along this curve would reproduce Figure 2. Below this curve μ would be less than zero, implying that the system was supplying energy to the incident radiation. Along the vertical axis at $T_Q = 300K = T_A$, the Carnot efficiency of the thermal conversion part of the system is zero and the combined system is equivalent to a pure quantum system. Efficiency and available energy plotted versus threshold frequency along the vertical axis would reproduce Figure 4. The region between the vertical axis and the curve $\mu = 0$ represents combinations of ν_Q and T_Q for which the system has both a quantum and a thermal part. It is instructive to explore further optimization of the system along two paths in this region. If we find the temperature which maximizes the efficiency for a given ν_Q, then we will trace out the lower portion of the $\mu = 0$ curve. This approach to optimization leads to a pure thermal system. If we find the threshold frequency which maximizes the efficiency for a given T_Q, then we trace out the dashed curve in Figure 6. This approach to optimization leads to systems with both a quantum and a thermal conversion part.

If we plot overall system efficiency η_{Q-T} and the individual contributions to overall efficiency of the quantum part η_Q and the thermal part η_T versus T_Q along this dashed curve, we get the results presented in Figure 7. The overall system efficiency increases from that of a pure quantum system at $T_Q = 300K$ ($\eta_{Q-T} = \eta_T = 0.31$) to that of a pure thermal system at $T_Q = 862K$ ($\eta_{Q-T} = \eta_T = 0.54$). The contribution of the quantum part of the system to overall efficiency decreases monotonically from 0.31 at $T_Q = 300K$ to zero at

T_Q = 862K while that of the thermal part increases from zero at 300K to 0.54 at 862K. The quantum and thermal parts make equal contribution to overall efficiency at T_Q = 450K where each is 21%.

5.0 THERMALLY DECOUPLED QUANTUM/THERMAL CONVERSION

Figure 8 is a schematic of a thermally decoupled combined quantum thermal conversion system. The spectrum of incident radiation is split into a low frequency part and a high frequency part by a dichroic beam splitter (alternatively, the quantum process, which absorbs high frequencies but passes low frequencies, could be placed in front of the thermal process). The high frequency part of the incident spectrum is directed to a quantum receiver operating at temperature T_Q while the low frequency part is directed to a thermal receiver operating at a temperature T_T. The quantum and thermal parts of the system then each operate upon their part of the spectrum as previously described.

The efficiency of the thermally decoupled combined quantum/thermal conversion process is given by

$$\eta_{Q/T} = \left\{ \int_0^\infty [I_S(\nu) + I_A(\nu) - I_Q(\nu,\mu,T_Q)]\mu\sigma_{DBS}(\nu,\mu,T_Q,T_T)d\nu + \int_0^\infty [I_S(\nu) + I_A(\nu) - I_T(\nu,T_T)]h\nu\left(1 - \frac{T_A}{T_T}\right)[1 - \sigma_{DBS}(\nu,\mu,T_Q,T_T)]\sigma_T(\nu,T_T)d\nu \right\} \Big/ \int_0^\infty [I_S(\nu)h\nu \quad (11)$$

where $\sigma_{DBS}(\nu,\mu,T_Q,T_T)$ is the transmissivity of the dichroic beam splitter which is chosen to match the absorptivity of the quantum process. As before, we will assume that

$$\sigma_{DBS}(\nu,\mu,T_Q,T_T) = \begin{cases} 0 & \nu < \nu_Q(\mu,T_Q,T_T) \\ 1 & \nu > \nu_Q(\mu,T_Q,T_T) \end{cases} \quad (12)$$

where ν_Q is the excitation threshold of the quantum system. The absorptivity of the thermal receiver is given by σ_T. For the reasons discussed in section 2, it is desirable to not absorb very low frequencies in the thermal receiver. We will assume that

$$\sigma_T(\nu,T_T) = \begin{cases} 0 & \nu > \nu_T(T_T) \\ 1 & \nu < \nu_T(T_T) \end{cases} \quad (13)$$

In equation 11 I_Q is the spectrum of light emitted from the quantum receiver as given by Equation 6 and I_T is that emitted from the thermal receiver as given by Equation 3. All other terms have been defined previously.

The efficiency of the thermally decoupled combined quantum/thermal conversion system is a function of μ, T_Q, T_T, ν_Q and ν_T. Inspection of equation 11 shows that the maximum system efficiency occurs at the lowest possible temperature of the quantum receiver which is the ambient temperature. We will assume in the following that $T_Q = T_A$. If we now examine maximizing the overall conversion efficiency with respect to the remaining parameters, we find that the conditions on μ which result in maximizing $\eta_{Q/T}$ for a given ν_Q, T_T, and ν_T are the same as for a pure quantum system (the optimum μ is a function only of ν_Q and is that given in Figure 4). Similarly, the conditions on ν_T which result in maximizing $\eta_{Q/T}$ for a given ν_Q, T_T, and μ are the same as for a pure thermal system (the optimum ν_T is a function only of T_T and is that given in Figure 2).

If we now use these optimum values of μ as a function of ν_Q and ν_T as a function of ~~and~~ T_T, we get the results shown in Figure 9. The curve which runs from the lower left hand portion of the figure to the upper right hand represents the case where $\nu_T = \nu_Q$ and $\mu = 0$. Along this curve, both the thermal and the quantum parts of the system have zero conversion efficiency. Below this curve ν_T would be greater than ν_Q and the thermal part of the system would not work. Also, below this curve μ would be less than zero and the quantum part of the system would be supplying energy to the incident radiation. Along the vertical axis at $T_T = 300K = T_A$, the Carnot conversion efficiency of the thermal conversion part of the system is zero and the combined system is equivalent to a pure quantum system. Efficiency and available energy plotted versus threshold frequency along the vertical axis would reproduce Figure 4. The region between the vertical axis and the $\nu_Q = \nu_T, \mu = 0$ curve represents combinations of ν_Q and T_T for which the system has both a quantum and a thermal part. It is instructive to explore further optimization of the system along two paths in this region. If we find the temperature which maximizes the efficiency for a given ν_Q, then we will trace out the dotted line in Figure 9. If we find the threshold frequency which maximizes the efficiency for a given T_T, then we will trace out the dashed curve in Figure 9. Along both these curves, the system has both a quantum and a thermal part.

Consider the behavior of the system along the curve of optimum temperature (the dotted curve of Figure 9) as shown in Figure 10. The overall system efficiency increases along this curve from zero at $T_T = 300K$, $\nu_Q = 0\ s^{-1}$ to 54.7% at $T_T = 834K$, $\nu_Q = 7.83 \times 10^{14}\ s^{-1}$ ($\lambda = 3.8 \times 10^{-7}$ m). This is a higher conversion efficiency then that achieved by either a quantum or a thermal system along, or by a thermally coupled combined quantum/thermal system. The contribution of the thermal part of the system increases along this curve from zero at $T_T = 300K$ to 46.3% at T = 834K, the temperature of each system efficiency. The contribution of the quantum part of the system first increases from zero at $T_T = 300K$, $\nu_Q = 0\ s^{-1}$ to a peak of 31% at $T_T = 625K$, $\nu_Q = 3.16 \times 10^{14}\ s^{-1}$ ($\lambda = 9.52 \times 10^{-7}$ m) and then decreases, but still contributes 8.4% at $T_T = 834K$, the temperature of peak system efficiency. The quantum and thermal parts make equal contributions at $T_T = 700K$ where each is 26%.

Now consider the behavior of the system along the curve of optimum threshold frequency (the dashed curve in Figure 9) as shown in Figure 11. This curve is analogous to the dashed curve in Figure 7 for a thermally coupled system. The overall system efficiency increases along this curve from that of a pure

quantum system at T_T = 300K ($\eta_{Q/T}$ = 31%) to a peak of 54.7% at T_T = 834K and $\nu_Q = 7.83 \times 10^{14}$ s^{-1} ($\lambda = 3.8 \times 10^{-7}$ m). This is, of course, the same maximum system efficiency reached along the path of optimum T_T discussed in the preceeding paragraph. The contribution of the thermal part of the system along this curve first increases from zero at T_T = 300K until it reaches 46.3% at T_T = 834K, the temperature of peak system efficiency, and continues to increase until it reaches 51.5% at T_T = 858K, $\nu_Q = 10^{10}$ s^{-1} ($\lambda = 3 \times 10^{-8}$ m). After this, it decreases monotonically to zero at high temperature. The contribution of the quantum part decreases monotonically from an efficiency of 31% at T_T = 300K to zero at high temperature. However, as discussed before, the quantum part contributes 8.3% at the conditions of maximum system efficiency.

6.0 CONCLUSIONS AND RECOMMENDATIONS

For a pure quantum system compared to a pure thermal system, optimum thermal conversion is more efficient (by a factor of 1.74) then optimum quantum conversion. This is largely because only a fixed portion of each photon absorbed by the quantum process is available to do work. The rest is immediately thermalized and rejected as waste heat. In a thermal process, the full energy of each photon is available for conversion to useful work with Carnot efficiency. On the other hand, optimum thermal conversion occurs at high temperature (T_T = 862K). Since costs generally increase with temperature, it may be that a quantum conversion system will be cheaper than a thermal conversion system inspite of its lower efficiency.

For a thermally coupled combined quantum-thermal conversion system, the peak efficiency of 54% occurs at T_Q = 862K, $\nu_Q = 2.22 \times 10^{14}$ s^{-1} ($\lambda = 1.35 \times 10^{-7}$ m), $\mu = 0$. Under these conditions, the contribution of the quantum part of the system is zero. From an efficiency point of view, thermally coupling quantum and thermal conversion processes does not favor quantum conversion. However, since costs generally increase with temperature, the cheapest system may operate at a temperature below that of maximum system efficiency. At temperatures between 300K and 862K, the thermally coupled combined system has a higher efficiency than either a pure quantum system or a pure thermal system operating alone and may be cheaper than either operating alone.

However, the thermally coupled system severely penalizes the quantum component because the thermal component has a higher peak efficiency achieved at high temperature where the quantum component has a very low efficiency. One manifestation of the penalties thermal coupling imposes on the quantum component is demonstrated by the latitude one has in choosing system parameters without greatly effecting overall efficiency. In Figure 6, the parameter which most directly effects the quantum component is ν_Q, displayed along the vertical axis, while the parameter which most directly effects the thermal component is T_Q, displayed along the horizontal axis. The contours of constant overall system efficiency are generally parallel to the horizontal axis, i.e., T_Q can be varied over a considerable range without appreciably effecting overall system efficiency, while a small variation in ν_Q usually has a much stronger effect on overall system efficiency.

For a thermally decoupled combined quantum thermal conversion system, the

peak efficiency is greater (54.7% versus 54%) and occurs at a lower temperature (834K versus 862K), then the thermally coupled system. At peak system efficiency, the thermal part contributes 46.3% and the quantum part contributes 8.3%, unlike the thermally coupled system for which the quantum component contributes nothing under conditions of peak efficiency. The value of ν_0 under conditions of peak efficiency is 7.83×10^{14} s^{-1} (λ = 3.8×10^{-7} m). This is in the near ultraviolet. In other words, thermodynamics requires that this system portions the ultraviolet light to the quantum conversion part and the rest of the solar spectrum to the thermal conversion part. It happens that real quantum conversion processes often have excitation thresholds in the ultravoilet, while ultraviolet light is usually considered harmful to the components of a real thermal system (i.e., ultraviolet light causes devitrification of quartz, a material otherwise well suited for the window of a high temperature receiver).

The points just discussed demonstrate that the thermally decoupled system is much kinder to the quantum component than the thermally coupled system. This is because the thermally decoupled system allows the quantum component to operate at ambient temperature. This is further illustrated by the latitude one has in choosing system parameters without greatly effecting overall efficiency. In Figure 9, the parameter which most directly effects the quantum component is ν_0, displayed along the vertical axis, while the parameter which most directly effects the thermal component is T_T, displayed along the horizontal axis. The contours of constant system efficiency generally lie parallel to the vertical axis, i.e., ν_0 can be varied over a considerable range without appreciably effecting overall system efficiency, while a small variation in T_T has a much stronger effect on overall system efficiency. Since the temperature of the thermal conversion part of the system can be controlled by the rate of heat transfer while the excitation threshold of the quantum system is not so readily controlled, this aspect of the thermally decoupled system has important practical implications.

Another indication of the greater role the quantum component plays in a thermally decoupled system than in a thermally coupled system is seen by considering the conditions under which the quantum and thermal part contribute equally to the overall system efficiency of each type of system. This occurs for a thermally coupled system at T_0 = 150K where each part contributes 21% and for a thermally decoupled system (along the path of optimum temperature) at T_T = 700K where each contributes 26%.

It is clear from the above discussion that the thermally decoupled combined quantum/thermal conversion system has considerable potential. However, there is still a large degree of uncertainty about the best operational conditions for the system and about its competitive position relative to the other types of systems. One important operational factor not yet considered is the effect of concentrating the incident sunlight. It is known that concentrating the incident sunlight, with other system parameters fixed, improves the performance of pure quantum and pure thermal conversion systems. As the concentration is increased, heat must be transferred out of the system at an increasing rate to keep temperature constant. In a thermally decoupled system, the quantum part is operating near ambient temperature while the thermal part is operating at high temperature. Thus, it will be harder to transfer heat out of the quantum part than out of the thermal part. This means that the optimum operating conditions may call for

a different degree of concentration for the two parts. Other operational factors which determine system configuration also need to be examined. Guided by this analysis a concept for a practical system should be developed. This concept should include all factors of importance to a real system such as the actual quantum process to be used, the limitations of real dichroic beam splitters, the actual thermal process to be used, etc. Finally, the concept should be laid out in enough detail to estimate cost and this cost should be compared to the cost of competitive systems.

7.0 REFERENCES

1. Haught, A.F., 1984, "Physics Considerations of Solar Energy Conversion," to be published in the ASME Trans., Journal of Solar Energy Engineering.

2. Bolton, J.R., 1978, "Solar Fuels," Science 202, No. 4359, 705.

3. Ross, R.T. and T.L. Hsiao, 1979, "Limits on the Yield of Photochemical Solar Energy Conversion," J. Appl. Phys., 48, No. 11, 4783.

Thermal System

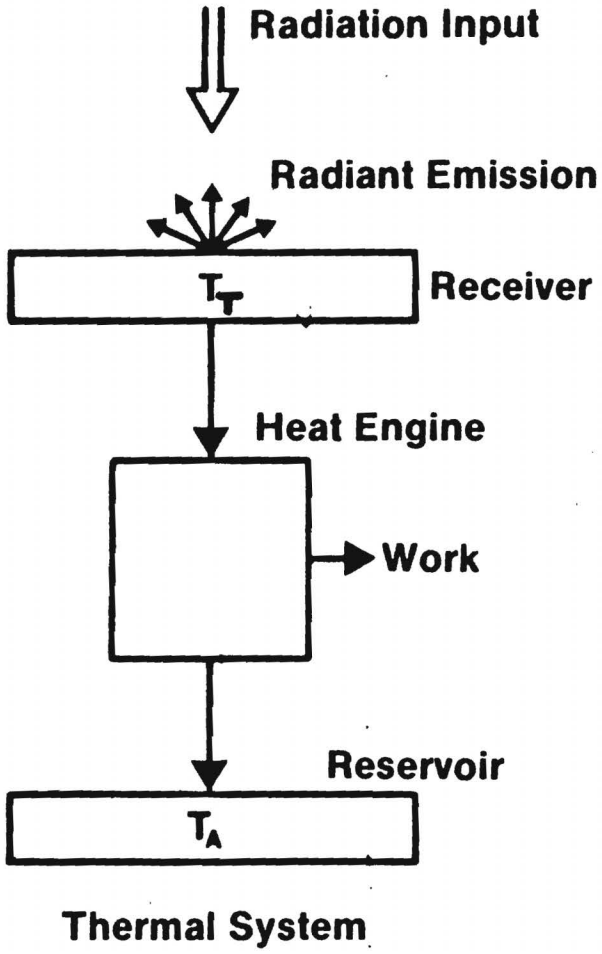

FIG. 1

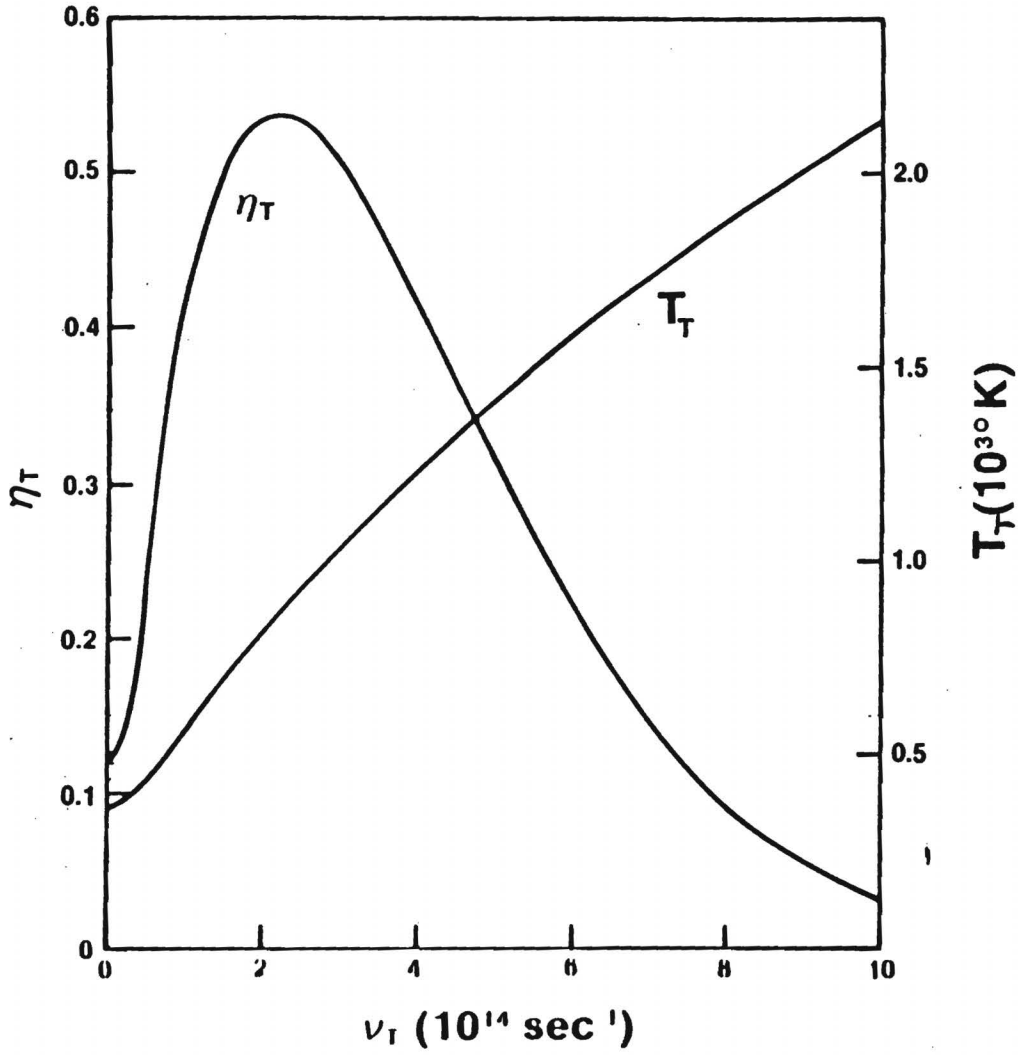

FIG. 2

From: Physics Considerations of Solar Energy Conversion by Alan Haught, United Technologies

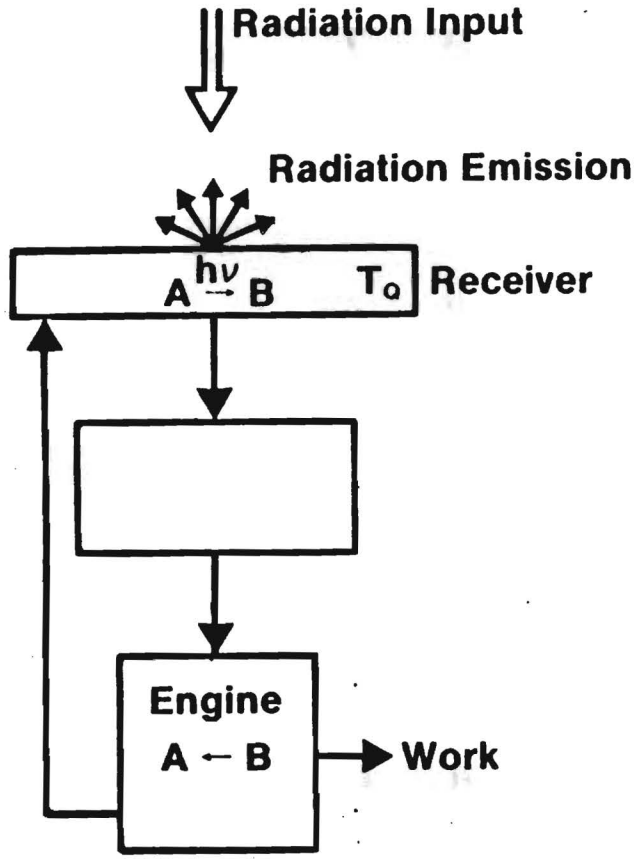

Quantum System

Conversion Efficiency for Quantum System

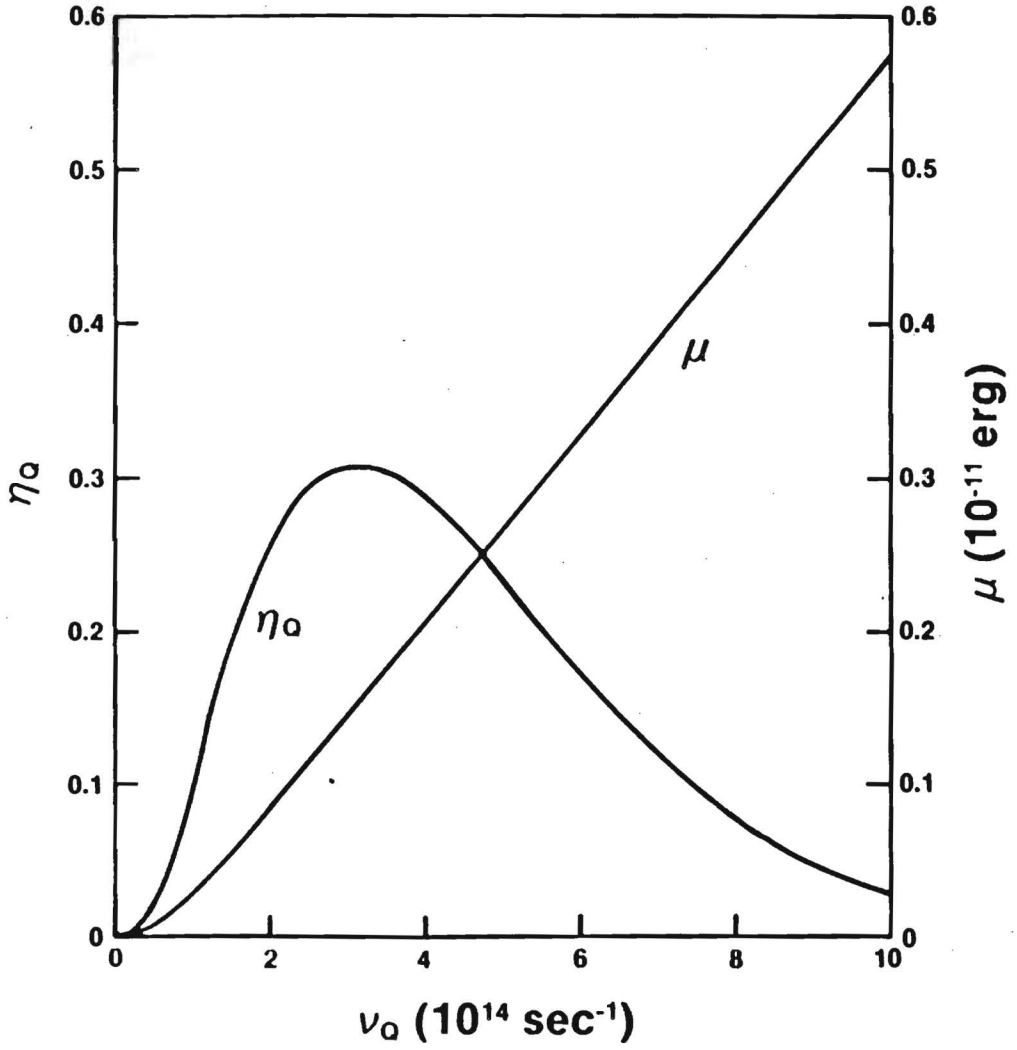

FIG. 3

Quantum/Thermal Conversion

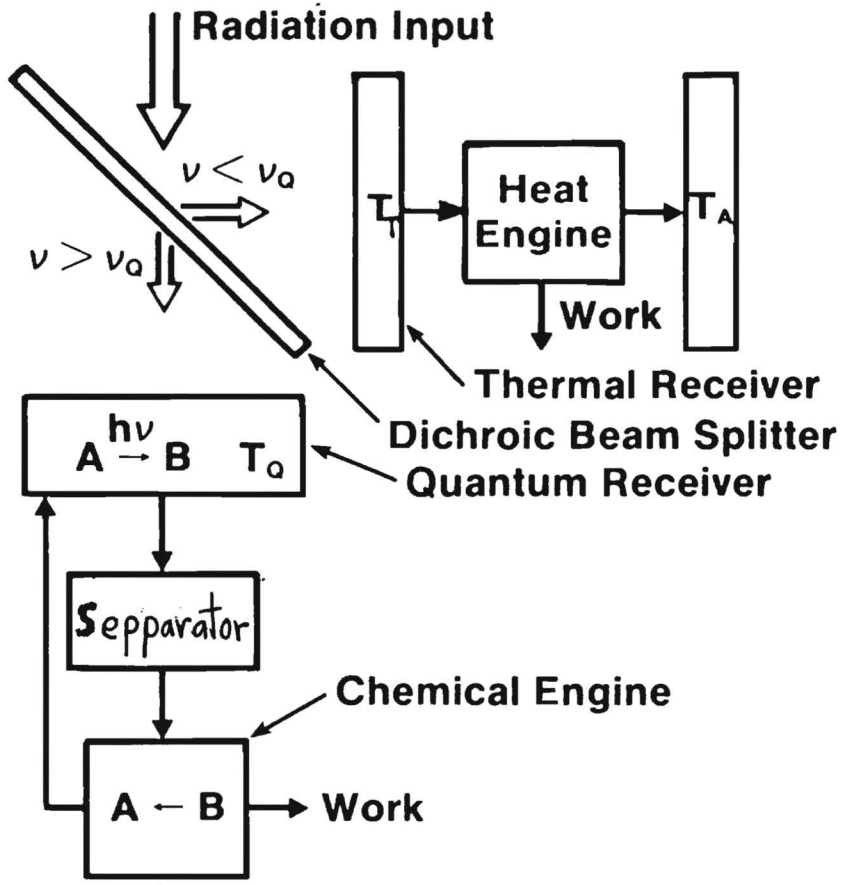

FIG. 5

Conversion Efficiency for Thermally Coupled Combined Quantum/Thermal System

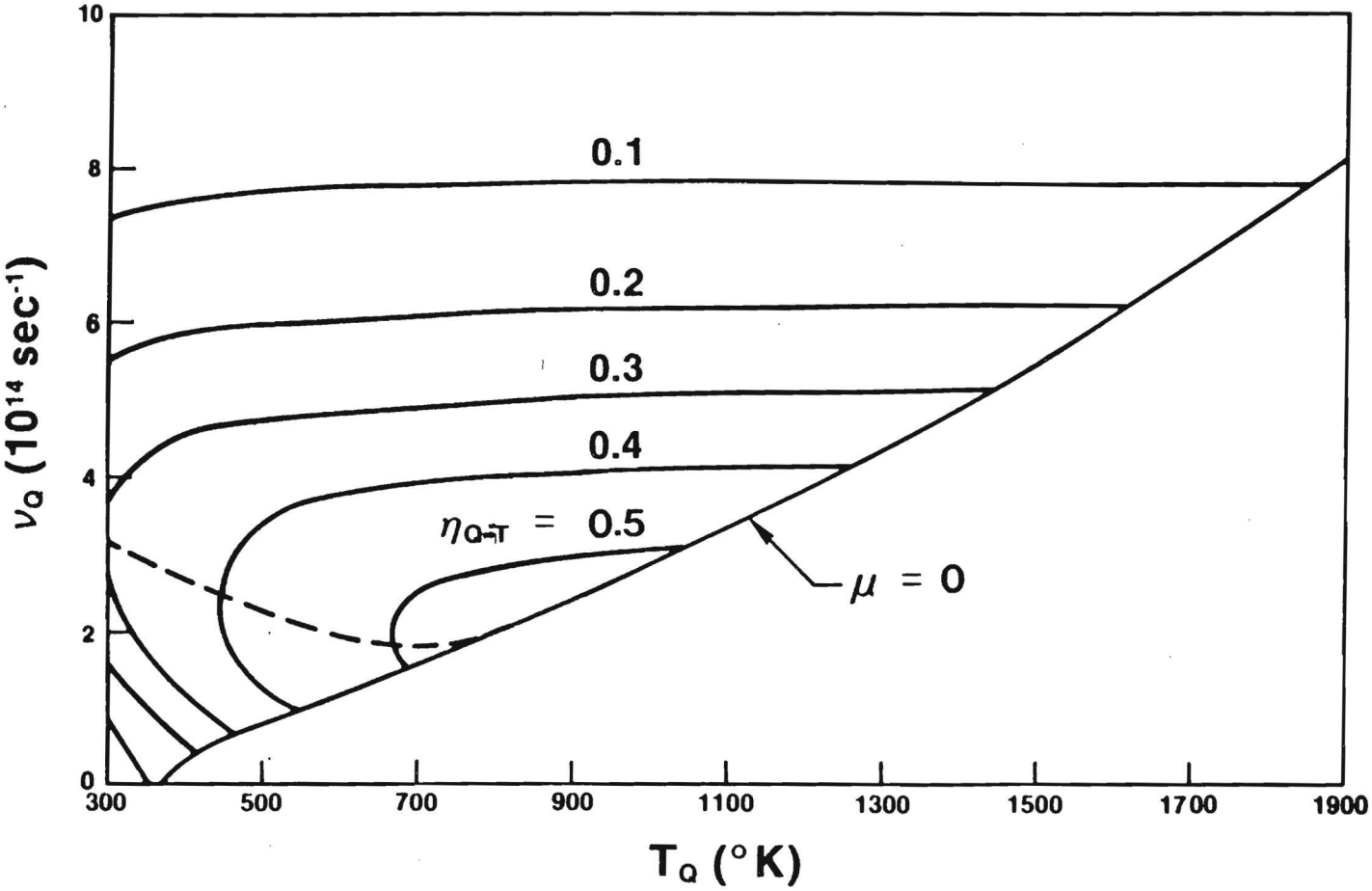

From: Physics Considerations of Solar Energy Conversion by Alan Haught, United Technologies

Thermal Conversion for Thermally Coupled Combined System

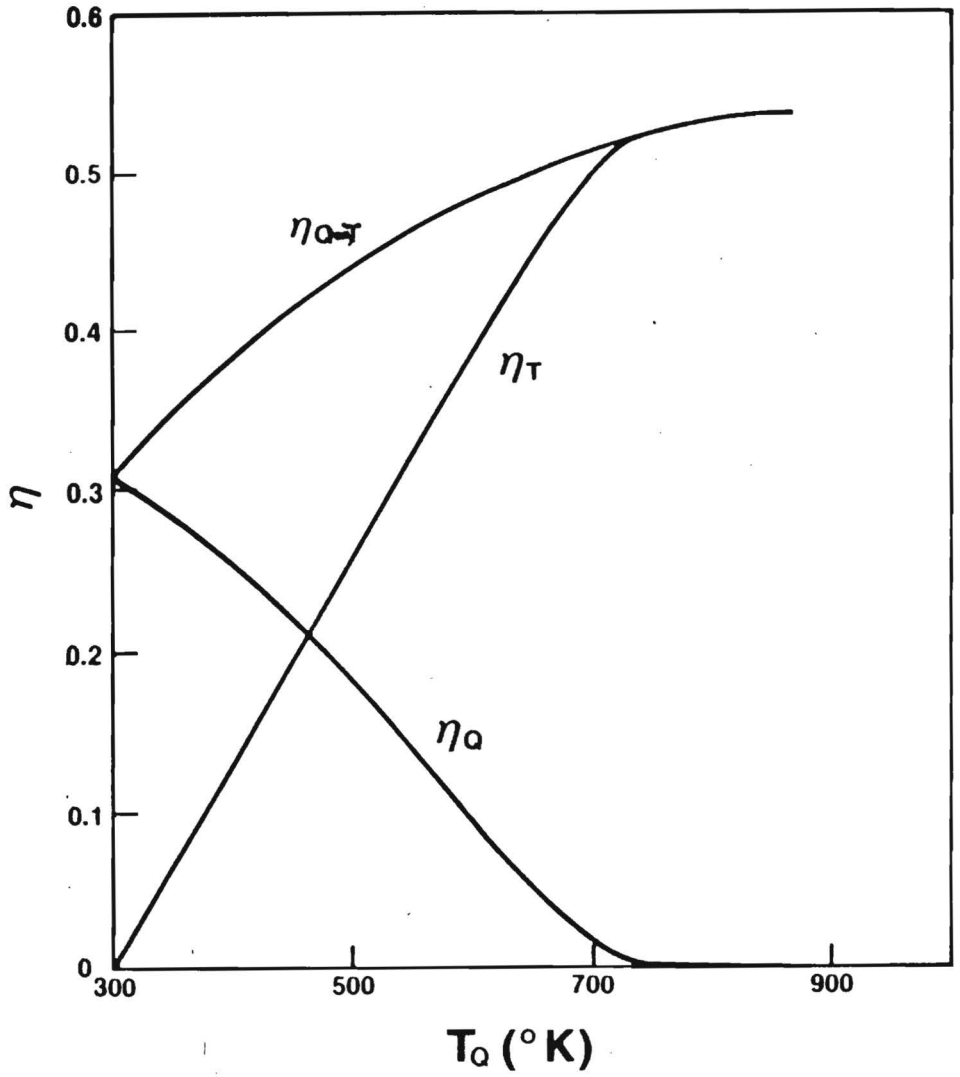

From: Physics Considerations of Solar Energy Conversion by Alan Haught, United Technologies

FIG. 7

Thermally Coupled Combined Quantum Thermal Conversion

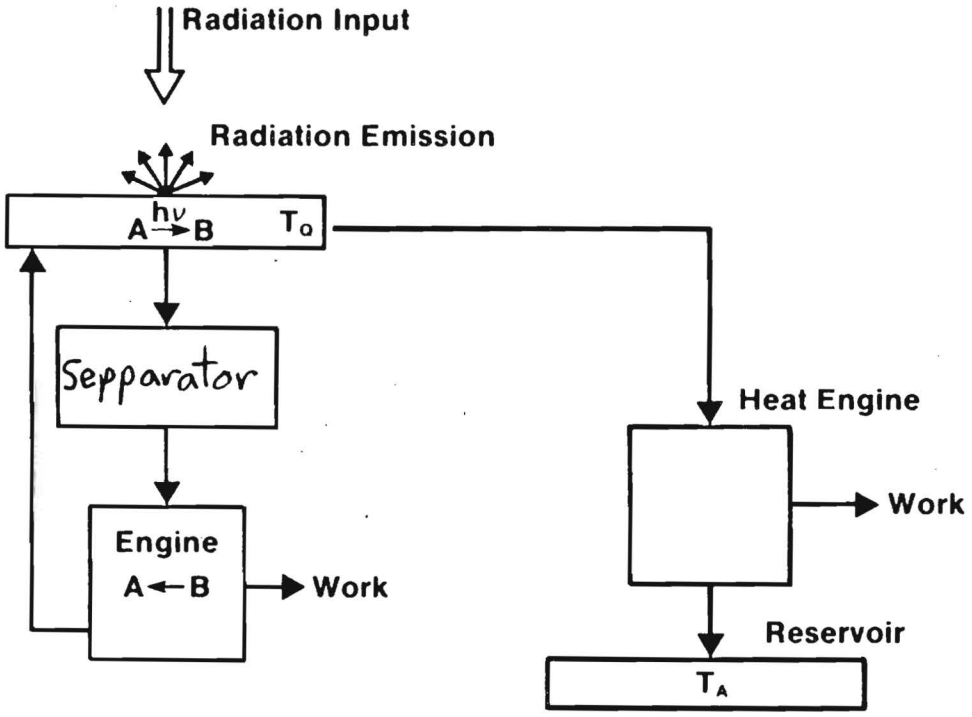

FIG. 8

Thermally Decoupled Combined Quantum/Thermal System

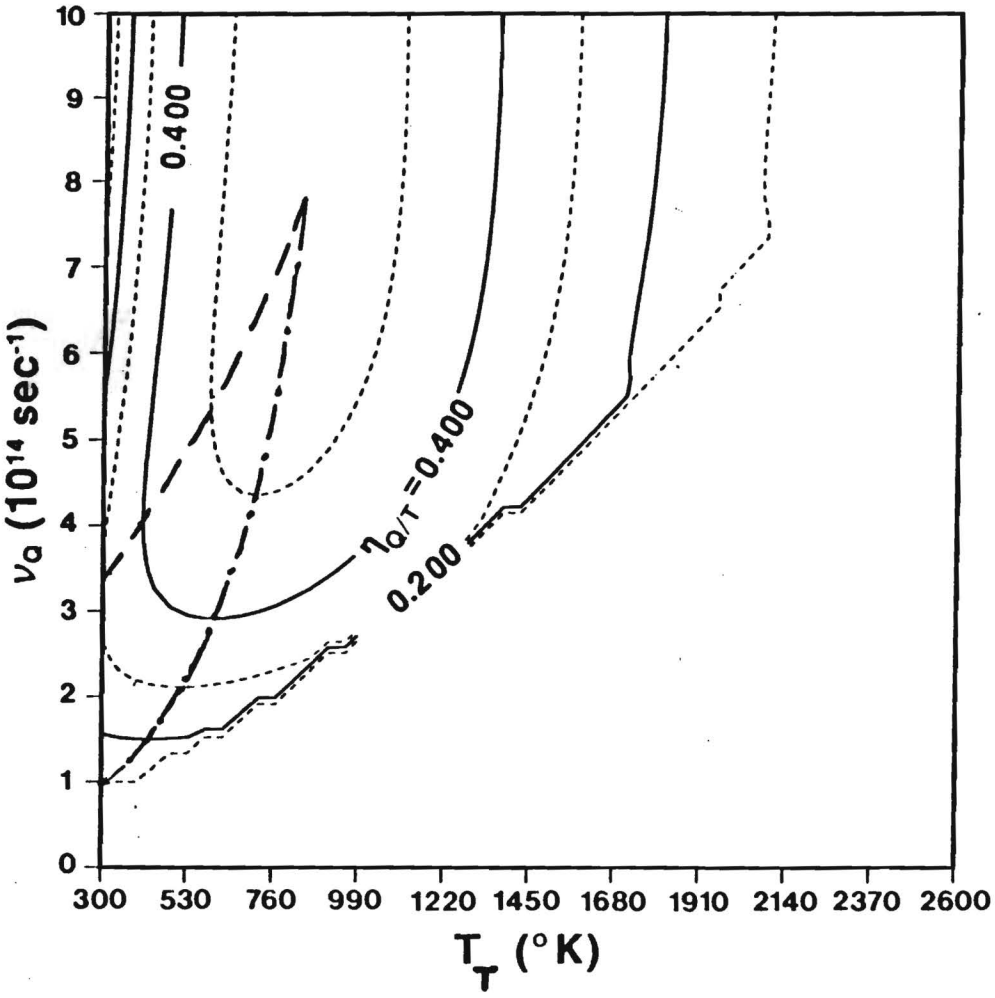

FIG. 9

Split Between Quantum and Thermal Conversion for a Thermally Decouple Combined System

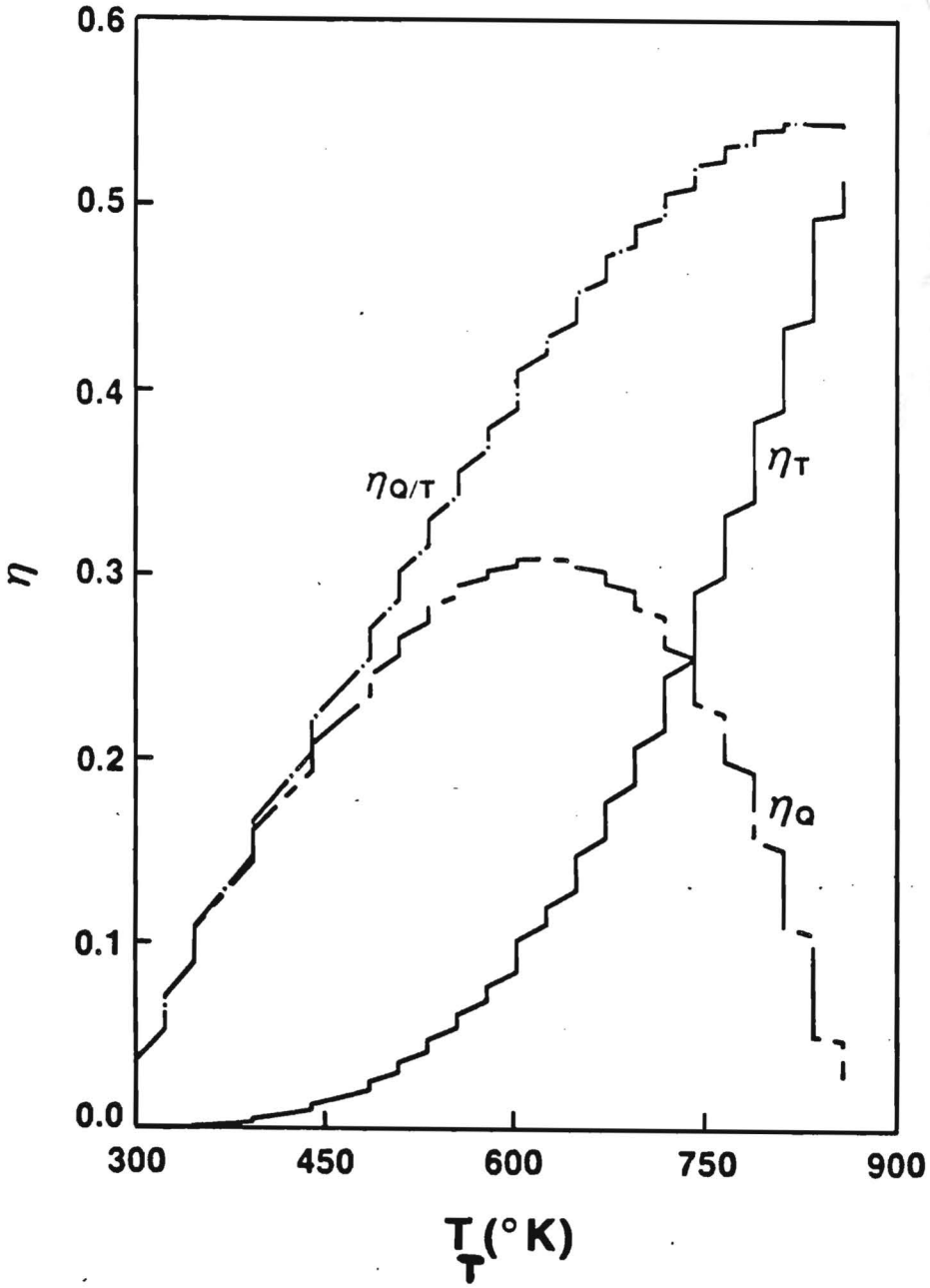

FIG. 10

POLYMERIC GLAZINGS

Paul Schissel
Solar Energy Research Institute
Golden, Colorado

Polymeric glazings are used as coatings to protect silver mirrors and as free-standing films to protect other solar system elements. Experiments are in progress to evaluate and improve films for these applications.

Introduction

Polymer-glazed mirrors may provide lower-cost alternatives to current glass mirror designs. The glass mirror fields account for about half of the cost of a central receiver power system, and it is estimated that central receiver system costs need to be halved to be economically viable. Polymer-coated aluminum mirrors have been used in field tests that indicate life spans of at least several years. The (solar-weighted) reflectance of aluminum mirrors is limited to about 85% by the aluminum, while polymer-coated silver mirrors can have reflectances of 96%. System studies suggest that the difference in reflectances can have an important cost impact that probably will exclude the use of aluminum. Polymer-protected silver mirrors that can withstand outdoor use with sufficient lifespans are not yet developed. This study was undertaken to evaluate polymer-coated silver mirrors with reflectances greater than 90% that can approach a lifespan of five years.

Results

Evaluation of silver mirrors has been initiated and is continuing, using real-time outdoor screening tests along with accelerated weathering devices

(Weather-Ometer* and QUV**). Mechanistic studies of degradation processes also in progress [1,2]. The experimental approach is multifaceted. Met lized films currently available from industrial sources are tested, c mercially available polymeric films are silvered and tested, and polyme films are formed (solution cast or plasma polymerized) onto silver fil which are deposited on a glass substrate for testing.

The metallized films from industrial sources are identified in Table 1 (ser 107, 207, 507, 407). The first film (FEK 244) is the only aluminized f documented in this study. It is used as a standard comparison mater because long-term outdoor data for FEK 244 exist. The solar-weighted, he spherical reflectances are listed before degradative exposure, after f weeks exposure in the Weather-Ometer, and, for other samples, after six-we outdoor exposure. Similarly, values are listed for the coated sil mirrors: polycarbonate (PC), acrylic/polyester (YS94), and Teflon (FE Polycarbonate mirrors discolored significantly, and their testing was c continued. The other materials are essentially unchanged during th initial, short-term tests. As noted earlier, the reflectance of alumin mirrors is limited to about 85% while silver mirrors yield about 95%. materials of Table 1 are being supplemented by other commercial polyme films [Teflon, polymethylmethacrylate (PMMA), polyacrylonitrile (PAN)] t are silvered using vacuum sputtering and then coated with a protective bac (sputtered aluminum or Inconel, FEK 244, Scotch tape, PMMA, PAN).

Empirical evidence has shown that PMMA is stable during long-term out exposure [3] and the field experience with FEK 244 demonstrates that PMMA protect aluminum. We are emphasizing PMMA coatings, recognizing that PMMA probably will not provide sufficient protection for silver [4]. Tab also lists a series of PMMA and PAN films solution-cast onto silver films were deposited on glass (Corning 7809). The silver films for these sam were formed on glass using the wet chemical process (series 607, 707,

---

*Weather-Ometer is a registered trademark of the Atlas Electric Dev Company, Chicago, Ill.

**QUV is a registered trademark of the Q-Panel Company, Cleveland, Ohio.

Table 1. Exposure Results

Series	Product	Company	Solar-Weighted Averages (Hemispherical Reflectance)		
			Weather-Ometer		Outdoors
			Initial	4 Weeks	6 Weeks
107	Acrylic/AL (FEK 244)	3M	85.5	85.5	85.5
207	PC/AG/Mylar	Sheldahl	92.3	84.0	84.9
507	PEst/AG (YS94)	3M	96.3	96.0	94.0
407	Teflon/AG/Inconel (FEP)	Sheldahl	95.6	94.6	95.1
607	PMMA/AG/7809 (1% National Starch)	SERI	87.0	78.9	84.3
707	PMMA/AG/7809 (1% Uvinol 400)	SERI	88.0	67.3	87.0
807	PMMA/AG/7809 (1% Tinuvin P)	SERI	87.3	87.9	86.4
907	PMMA/AG/7809	SERI	87.9	77.9	86.2
117	PAN/AG/7809	DU	87.9	88.4	88.0
	$PMMA/AG_{SP}/7809$	SERI	93.6	--	--

907, 117). The reflectances for these samples are only about 88% compared t
the last entry of Table 1 where the reflectance is about 94%. The latt
sample is different in that the silver is vacuum-sputtered onto the glass, a
we have observed the same improvement in reflectance with PAN film on vacuu
sputtered silver compared to wet-processed silver.

A series of experiments demonstrates that the diminution of reflectance usi
wet-processed silver is not a chemical effect. For example, wet-process
silver has a reflectance of about 96% before being coated by PMMA, althou
after coating, the reflectance drops to 88%. When the PMMA film is redi
solved with the same type solvent, the reflectance of the silver returns
its original value, 96%, and transmittance measurements of the redissolv
polymer compared to the original polymer solution are also unchanged. Polym
coated onto wet-processed silver has a slight yellow hue that is not prese
when vacuum-sputtered silver is used. The yellowing phenomenon is observ
for different polymer types or even when a drop of solvent (toluene) is depo
ited on bare silver. We conjecture that the surface of wet-processed silv
is rougher than that of vacuum-sputtered silver, resulting in the loss
reflectance. The effect on reflectance is illustrated in Figure 1 where t
initial reflectance of PAN/Ag/7809 (series 117, Table 1) is shown as
function of wavelength. The dip in reflectance at 0.4 μm is absent when spu
tered silver is used.

Table 1 illustrates that, in general, Weather-Ometer tests are harsher t
outdoor exposures for PMMA samples. Three ultraviolet screens are included
this initial test set, and the Tinuvin P/PMMA (series 807) sample demonstra
an improved stability. Similarly, pure PAN film is unchanged in the Weath
Ometer tests; however, outdoors it partially delaminated. Where the PAN f
had not delaminated, its reflectance was unchanged (series 117, Table 1).
PAN the outdoor tests were harsher than the Weather-Ometer. Laboratory exp
iments at the University of Denver, Colo., have shown that the adhesion of
to silver can be improved, and tests are in progress to determine if adhes
is also improved for outdoor exposures.

Mechanistic studies of photodegradation of PMMA/Ag mirrors have corrobora
the empirical observation that PMMA is stable in sunlight [1]. PMMA-coa

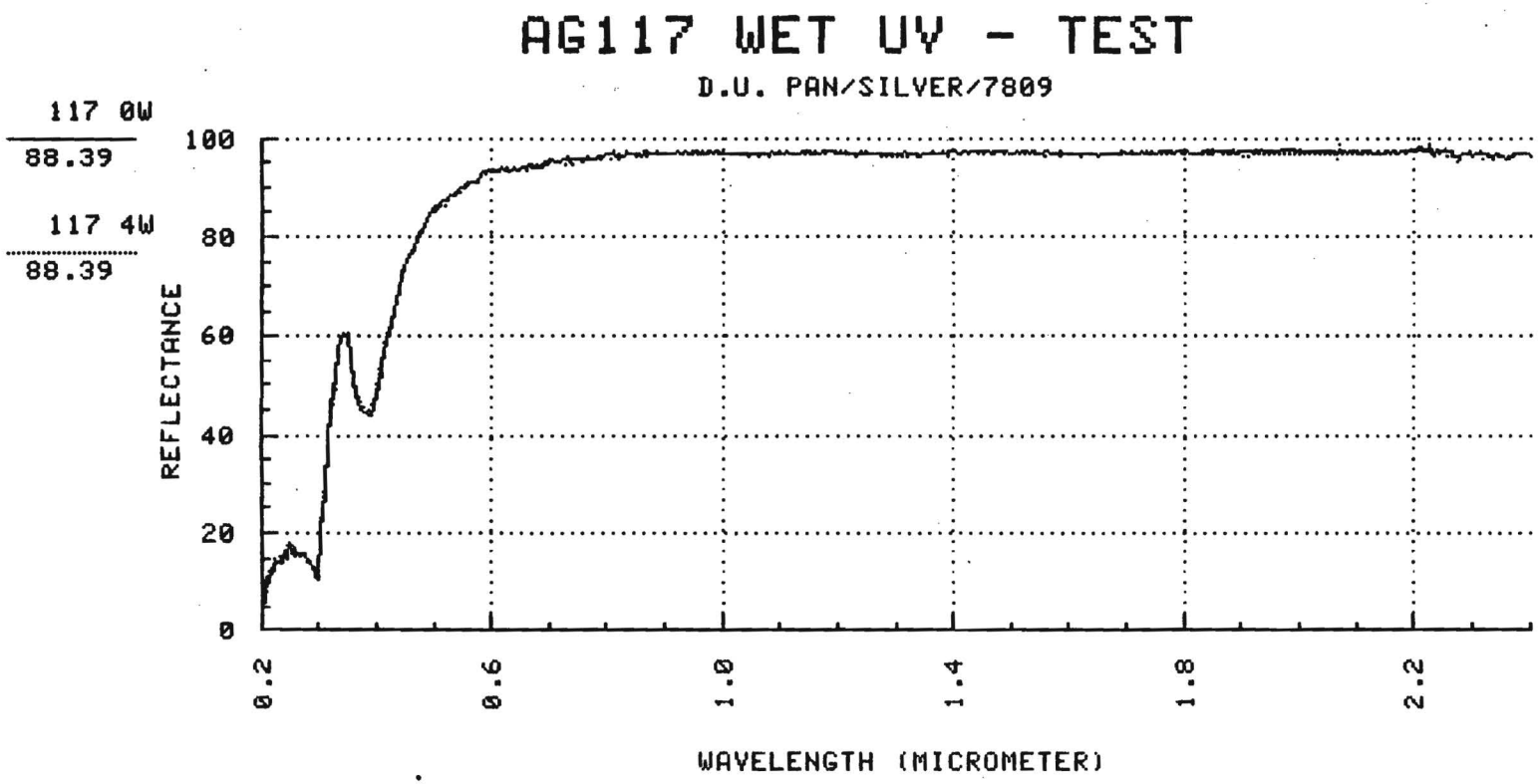

Figure 1. Reflectance Versus Wavelength, 7809 Glass Substrate, Wet-Processed Silver-Cast Polyacrylonitrile

mirrors have been studied in a controlled environment (ultraviolet, te perature, ambient atmosphere, etc.) in a configuration that allows dire observation of the chemical changes using infrared spectroscopy. A comparis of the accelerated degradation of PMMA/Ag mirrors with and without chlori contamination on the silver is available [1]. Without chlorine no changes a observed in the infrared spectra after exposure to ultraviolet radiation f 3.75 h with a solar wavelength distribution, but with the intensity increas by a factor of 16. If the silver surface is contaminated with chlorine (exposure to HCl, Cl_2, or by use of AgCl rather than Ag) before PMMA solution-cast onto the mirror and then the degradation is carried out sir larly to the chlorine-free case, changes in the infrared spectra are obser in only one minute. The polymer is now photosensitized to solar radiati We conjecture that solar photons can produce chlorine radicals that react w the PMMA [5]. Measurements are planned to determine if chlorine sensitizat or effects of other atmospheric pollutants are involved in mirror failu during outdoor use.

One approach to lowering mirror costs is to use the stretched membrane conc where the metallized polymeric film is only rim-supported (see companion pa by L. M. Murphy). Other, nonmetallized applications for glazings also requ good mechanical properties in addition to the optical properties for polyme films. One example is the dome concept where a thin polymeric film is a supported to enclose a polymeric-mirror heliostat. Work on chemically-bo ultraviolet screens to stabilize laminated polymeric films is in progress (companion paper by R. Liang).

Acknowledgments

The author thanks the members of the Materials Research Branch of the So Energy Research Institute for their contributions. Professor D. M. Smith the University of Denver provided information on PAN films, and Drs. A. Gu and R. Liang are conducting work on stabilized, laminated films at the Propulsion Laboratory.

References

1. Webb, J. D. et al., Polymer Degradation on Reflecting Metal Films: Fourier Transform Infrared (FTIR) Reflection-Absorbance Studies, SERI/TP-255-2054, Golden, CO: Solar Energy Research Institute, 1983.

2. Smith, D. M., private communication, Denver, CO: University of Denver, August 1983.

3. Rainhart, L. G., and Schimmel, W. P. Jr. Solar Energy, Vol. 17, 1975, p. 259.

4. Brauman, S. K., MacBlane, D. B., and Mayo, F. R., Reactivity of Polymers with Mirror Materials, Subcontract No. XP-9-8127-1, Golden, CO: Solar Energy Research Institute, 1982.

5. McNeill, I. C., and Neil, D., Eur. Polymer J., Vol. 6, 1970, pp. 143, 569.

ADVANCED CONCENTRATOR RESEARCH: TWO EXAMPLES

by

L. M. Murphy, Ph.D.
Group Manager
Thermal Systems and Engineering Branch

Solar Energy Research Institute
Golden, Colorado 80401

INTRODUCTION

This paper briefly describes the major research efforts and findings at the Solar Energy Research Institute (SERI) on two innovative, potentially low-cost, concentrator concepts. The first concept discussed is the stretched-membrane heliostat, and the second is the polymer-enclosed parabolic dish.

STRETCHED-MEMBRANE HELIOSTAT

The need for heliostats with dramatically improved costs and performance was established by the value-based cost goal analysis developed by a joint industry/ Department of Energy cost-goal committee in 1981 [1]. The stretched-membrane concept can potentially meet a significant portion of that need. In this concept a reflector film—which can be metal, a polymer, or a composite—is stretched on a hollow torroidal frame that offers a structurally efficient and optically accurate surface (see Figure 1). This design, although intended primarily to improve heliostat concentrator performance and lower costs, may well offer the same opportunities for improvements in photovoltaic and daylighting applications as well.

To date, SERI's effort, detailed in Murphy [2], has focused on concept configuration, development, cost and performance analysis, and scale-model testing. Technical issues

investigated include fabrication and attachment approaches, focusing and optical requirements, and the structural behavior of membranes and support structures. This last issue includes analysis of linear and nonlinear deformation, buckling of the support frame, thermal mismatch considerations, wind spillage effects, and the optimal strength and sizing of the membrane's support structure.

We costed several stretched-membrane concepts. We also designed and fabricated a number of bench-scale and field-test scale hardware elements, including two prototype concentrators 2 m in diameter and a potentially low-cost two-axis tracking support base; seven stretched-membrane reflective modules of various designs 1 m in diameter, which were tested for optical accuracy using a SERI-designed laser ray trace instrument test bed; and a reflector 3 m in diameter based on a commercial trampoline as an initial prototype. Further, we also tested a number of mechanisms for attaching membranes to support structures that are appropriate to either low or high production levels and evaluated seven candidate metallized polymers as potential reflective surfaces for stretched-membrane and other innovative concentrators.

The major advantages emerging from the research include the following: the reflector, support frame, and support structures can be made extremely lightweight and inexpensively because this concentrator makes the most effective use of material with high average stress levels in the reflector and suppport frame. Also, the simplicity of the design, which results in many fewer parts, should help reduce costs. We anticipate a 75% weight reduction of the reflector and support structure (down to the drive attachment) compared with the second-generation glass and metal heliostat concentrator. We also expect a better than 50% cost reduction for the reflector assembly and support structure compared with corresponding elements of the second-generation concentrator. Finally, we envision optical accuracies and annual energy delivery potential close to those attainable with current glass and metal heliostats. To get this high optical performance requires focusing, which can be accomplished in one of two ways [1], and a high quality polymer reflective surface.

Much development work still remains to verify and realize the full potential of the stretched-membrane concentrator. Remaining research is in three areas: systems performance and cost, materials, and mechanical and structural development.

Detailed costing and production analyses as well as a comparison of the annual cost of delivered energy with second-generation heliostats are needed. Optical surface accuracy analyses for membranes in real environments, correlated with and confirmed by experiments, should be used to support these system performance studies. We also need an impact assessment of seams, nonuniform and backside pressure loading, and ring imperfections as well as optimization studies that include the effects of weight reduction limitations, size constraints, and the applicability of scaling relationships.

Materials issues include determining the availability of durable, highly reflective polymer films for use with metallic structural membranes. We need more understanding on bonding or welding membranes (to the main structural frame and in forming wide sheets from multiple narrow sheets) in large-scale production environments. Testing and industry involvement are warranted at an early stage. Long-term materials issues include possible cost reductions through the development of polymer mirror laminates and polymer composite structural elements (i.e., the frame).

The most important issues on mechanical and structural research and development include refining the definitions of practical limits for further weight reductions (including the establishment of more precise buckling criteria for both local and gross stability as a function of heliostat size and design tension) and determining ways to enhance the buckling resistance of thin, tubular structures. In particular, we need to investigate the in-plane stability question, relating to the membrane tensioning and support frame, and verify the applicability of structural-stability scaling relationships by testing increasingly larger hardware elements. Furthermore, snap-through "oil canning" of laminated, curved membrane reflectors and aerodynamic load-reduction schemes for the reflector assembly should be studied.

POLYMER-ENCLOSED DISH CONCEPT

There is a need for small modular process heat systems that deliver energy in the 540° C (1000° F) temperature range, and the low-cost dish technology was suggested as a possibility to meet this need. One concept has a polymer dome enclosing the dish (see Figure 2).

A systems engineering study was performed to identify problem areas and research issues, and to study technical feasibility as well as performance and areas likely to drive the cost up. We reviewed previous thermal dish development and cost and systems studies; analyzed, assessed, and recommended solutions for numerous limiting thermal performance issues; and established bounds for likely dish costs. Performance models were developed and used for the trade off studies. Finally, conceptual designs for reconfigured dishes and receivers were developed.

Analysis findings indicated that this concept is feasible. There are, however, numerous technical challenges that must be overcome. In addition to the issues identified with polymer-enclosed heliostats, the major technical problem appears to be the "beam walk-off problem" where the beam is no longer focused at the receiver but at some other point, which can result in exceedingly high flux levels on the dome enclosure. This can be caused by malfunctions in the tracking mechanism or by intentionally moving the dish off focus during maintenance.

Also, in moving toward low-cost dish concepts, we found that a much smaller focal-length-to-diameter ratio (f/D) [i.e., about 0.25 versus about 0.60 for current designs (see Figure 3)] is desirable to reduce the structural weight associated with both the dish and the strucutral support of the receiver and to take advantage of the additional strength of the resulting enhanced curvature effects. Further, the smaller f/D dishes allow smaller enclosure diameters while still solving the beam walk-off problem (see Table 1).

Reconfiguration of the smaller f/D concept requires an external receiver. However, the external receiver can be smaller, lighter, and less expensive than a corresponding cavity receiver. Thus, using this smaller external receiver can partly compensate for the lower efficiency of the external receiver. Furthermore, by using selective coatings, analysis has shown that the performance of the external receiver can be fairly close to that for a cavity up to temperatures of 540°C (1000°F). Moreover, an evacuated enclosure looks feasible and can improve the performance even more. Note that for temperatures significantly above 540°C (1000°F), the external receiver will not perform as well as the internal cavity receiver. Also, the external receiver, if optimized for high efficiency and with the smaller f/D ratio dish, appears to have merit whether the dish is enclosed or not and possibly can be used for electric applications using existing materials and current Rankine-cycle steam technology.

Systems analyses show that the reconfigured enclosed dish is potentially more cost-effective on annual cost of delivered energy basis compared with the unenclosed conventional dish. However, the benefits of the enclosed thermal dish are not enough to make thermal dishes more cost-effective than some other solar thermal technologies (i.e., central receiver) above the 5-MW size range. Based on standard economic assumptions the delivered energy costs for dish systems (whether enclosed or not) appear to be 50%-100% greater than for central receivers using second-generation glass and metal heliostats for 5-MW or larger sizes. However, for very small sizes, other issues may lead to the selection of dishes. For instance, utilities are interested in very small modular applications of dish technology because of the lower capital cost and the potential to incrementally add to the generating capacity of the system.

Systems analyses also show that thermal transport costs for thermal dishes are exceedingly high using current technology or anticipated advances of this technology in the near term. These transport costs alone may exceed the value-based cost goal levels set in 1981 for collector subsystems. Polymer enclosures aggravate these already high costs for transport, and, thus, some of the anticipated advantages of enclosures are lost.

The results from the analysis of the enclosed dish concept indicate that the enclosure concept itself does not appear to merit strong continued research emphasis. However, the lower f/D dish concept with an external receiver appears to have significant merit whether the dish is enclosed or not, up to operating temperatures of 540° C (1000° F). Clearly, a range of materials, thermal, structural, and systems research issues remain to develop the "deep dish" concept and to verify its potential. These include those issues related to receiver coatings, small external boiler receivers, low-cost, accurate deep profile shell structures, and much improved transport subsystems.

REFERENCES

1. Edelstein, R. et al., Final Presentation of the Solar Thermal Cost Goals Committee, presented to the U.S. Department of Energy, Washington, D.C., 26 February 1982.

2. Murphy, L. M., Technical and Cost Benefits of Lightweight, Stretched-Membrane Heliostats, SERI/TR-253-1818, Golden, CO: Solar Energy Research Institute, 1983.

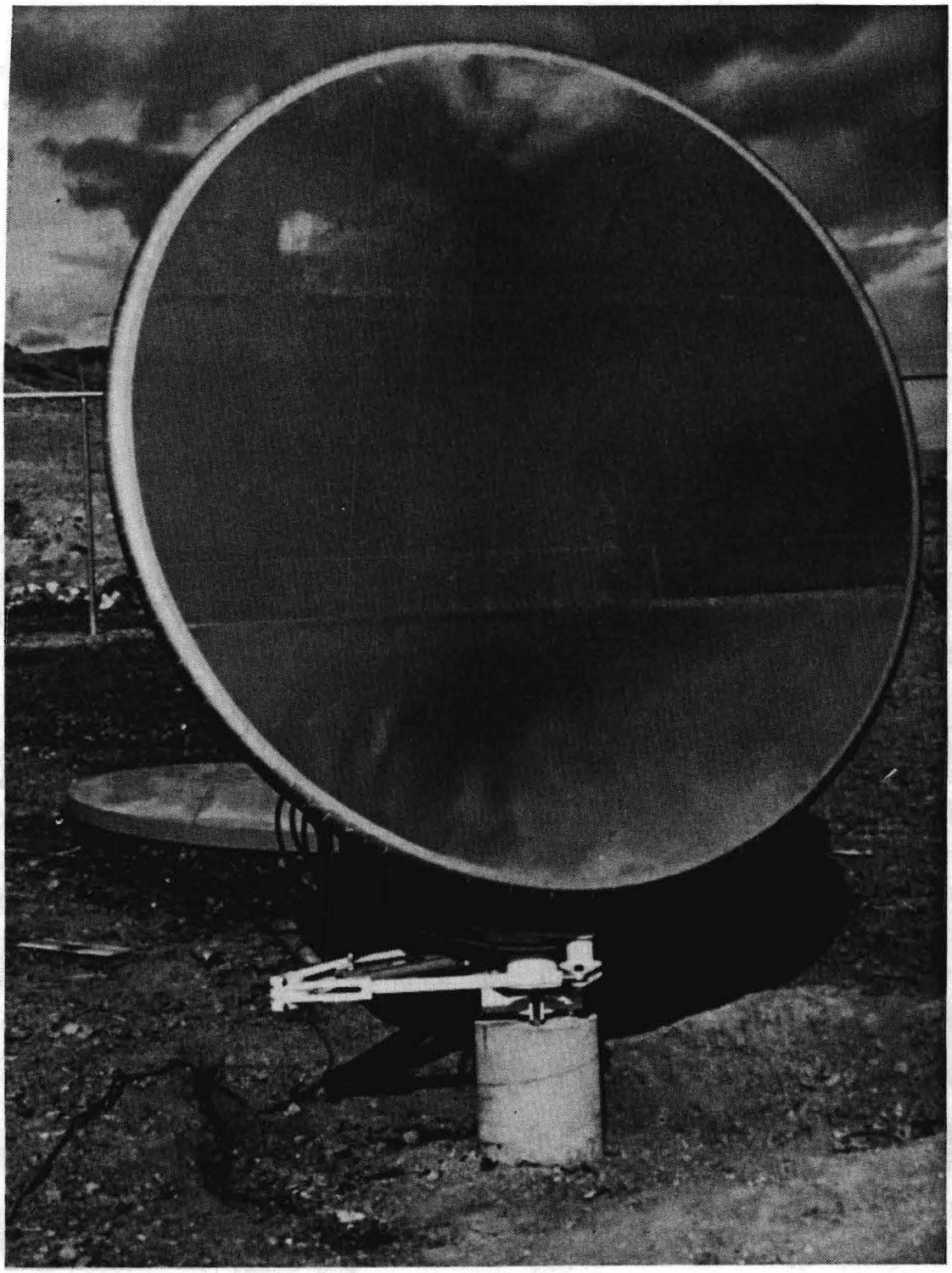

Figure 1. Two-Meter Diameter, Stretched-Membrane Heliostat Research Experiment at the SERI Test Site

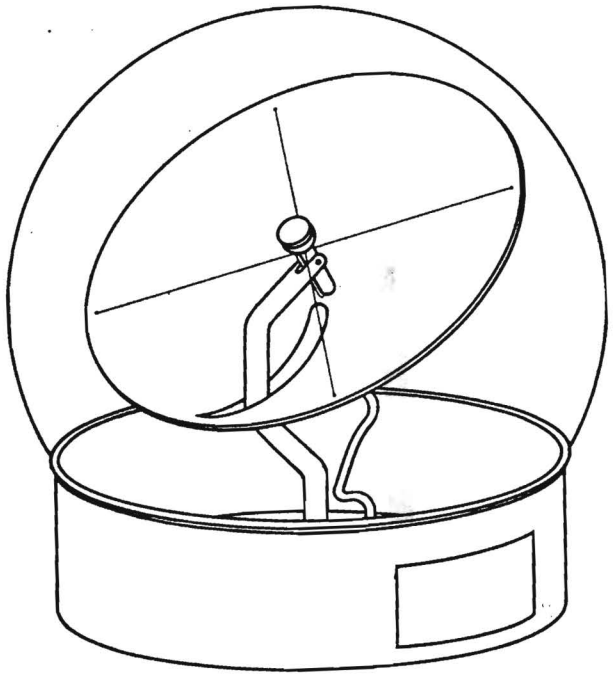

Figure 2. Conceptual Design of a Polymer-Enclosed Thermal Dish Having a Small f/D, an External Receiver, and a Single Post Receiver Support

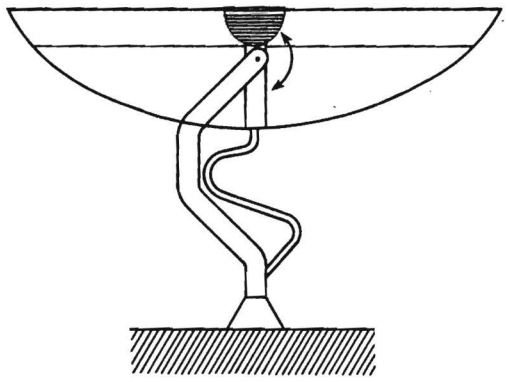

Figure 3. Side Section of a Deep Profile Thermal Dish (f/D = 0.25) Conceptual Design

Table 1. Various Dome Geometric and Flux Requirement Parameters Shown for Several Polymer-Enclosed Dish Geometries. Note that for f/D = 0.60, a dome diameter three times as large as the dish is required to assure that the most severe flux on the enclosure surface is at or below 15 suns. For f/D = 0.25, a dome only 30% larger than the dish is required.

DISH DIAMETER, M	10	10	10
FOCAL LENGTH, M	9	6	2.5
RIM ANGLE, ^{o}	31	45	90
MINIMUM DOME RADIUS BASED ON GEOMETRY, M	9	6	5.6
$\frac{\text{MINIMUM DOME DIAMETER}}{\text{DISH DIAMETER}}$	1.8	1.2	1.1
WORST CASE FLUX AT 1.1 X MINIMUM DOME DIAMETER	267	260	16
MINIMUM DOME DIAMETER TO GET 15X CONCENTRATION, M	41	29	13

University of Houston Materials Research:

Photoeffects in Solar Materials

A. Ignatiev
Department of Physics and Chemistry
University of Houston
Houston, Texas 77004

Abstract

The elevated temperature behavior of solar materials under concentrated solar irradiation has been shown to be significantly dependent on the solar component of the radiation. Chromium and the solar absorber coatings black chrome and black cobalt have exhibited reduced oxidation (degradation) rates under solar heating as compared to infrared (oven) heating while iron has shown an increased oxidation rate under solar irradiation. Aluminum samples studied have exhibited both behaviors. Basic mechanisms have been determined for these here-to-fore unknown photoeffects in solar materials and it is expected that such effects will not only be present, but prominant in most all materials used in for solar enviroments.

Introduction

The stability of materials at elevated temperatures has long been a point of great interest in materials research.[1,2] Until recently, however, such interst has centered principally on the stability of a material under high temperatures generated by the absorption of either infrared or particle radiation. Such are not the conditions encountered by materials used at elevated temperatures in solar apparatus. In this case the materials are exposed to concentrated solar radiation of wavelengths from ~0.3 μm to ~ 2μm. Radiation from this solar spectrum is by and large absorbed over a much shallower depth (up to a factor of 100 to 1000 shallower[3]) than infrared radiation and hence this surface localized absorption can lead to surface temperatures much higher than the measured bulk temperature. Such an effect may prove deliterious on several fronts. In addition, the ultraviolet and near ultraviolet components of the solar radiation may induce various chemical changes at the surface which may prove to be either beneficial or deliterious in terms of affecting the long term stability of the material in a solar enviroment.

It is clearly an enhancement of long term stability under elevated temperatures in solar enviroments that is sought after in solar materials. The work described below will show that such an enhancement can become a possibility when the basic mechanism responsible for the noted photoeffects are identified and characterized. It is with that knowledge as an input that efforts can be made to generate new solar stable materials.

Photoeffects in Solar Material Absorber Coatings

We have discussed in the past specific photoinduced effects active in

black chrome[3,5] and black cobalt[6] and wish to note here some of the specifics of the studies as background for our current investigation of photoeffects in metals and ceramics. For both black chrome and black cobalt (formed by oxidation of plated cobalt metal[7]) it was observed that the reflectance of the samples changed less from the "as prepared" case upon solar heating than upon infrared (oven) heating. The differences were in fact quite significant (Figure 1) with for black cobalt $\Delta\alpha \approx -0.11$ under oven heat at 460°C in air for 50 hours whereas $\Delta\alpha \approx -0.5$ for an identical solar heated sample under equivalent (bulk) temperature conditions.

The basis for such a photoeffect was investigated by applying the surface sensitive techniques of Auger electron spectroscopy (AES), x-ray photoelectron spectroscopy (XPS) and mass spectrometry. It was found in both cases that the effect was photodesorption of oxygen bearing species (CO_2) from the surfaces of absorber coatings as a result of the near ultraviolet irradiation. This photodesorption reduced the number of oxygen species at a surface available for oxidation and hence reduced the rate of oxidation - oxidation being the principal degradation mode in black chrome and black cobalt. It is seen here that the photoeffect in these two systems has been quite beneficial and should therefore be utilized to its fullest extent when designing solar absorber systems.

Metals

A large variety of metals are, expected to be, utilized in the concentrated solar enviroment. These include iron, chrominun, aluminum, copper, nickel and various steels. It is of importance, therefore, to define and characterize any photoeffects that significantly affect the sta-

bility in these systems.

Chrominum samples exposed to ~700 kW/m^2 solar simulated radiation exhibited two modes of behavior depending on cleaning history of the sample surface. Samples cleaned in ultrahigh vacum by argon ion bombardment such that the surface was atomically clean showed no photoeffects under irradiation. However, samples not cleaned, i.e. retaining the native oxide and other surface impurities, showed marked photodesorption of CO_2 upon solar irradiation (Figure 2). The desorption efficiency was measured by mass spectrometry to be ~ 3×10^{-6} molecules/photon under irradiation at 3000Å and varied linearly with photon flux. The wavelength threshold for the photodesorption was near 5000Å (~2.5eV) and thus that effect did not correspond to any know photo induced effects in metals. The threshold behavior did, however, nearly correspond to that expected for photodesorption from Cr_2O_3. There are presently discussions underway which address the discrepency in the measured and expected desorption thresholds for Cr_2O_3, (2.5 eV vs 3.4 eV)[8,9] with the basis for the discrepency lying in the most appropriate description of the basic mechanism responsible for the desorption[10,11]. It is fair to say, however, that a photo desorption mechanism(s) is active in Cr_2O_3 and similar to the previously noted black chorome absorber coatings it reduces significantly the oxidation rate of the chromium.

Iron samples exposed to solar simulated radiation showed no photodesorption effects when the surface was atomically clean. They did, however exhibit photodesorption of CO_2 at an efficiency almost two orders of magnitude lower than that of chromium for a native oxide coated surface. On the

other hand, iron samples exposed in air to solar simulated radiation at elevated temperatures showed a new photoeffect. The samples exposed to 600 to 700 kW/m^2 fluxes at 410°C, 505°C and 614°C all showed increased rates of oxidation under solar irradiation as compared to oven heating in air. Figure 3 shows AES depth profiles (obtained by bombarding with argon ions) of a solar simulator irradiated iron sample and an equivalent sample heated in an oven. It is clear that the solar irradiated sample has an oxide coating that is ~ 30% thicker than that of the oven heated one, i.e. it has undergone enhanced oxidation under the influence of the solar simulated radiation. The basis for this is believed to be enhanced dissociation of molecular oxygen at the iron surface by the solar photons thus generating more highly reactive oxygen atoms for participation in the oxidation process.

We have then, in the case of iron a detrimental effect due to solar irradiation of a material and must clearly include this possibility in the utilization of iron in concentrated solar environments.

Irradiation of aluminum by concentrated solar simulated radiation results in different effects in two specific temperature regimes, below 400°C and above 400°C with a flux dependence also observed above 400°C. The AES depth profile of an aluminum sample solar irradiated for 2 hours at 520°C in air at ~ 1.3 MW/m^2 is shown in Figure 3a. For comparison, a depth profile of a sample irradiated at 520°C in air at ~ 250kW/m^2 is shown in Figure 3b and a depth profile for a sample heated in an air oven at 520°C is shown in Figure 3c. Several points can be made in the comparision.

1) The high flux solar heated sample has a thinner oxide (~ 250Å) as determined from the ion etch rate during profiling, than the low

flux solar heated sample (~350Å) or the oven heated sample (~350Å) or the oven heated sample (~350Å).

2) The stoichiometry of the high flux sample exhibits a higher oxygen to aluminum ratio in the surface region than does the low flux sample. However, the stoichiometry is quite similar to that of the oven heated sample. The stoichiometries of the oven heated and high flux heated samples as obtained from the figures are approximately: oven - $A\ell_3O_6$; high flux - $A\ell_3O_{5.5}$. These stoichiometries are obtained from the atomic concentrations in the depth profiles as determined from the AES peak-to-peak heights and AES sensitivity factors(12). The sensitivity factors have ~30% uncertainty in them and are dependent on apparatus used. Therefore, it is appropriate to denote (as is expected) the surface region of the oven heated aluminum sample as fully oxidizied $A\ell_2O_3$. The surface region of the high flux heated sample is then also $A\ell_2O_3$, however the low flux heated sample is noticably different at ~ AℓO, i.e. denoting a not fully oxidized surface region.

3) The top few 10's of Angstroms of the high flux heated sample are much reduced in oxygen concentration with most of the aluminum reduced to the metallic state.

The above differences, although detailed only for samples treated at ~500°C are consistantly observed for samples treated at 470°C, 400°C and 430°C.

Irradiation of aluminum samples below ~400°C results in very little difference between oven heated, high flux solar heated and low flux solar heated samples. The stoichiometries are all near Al_2O_3 and the thickness are all comparible and quite thin (~50Å).

The mechanisms responsible for the noted behavior of aluminum exposed to concentrated solar simulated radiation are not yet fully understood, however, several points can be made. The observed thinner oxide under the high flux irradiation probably indicates a surface temperature much higher than that measured by the thermocouple. Less oxide growth has been observed in aluminum above 600°C. The reduced amount of oxygen within the very top layers of the high flux sample indicate the presence of an active photo induced effect which reduces the oxide at the surface of the sample. Such an effect may be photodesorption of oxygen hearing species, and this can be and is currently being tested for by the irradiation of an oxidized sample in vacuum while monitoring desorbed species by mass spectrometry.

The lower oxygen to aluminum ratio in the low flux heated sample as compared to the high flux or oven heated samples may have its basis in lower thermal gradients in the sample due to the low flux condition, and a reduced, but still active photodesorption effect. The lower thermal gradients generating sample temperature uniformity approaching that of the oven heated samples, results in oxidation of the sample quite equivalent to that observed in the oven heated sample. The reduced oxygen to aluminum ratio in this surface region as well as some enhanced oxide reduction in the very, top surface of the sample is then a result of photodesorption of oxygen hearing species under the low flux conditions. The decrease in reduc-

tion of the oxide at the very top surface in the low flux sample as compared to the high flux sample directly indicates the effect of solar flux on the samples. Quantitative measurements are now underway to describe the effect more fully.

CERAMNICS

In working with the aluminum system we have begun to grow thick (3-5μm) thermal $A\ell_2O_3$ layers on aluminum for the initial evaluation of specific photoeffects in ceramics. Preliminary measurements show two effects: i) photodesorption of oxygen bearing species for aluminum oxide solar irradiated at a flux of 1.5MW/m^2 and a temperature of approximately 400°C in vacuum; (i) discolaration of the coating - darkening, under ~ 1.5 MW/m^2 in air at ~ 400± 100°C. Optical measurements to define changes in reflectance are to be undertaken, as are high resolution (1μm spacial resolution) AES measurements to define the basis for the discoloration. The discoloration (darkening) clearly increases the solar absorptance of the aluminum oxide sample and could result in locally high energy absorption leading to the cracking and melting previously observed at GIT and SANDIA.(13)

CONCLUSIONS

It has now been clearly shown that a number of solar relevant materials exhibit strong photo-induced effects which may be deliterious or beneficial. It is such effects that must be identified characterized, and understood with respect to the basic mechanisms responsible for them. With this knowledge it is then possible to design solar system components that are highly stable under concentrated solar enviroments.

ACKNOWLEDGEMENTS

The assistance of A. Mesawri and A. Zomorrodian is greatly acknowledged. Support for this work has been provided by the Department of Energy - STARC and by the University of Houston Energy Laboratory.

References

1. High Temperature Oxidation - Resistant Coatings, ed., National Research Council (Nat. Head of Sci., (1970).

2. I.E. Campbell and E.M. Sherwood, High Temperature Materials and Technology, (Wiley, New York, 1967).

3. J.P. Jackson, Classical Electrodynamics, p. 225 (Wiley, New York 1965).

4. G.B. Smith, G. Zajac and A. Ignatiev, Solar Energy 29, 279 (1982).

5. A. Ignatiev, G. Zajac and G.B. Smith, Proc. SPIE 324, 170 (1982).

6. A. Ignatiev, Yearly Prog. Report, DOE - STARC, Task 2 (Houston, 1982).

7. G.B. Smith, A. Ignatiev and G. Zajac, J. Appl. Phys. 51, 4186 (1980).

8. L. Korenblit and A. Ignatiev (Submitted for publication).

9. G.W. Fabel, S.M. Cox and D. Lichtman, Surf. Sci., 40, 571 (1973).

10. P. Mark, R.C.A. Review 26, 461 (1965).

11. D. Lichtman and Y. Shapira, in Chemistry and Physics of Solids - II, ed., R. Vanselow p. 397 (CRC Press, 1978).

12. Handbook of Auger Spectroscopy, ed. L.E. Davis et. al. (Physical Electronics, Minn, 1976).

13. P. Doherty and R. Davis, J. Appl. Phys. 34, 619 (1963).

14. High Temp. Materials and Thermal Science Coord. Meeting, (SERI, Golden 1983).

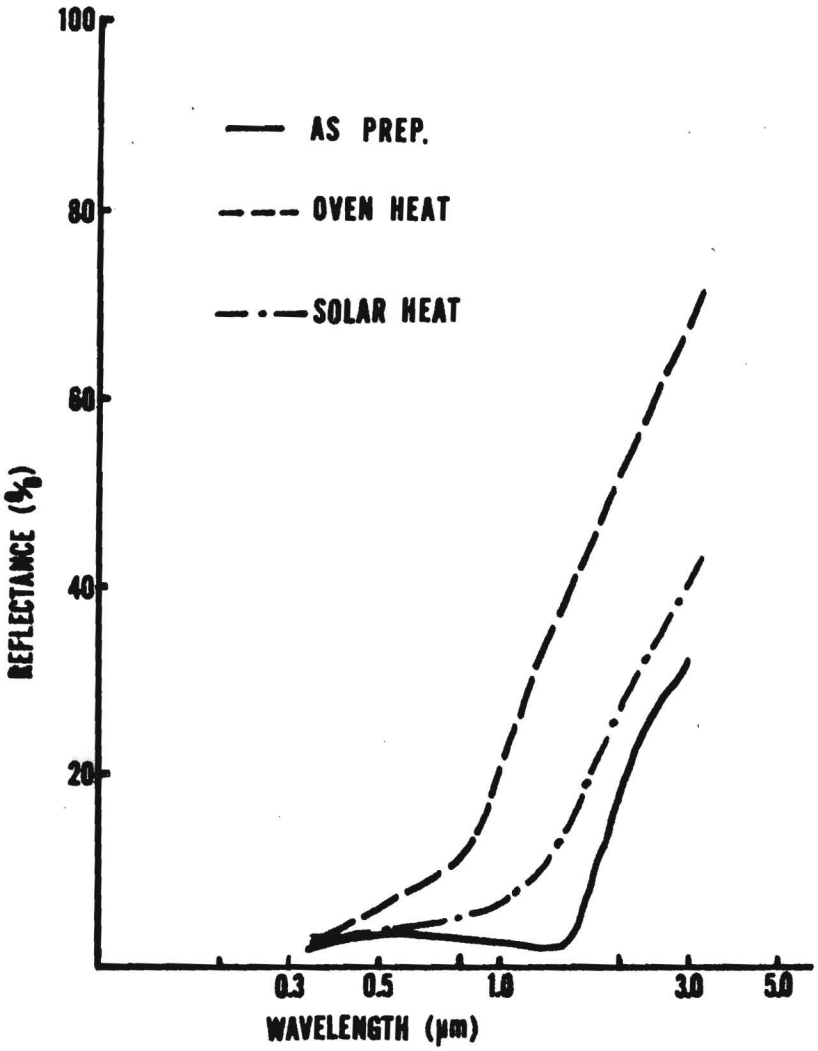

Figure 1. Spectral hemispherical reflectance for black cobalt samples that were solar simulator irradiated in air at 600 kW/m^2 and 460°C for 50 hours, oven heated in air at 460°C for 50 hours and for and "as prepared" sample.

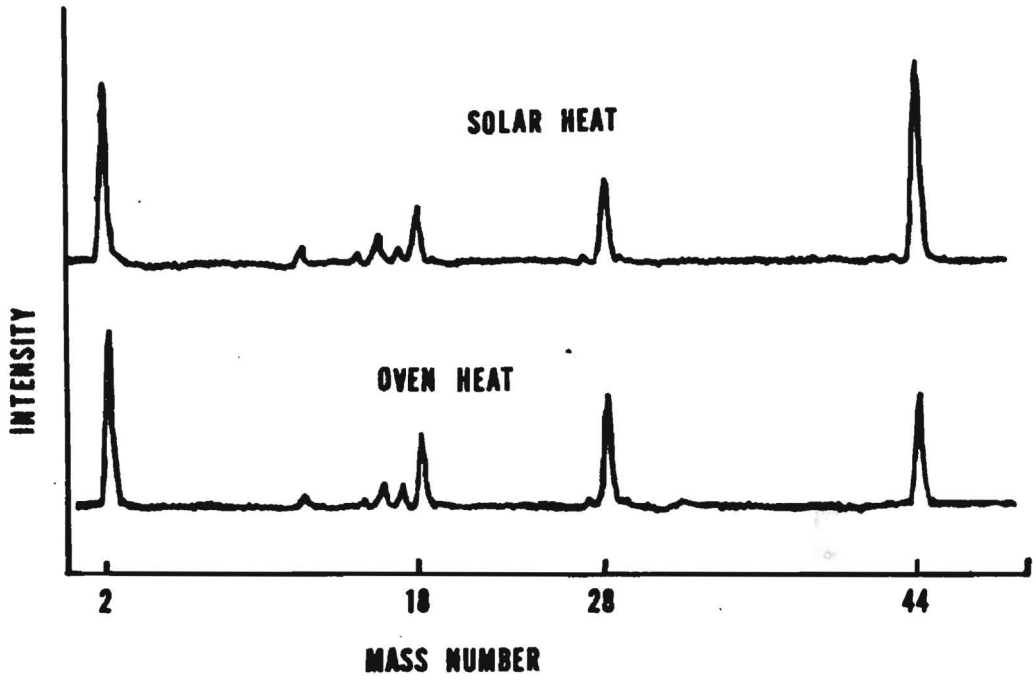

Figure 2. Mass spectra of solar-simulator irradiated, air exposed chromium (660 kW/m^2 at 410°C in $5x10^{-10}$ torr) and infrared heated air exposed chromium (410°C). Note the large increase in the 44 amu (CO_2) peak under solar simulated irradiation.

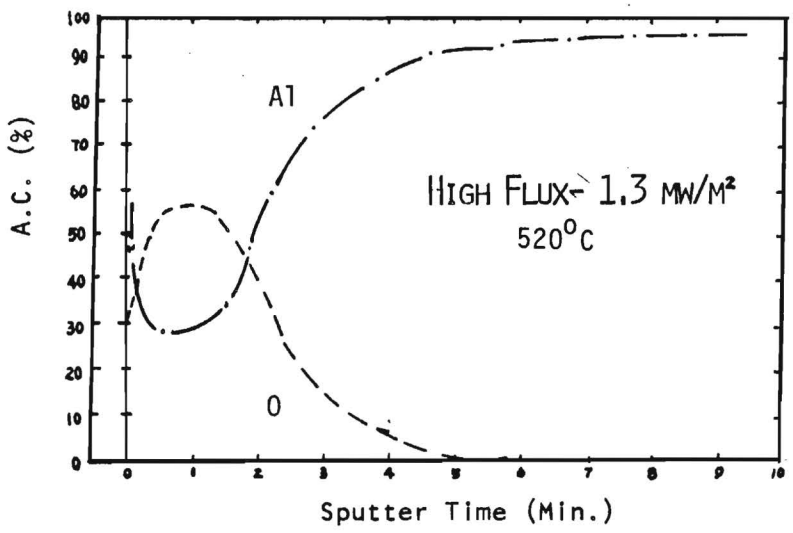

A

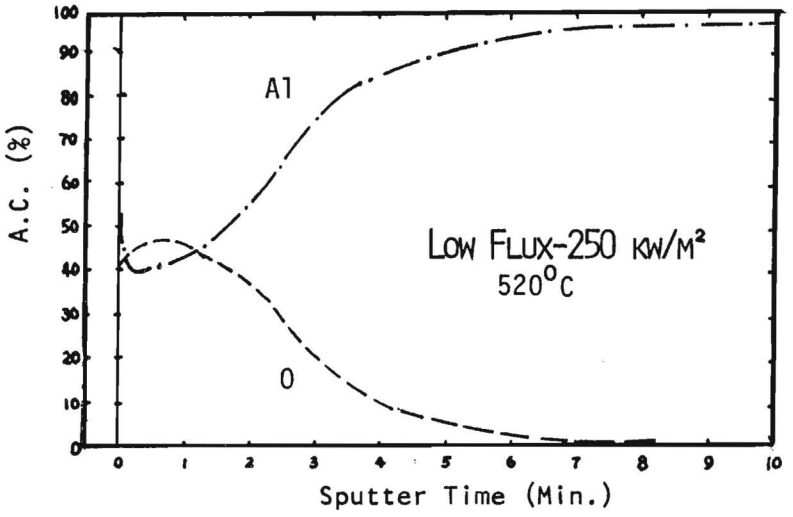

B

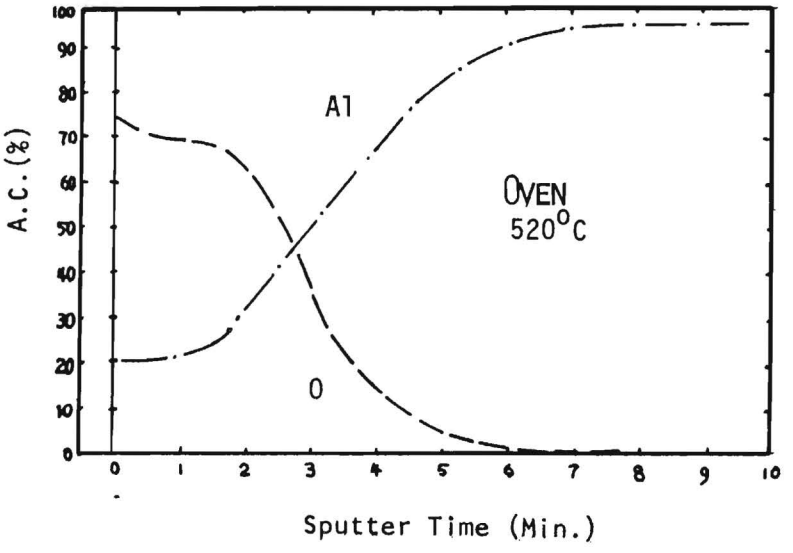

C

Figure 3. AES depth profiles giving the atomic concentration of oxygen and aluminum for aluminum samples heated under different conditions.

GEORGIA TECH SOLAR THERMAL CERAMICS RESEARCH

Steve H. Bomar, Jr.
Georgia Institute of Technology
Engineering Experiment Station
Atlanta, Georgia 30332

INTRODUCTION

Application of solar thermal technology to the production of chemicals and fuels provides a means of storing solar energy and offers possibilities for carrying out chemical reactions which cannot be accomplished using ordinary processing techniques. In the foreseeable future, solar thermal energy is likely to be more expensive than process energy derived from fossil fuels. Thus, it seems necessary to exploit the unique characteristics of solar thermal energy insofar as possible, especially the opportunity for direct interaction between the reacting species and the intense radiant flux.

Suitable transparent window materials and high temperature structural and insulating materials are crucial to the development of direct flux, solar thermal reactors. Receivers used for solar chemical applications will be required to work in environments peculiar to this service. Although the chemical processes which might be conducted in solar thermal reactors are not clearly defined at this time, it is possible to foresee tentative operating specifications and to proceed with materials evaluation and development. The operating specifications selected for this study are:

(1) Capability for service in radiant fluxes up to the range of 2000 to 3000 kW/m^2,

(2) Capability for service at temperatures up to the range of 1200 to 1500 °C,

(3) Capability for operation in various oxidizing and reducing chemical environments and in water vapor,

(4) Lifetimes of hundreds of hours with diurnal thermal cycling,

(5) Available in sizes suitable for commercial reactors and at acceptable cost.

MATERIALS FOR HIGH TEMPERATURE SOLAR RECEIVERS

This materials research program has the following objectives:

(1) To identify window materials and ceramic structural and insulating materials suitable for use in solar thermal chemical reactors,

(2) To conduct test programs in a solar thermal environment, supported as necessary by laboratory and analytical testing, for quantification of the performance of candidate materials,

(3) To define the service life of currently available window and ceramic materials as a function of flux, operating temperature, and atmosphere,

(4) To identify development needs and conduct research which leads to improved materials performance.

The most commonly used high temperature window material for laborator application is transparent fused quartz. Its advantages are excellen thermal shock resistance, high transmittance in the visible spectrum, an relatively high melting temperature. Fused quartz suffers from importan disadvantages, however, including the tendency to devitrify (crystallize) a temperatures above about 900° C, especially in the presence of water vapor rather poor resistance to abrasion, and limited availability in large sizes Another silica-based transparent window material is 96-percent silica glas (Vycor), which is manufactured by a phase-separation process from borosili cate glass. This material has a lower melting temperature than fused quart but may be more resistant to devitrification. Still another candidat window is borosilicate glass (such as Pyrex or Kimex) but these materia have much lower softening temperatures than fused quartz.

Other candidate window materials are aluminum oxide and magnesium-aluminum spinel. Sapphire (single crystal alumina) is transparent but prohibitively expensive in large sizes. Translucent, polycrystalline aluminas approaching transparency in thin pieces are commercially available (Lucalox by General Electric and Vistal by Coors Porcelain Company) and offer the attractive combination of being chemically inert and having very high melting temperatures. Magnesium-aluminum spinels are being developed for military use as infrared windows and are also transparent in the visible portion of the spectrum. Other, less promising candidates exist, but are not discussed here.

A test program was conducted at the Advanced Components Test Facility (ACTF) at Georgia Tech for the purpose of measuring the solar transmittances and steady-state operating temperatures of nine different potential window materials in various diameters and thicknesses, both with and without a thermal cavity behind the specimens. Transmittances were measured with a Gardon-type calorimeter; incident solar fluxes were in the range of 1000 to 2000 kW/m^2 and test times ranged from 3 to 60 minutes. The results of these tests are shown in Table 1 for the more important materials.

In the absence of the thermal cavity, steady-state temperatures of the transparent materials were 150 to 250° C, which was too low to realistically simulate operation in a solar receiver. The addition of a ceramic cavity behind the specimens raised operating temperatures to the range of about 400° C, but the presence of the water-cooled calorimeter within the cavity prevented attainment of higher temperatures. Three specimens of Vistal, 2 to 4 mm thick, all cracked upon heating, evidently because of flux

TABLE 1. Window Materials Tests

Material	Melting Temp (°C)	Solar Transmittance	Remarks
Fused Quartz	∿1700	0.91	"Standard" high temp window mat'l
Vycor	∿1500	0.96	96% silica glass (Corning)
Pyrex	∿ 800	0.92	Borosilicate glass, 80% SiO_2
Sapphire	2030	0.92	Transparent, single crystal Al_2O_3
Vistal	2030	0.85	Translucent, polycrystalline Al_2O
Spinel	2030-2060	0.65	Translucent, polycrys. $MgO \cdot Al_2O_3$

absorption and the resulting thermal shock. The spinel did not crack but was only 1 mm thick. Transparent specimens suffered no visible damage.

Two 15-cm diameter fused quartz windows were run in the aperture of cavity test fixture in the presence of steam, carbon monoxide and sulfu dioxide for cumulative times of about 15 hours each. Both exhibited sever devitrification on the surface facing the cavity after four to eight hours o operation. The operating temperature of that window surface is believed t be at least 100° C lower than the usual devitrification threshold temperatur for fused quartz, suggesting that a photon-induced process contributes t crystallization. A Pyrex window tested in this cavity fixture sagged notice ably when its temperature reached the range of 600° C during a two-hour ru Vycor has not yet been tested for extended times in this test receiver. the basis of cost and test results, fused quartz or 96-percent silica gla appear to be the most suitable window materials, but methods to inhib devitrification of fused quartz must be found and Vycor remains to be test in long-term service under concentrated solar flux.

Several pure ceramic materials and commercial, high-alumina castables have been tested at the ACTF in the cavity test receiver for the purpose of evaluating their performance as potential structural components in solar thermal chemical reactors. It has been empirically observed that uncooled ceramic materials exhibit failure at flux levels on the order of 1000 kW/m^2 and it is clear that better materials performance is required for solar thermal receiver applications.

The ceramic materials test program at Georgia Tech has initially concentrated on quantifying the behavior of readily available structural materials, particularly high-alumina castables. These are hydraulic-setting ceramic compositions which can be cast in place or in molds. The test materials were exposed to solar fluxes of 1000 to 2000 kW/m^2 in a cavity test fixture, which permitted control of operating temperature and atmosphere. Usual test temperatures ranged up to 1400° C and test atmospheres included air steam, carbon monoxide and sulfur dioxide. A summary of test results for five materials is shown in Table 2.

The most notable test observation is the apparent deterioration of all materials far below their rated service temperatures. It has been observed during tests that surface color changes occur within one or two minutes after the temperature of the test cavity is raised. Post-test examinations reveal evidence of internal melting and intergranular cracking. X-ray diffraction of the alumina castables shows some enhancement of mullite content at the expanse of α-alumina after testing to the stage of internal melting, and electron microprobe analyses show higher iron content in the darkened areas than in undarkened areas of the same specimen. Other materials, such as refractory fibrous blankets and boards, firebricks, castables, and pure ceramics are being investigated.

TABLE 2. Ceramic Structural Materials Test Results

Material	Service Temp. (°C)	Remarks
Slip-cast fused silica (SiO_2)	1000	Devitrified after 10-15 hours in oxidizing atmospheres and steam at 1000° C and up
Cordierite ($2MgO\ 2Al_2O_3\ 5SiO_2$)	1130	Cracked after about 2 hours at 1200° C
Alumina (Al_2O_3)	1600	McDanel 998, cracked by thermal shock
High-density alumina castable (60% Al_2O_3	1650	Darkened, internal melting, intergranular cracking after 4 hours at 1200° C
Low-density alumina castable (60% Al_2O_3)	1540	Darkened, surface and internal melting, intergranular cracking after 4 hrs, 1200° C

DAMAGE MECHANISMS

Tests of transparent fused quartz windows and ceramic structura materials under high-flux solar radiation have shown strong indications tha photon-induced processes occur. Such processes apparent are not found i ordinary furnaces at the same temperature, but the solar fluxes are an orde of magnitude higher than those found in furnaces at comparable temperatures.

The materials of interest in this program are dielectrics, which a nominally non-conductive at room temperature. Radiant flux in the visib spectrum can cause electron polarization within dielectric materials, and t availability of conduction electrons to participate in this dielectric lo mechanism is known to increase with temperature. Loss mechanisms other th electron polarization are not significant at the frequency of visible light

It appears that the electron polarization loss mechanism is relatively weak in dielectric materials, however, which accounts for penetration of t electromagnetic wave deep into the specimen (several millimeters). The hi intensity of the radiant flux seems to be able to induce material changes

a microstructural level even though the coupling between the electromagnetic wave and the material is not very strong. The presence of impurity elements, such as iron, appears to enhance the deposition of thermal energy within the volume of the ceramic.

Studies are in progress to clarify the controlling mechanisms for damage to ceramics and glasses under intense solar flux. This work should produce improved materials performance and perhaps clues to photon-induced processes which have commercial value.

HIGH-TEMPERATURE DIRECT ABSORPTION RESEARCH

Robert J. Copeland
Solar Energy Research Institute
Golden, Colorado

ABSTRACT

The Solar Energy Research Institute (SERI) is conducting research for high-temperature solar thermal receivers. A molten salt can serve as both the receiver heat transport and the thermal storage medium. Molten carbonates are the primary candidate salts for applications requiring temperatures of 850°C (1562°F) or higher. The receiver absorbs concentrated solar radiation directly on a salt film flowing down a wall in a cavity. This research has shown that depending on the receiver design, laminar, transition, or turbulent flow may be present. The heat transfer characteristics depend on both the optical properties and the film thickness. Predictions of molten-salt film thickness indicate a substantial variation in film thickness between flow regimes. A device has been constructed that can be used to verify the predictions and to provide data at low temperatures where none currently exist. Mathematical models of the heat transfer process in clear and blackened salts have been developed for both laminar and turbulent flow regimes. Blackened salts are preferred, but clear salts can also be employed.

INTRODUCTION

SERI researchers are investigating a direct absorption receiver and thermal storage (DARTS) concept for high-temperature solar thermal applications, particularly the heat transfer aspects of the absorption of the solar radiation. The objective is to generate data from which commercial scale central receiver systems can be designed. The research currently emphasizes modeling of the direct absorption process and measurements of liquid film thickness.

Temperatures on the order of 850°C (1562°F) and higher are needed for (1) fuels and chemicals (e.g., methane reforming), (2) electric power production (i.e., with gas cycles),

and (3) industrial process heat. Our approach is to employ molten salt as both the receiver and thermal storage media; the storage aspects are being researched under thermal storage program funding [1].

The molten salts being investigated are carbonates, chlorides, and hydroxides. Although sodium hydroxide is the cheapest media, it has the highest corrosion rate on containment materials; thus it will not be studied further at this time. Chlorides have low corrosion rates on ceramics but high rates on metals. Carbonates have low or modest corrosion rates on both metals and ceramics; the ternary eutectic of lithium, sodium, and potassium carbonate has been selected as the primary salt mixture for DARTS. Alternative salts are also being considered as backup to the ternary carbonate but at a reduced level of research.

Figure 1 illustrates the receiver concept. Low-temperature salt at 450° C is pumped to the receiver in the riser. A manifold distributes that salt over the top of the absorber surface. The molten salt runs down the absorber surface and is heated by the concentrated solar flux to a temperature of 850° C or higher. The salt is returned to ground level through the downcomer. The solar radiation enters the cavity through an uncovered opening. Secondary concentrators may be employed outside the cavity to improve receiver efficiency. Either the salt is blackened or black absorber surface is used with a relatively clear salt.

DIRECT ABSORPTION PROCESS

Figure 2 illustrates a section of the absorber surface with molten salt flowing over it. The surface is nearly vertical at angle χ. The solar radiation at a flux $F^{o}_{b\lambda}$ strikes the free surface of the salt at angle $\bar{\theta}$ and is bent to angle θ in the salt. The flux is partially absorbed in the salt film of thickness δ. The remaining flux is absorbed on the black absorber surface. The molten salt enters with constant temperature T_o and with nearly uniform velocity U_o. As the salt flows down the x-dimension, a velocity profile U(y) develops across the salt film. The free surface of the salt interacts by both radiation and convection with other surfaces and the air inside the cavity. That heat exchange is illustrated by a convective cooling coefficient h and an ambient temperature T_{amb} characteristic of the cavity. The principal factors affecting the heat transfer are

(1) flux level, (2) flow regime (laminar or turbulent), (3) salt optical properties, (4) absorber surface condition, and (5) salt film thickness. The convective heat transfer rate to the air has been calculated and is at least an order of magnitude smaller than any of the other factors.

We have chosen a 50-MW_t receiver based on the Boeing design [2] to be our baseline size. This size was selected because a number of other receiver designs are available to allow comparison, and data generated can be converted to larger and smaller sizes.

FLOW REGIMES

Figure 3 illustrates the shape of the absorber surface for the baseline design with an average receiver flux of 500,000 W/m^2. All three configurations are curved in the z-direction to maintain constant flux in that direction; the figure illustrates the surfaces as if they were flat. For the nominal case (100 m^2) active absorber surface, the flow is turbulent in the presence of maximum solar insolation and laminar for minimum solar insolation, which occurs as a result of viscosity changes with salt temperature. An all-laminar configuration can also be defined, but as illustrated it has an odd shape and may have flow distribution problems. An all turbulent configuration also has an odd shape and requires pumping of the salt back to the top of the absorber surface, once after being heated to 617°C and a second time after being heated to 783°C. Because of its more desirable geometry, the nominal case (turbulent and laminar flow) was selected for detailed analysis.

Figure 4 presents the calculated thickness of the salt film. At minimum solar insolation (a turndown ratio of 10:1 is assumed), the salt film is thin. These data assume laminar flow down the entire length, but the flow could become turbulent near the exit. At maximum solar flux, the flow is turbulent over the entire absorber surface. The film thickness is relatively constant at about 2 mm. Thus the film thickness near the exit could be as small as 0.25 mm or over 2.0 mm. Since the surface condition of the absorber seems to affect the transition from laminar to turbulent flow, we constructed a device to investigate those effects.

Figure 5 illustrates the apparatus constructed to measure flow thickness. A micrometer measures the thickness of the water, which is the medium. We have just initiated these

experiments, and the results to date indicate that under some flow conditions dry spots can develop, which could cause local overheating and damage to the absorber surface. Rough, melting surfaces distribute the flow well, avoiding dry spots. Additional tests are in progress to measure film thickness and velocity with that apparatus.

MATHEMATICAL MODELING

The direct absorption process shown in Figure 2 has been modeled for both laminar and turbulent flow regimes [4]. A computer program developed at SERI has been checked against previous models generated by Sandia for molten nitrate salt [3]. Good agreement was obtained with the earlier work, which was limited to conditions where the salt is isothermal in the y-direction. The SERI model is capable of predicting both x-direction and y-direction temperatures in the salt film. The model contains a number of simplifying assumptions, and additional work is in progress to incorporate more of the major variables.

The current model has been employed to calculate temperatures in the salt film for solar fluxes in the range of 100,000 to 1,000,000 W/m^2. The data are being generated parametrically because a receiver can be designed for small or large solar fluxes by making the absorber surface large or small; similarly the flow regime can be designed to be laminar or turbulent by the shape of the absorber surface (see Figure 3).

Figure 6 illustrates the typical data and conditions for laminar flow. Relatively small temperature differences are observed (e.g., 25° C maximum between the temperature of the wall and the salt). Note that these data are for a flux of 90,910 W/m^2. For laminar flow and a flux of 1,000,000 W/m^2, the wall is about 300° C hotter than the salt. Since receiver efficiencies and salt corrosion of the wall are adversely affected by the high wall temperatures, high fluxes and laminar flow conditions should be avoided in the design of the receiver. For turbulent flow conditions, the salt transfers heat by conduction and turbulent mixing. The heat transfer rates are much larger than in laminar conditions, and relatively small temperature differences between the wall and the salts can be obtained with either clear or black salts at high fluxes (i.e., 1,000,000 W/m^2).

We also used the model to investigate the temperature distribution in the x-direction (the vertical dimension from inlet to exit). The maximum temperature differences between

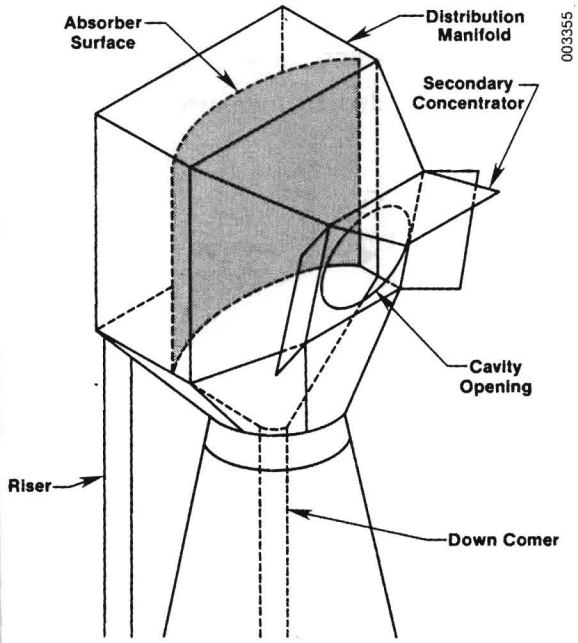

Figure 1. 50-MW_t DARTS Receiver

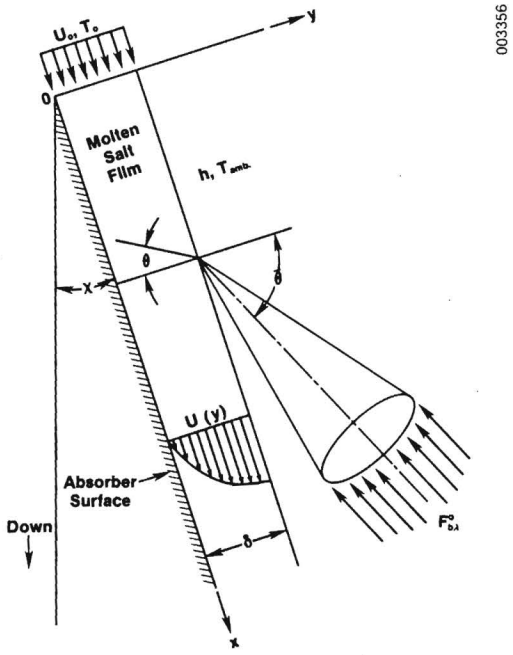

Figure 2. Direct Absorption Process

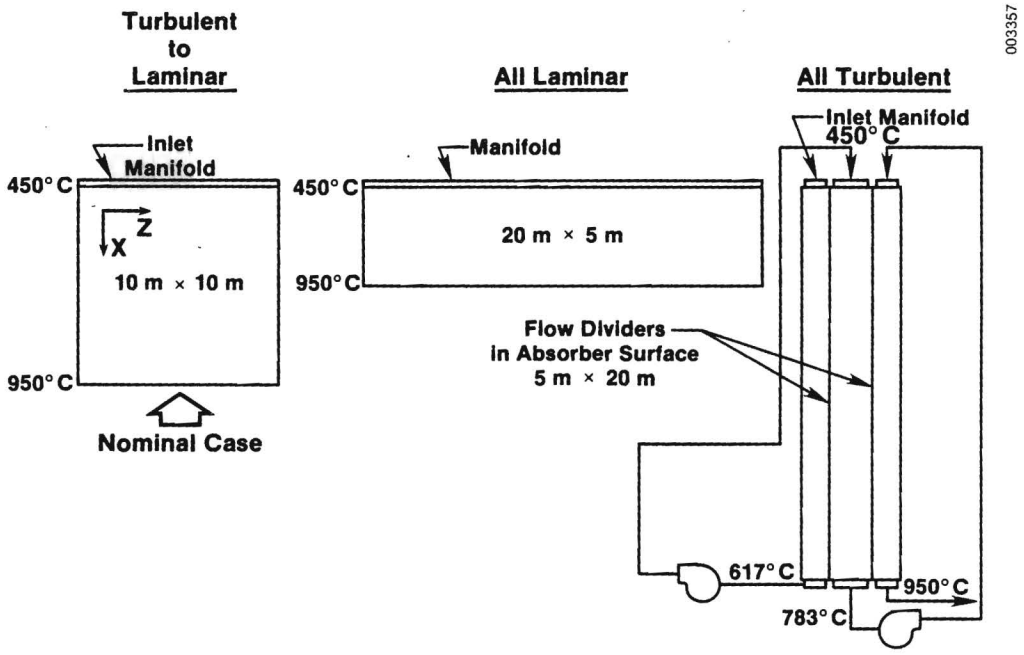

Figure 3. Flow Geometry, 50-MW_t, 100-m^2 Absorber

the wall and the salts occur at the exit. The model also shows that very small temperature differences occur in the inlet region, regardless of flux and flow conditions. Based on the current data, a flow length of 1 m or longer is needed to measure a significant temperature gradient.

FUTURE WORK

SERI plans to continue the current activities in film thickness measurements and improving the mathematical model. A direct absorption heat transfer experiment is planned to validate the mathematical model. Our initial work is directed to the application of maximum salt temperatures between 850° and 950°C. Long-range plans include research on application of temperatures up to 1100°C.

REFERENCES

1. Copeland, R. J., and R. Thomas Coyle, "Advanced High Temperature Molten-Salt Storage Research," Proceedings of the DOE Physical and Chemical Energy Storage Annual Contractors' Review Meeting, CONF-83 0974, 12-14 Sept., 1983, p.p. 54-58.

2. Boeing Engineering and Construction Company, Small Central Receiver Braxton Cycle Study, Livermore, CA: Sandia National Laboratories, draft, June 1983.

3. Abrams, M., The Temperature Distribution Along an Absorbing-Emitting Fluid Layer Flowing Over an Opaque Surface, SAND 76-8622, Livermore, CA: Sandia National Laboratories, August 1976.

4. Lazaridis, Anastas, Robert J. Copeland, and Jay Althof, "A Solar Irradiated Liquid Film Flowing Over a Solid Wall." Draft paper submitted to the ASME Solar Energy Division 6th Annual Technical Conference to be held in Las Vegas, NV, April 1984.

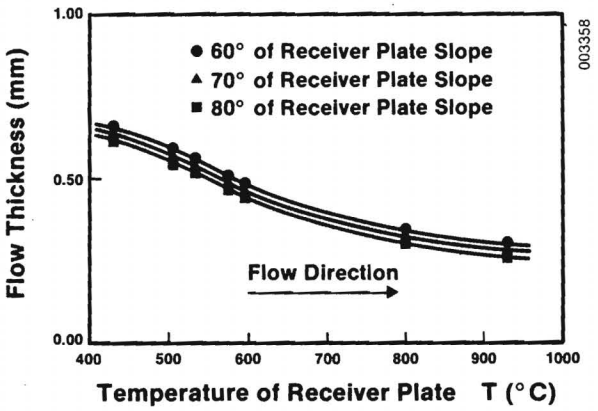

Figure 4. Fluid Thickness Flowing on Receiver Plate at 1/10 of Maximum Insolation

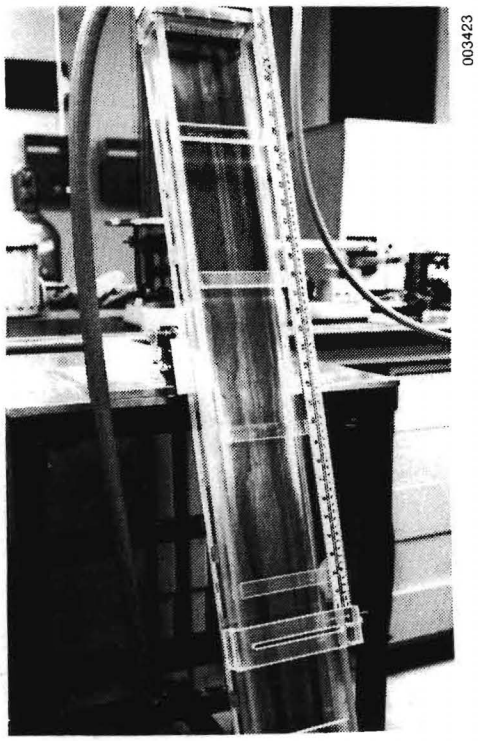

Figure 5. Apparatus for Measuring Flow Thickness

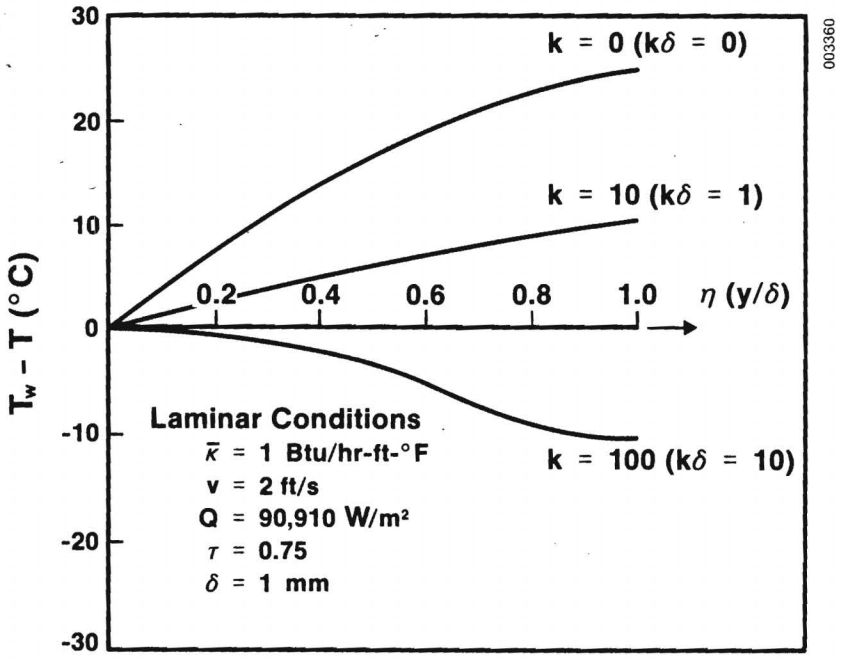

Figure 6. Effect of Optical Thickness on Temperature Profile in Liquid Film with Black Wall Substrate – Laminar Conditions

SMALL PARTICLE HEAT EXCHANGE RECEIVER
-SOLAR TEST RESULTS-

Arlon J. Hunt

Applied Science Division, Lawrence Berkeley Laboratory
University of California, Berkeley, California 94720

INTRODUCTION

The Small Particle Heat Exchange Receiver (SPHER) concept is a new approach to solar thermal conversion based on the direct absorption of concentrated sunlight by ultra-fine particles suspended in the working gas. The concept has been under investigation at Lawrence Berkeley Laboratory (LBL) since 1976. The central activity has been the development of the SPHER concept for a high temperature gas receiver. Earlier work analyzed the optical, physical, and thermodynamic processes of using small suspended particles as the solar absorber (Hunt, 1979). Experimental and analytic studies indicated that it was a practical approach and that it possessed significant advantages over conventional solar receivers.

Applications include heating a gas to high temperatures to provide industrial process heat or operate efficient heat engines, and direct solar processing of chemical feedstocks. An underlying goal of the project is to gain a basic understanding of the radiant heat exchange process in two phase, particle-fluid media to facilitate the development of direct radiant receivers for the processing of fuels and chemicals.

The SPHER, Mark I receiver was designed and built at LBL in 1981. It was tested in the summer of 1982 at the Advanced Component Test Facility (ACTF) at the Georgia Institute of Technology. The design and construction of the Mark I were described earlier (Hunt and Evans, 1982) and the solar test results in a recent report (Hunt and Brown, 1983).

PRINCIPLE OF OPERATION

The SPHER operates by injecting a very small mass of absorbing particles into the working gas. The gas-particle mixture passes into the solar receiver that consists of a hollow chamber equipped with a window. Concentrated sunlight enters through the window and passes into the gas-particle suspension. The particles absorb the sunlight and rapidly transfer the heat to the surrounding gas. The particles may react with the gas to form a clear exhaust.

The receiver in the test utilized carbon particles as the absorber and air as the working gas. After providing the heat exchange, the carbon oxidizes at temperatures from approximately 500 to 1000°C depending on the allotrope of carbon. The amount of carbon required is very small, less than 0.1% by mass of particles to air for most applications.

Advantages to this approach include high optical efficiency because of the characteristics of small absorbing particles and low chamber temperatures because the particles are nearly the same temperature as the gas and the absorption takes place within the gas, not on the chamber walls (easing material requirements and reducing radiant heat losses); moreover, the low pressure drop across the receiver improves turbine efficiency. Small-particle receivers can be scaled from the size suitable for a parabolic dish to multimegawatt central receivers.

EXPERIMENTAL SYSTEM

The main components of the experiment are the absorption chamber, particle generator, and air supply system. Ambient air is supplied by a Coanda effect air inducer. The particle generator produces carbon particles by the pyrolysis of acetylene in an argon carrier gas and mixes them with the incoming

air. Figure 1 shows the cross section of the Mark I receiver. Concentrated sunlight enters the bottom of the receiver through the window. The gas-particle mixture is routed into the annular manifold. Eighteen nozzles direct the gas flow into the chamber and produce a swirling motion. This motion organizes the flow and reduces the effect of nonuniform flux distribution.

The gas particle mixture circulates to the axis near the window where the quartz exhaust tube is located. The arrangement insures that the mixture passes through the maximum flux density region before exiting.

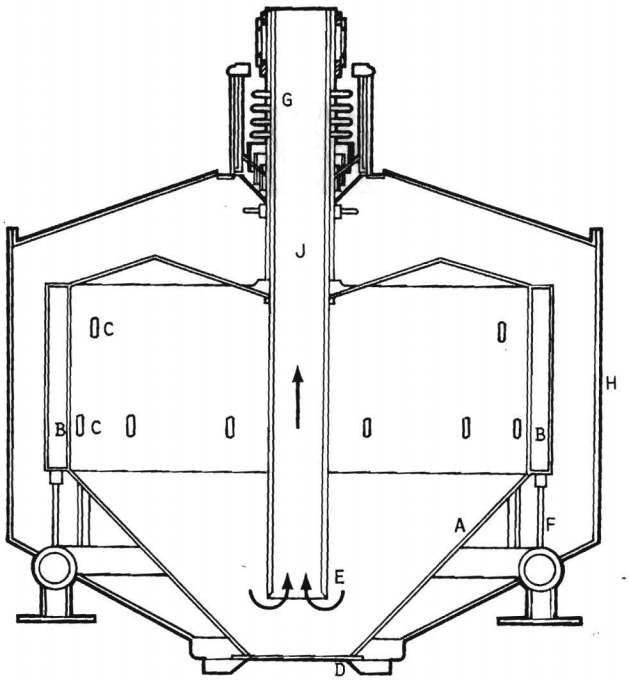

XBL 823-181A

Fig. 1. Cross section of the Mark I receiver.

Receiver wall temperatures were monitored by 26 thermocouples. A thermocouple with a four-component radiation shield determined the exhaust gas temperature. The output power was determined from the mass flow and the temperature rise. Solar input power was determined with a flux measurement system developed at the Georgia Institute of Technology. Accurate efficiency data

is not available because the calorimeters did not survive the intense solar heating at the focus, so the input power had to be estimated from other data.

The components were mounted on the ACTF tower, where 550 mirrors concentrated sunlight onto the receiver. The 20-centimeter-diameter window admitted 30 kW of sunlight with a flux density up to 200 W/cm^2. The receiver operation was monitored with thermocouples, pressure transducers, and laser probes that measured the absorption of light by the particle suspension.

RESULTS OF SOLAR TEST

Solar testing was conducted on 13 days for a total testing time of 35 hours. All major test objectives were met. The maximum output gas temperature was 750°C, and the output power exceeded 30 kW. "Burn out" or oxidation of the particles was achieved. The test established that concentrated sunlight can be absorbed directly within a working gas by small particles. The test also established that a window can be used successfully in a high-temperature environment and that carbon build-up on the window was not a problem.

Fig. 2 illustrates the test results by showing the chamber temperatures for two different particle loadings. The temperature of the output gas is indicated by the dashed line, and the average interior-wall temperature by the solid line. It can be seen that the gas temperature exceeds the wall temperature over the entire run. The increase in density of the particle suspension (from 0.46 to 0.88 gms/m^3) was accompanied by a dramatic rise in the gas temperature with almost no increase in the wall temperature. The large difference in temperatures between the walls and gas indicates that the gas-particle mixture was being heated directly by sunlight and not by the walls. This is an important result for future work because obtaining local-

ized heating in the gas is a key to achieving very high temperature radiant processing of chemicals.

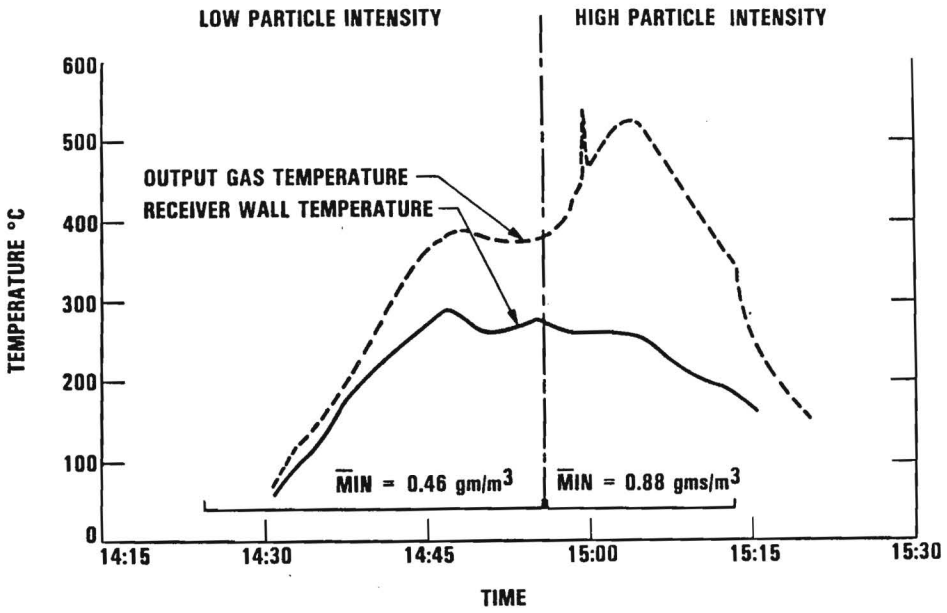

Fig. 2. Gas and wall temperatures vs. time.

ACKNOWLEDGEMENTS

The test program was supported by the San Francisco Operations Office of the Department of Energy, under the Assistant Secretary for Conservation and Renewable Energy, and the Director's Discretionary Fund under DOE Contract No. DE-AC03-76SF00098. The author would like to acknowledge the contributions of Leif Hansen, Donald Worth, Laurent Simionesco, Lauri Sariola and David Evans at LBL. The author would like to acknowledge the enthusiastic support of all the ACTF staff and in particular Tom Brown.

REFERENCES

Hunt, A. J. (1979). Proc. of the 14th IECEC, Boston, MA Lawrence Berkeley Laboratory Report LBL-8520.

Hunt, A. J. and Brown C. T. (1983). Lawrence Berkeley Laboratory report LBL 15807.

Hunt, A. J. and Evans, D. B. (1982) Report to the STTF Users Association, Lawrence Berkeley Laboratory Report LBL-13755.

OPTICAL PYROMETRY IN HIGH SOLAR FLUX ENVIRONMENTS

Paul Mackie
Engineering Experiment Station
Georgia Institute of Technology
Atlanta, Georgia 30332

Optical pyrometry is very appealing as a remote, non-contacting method of measuring surface temperatures, particularly in those cases where the attachment of thermocouples would be difficult, if not impossible (e.g. on glass surfaces). Furthermore, thermocouples are known to yield inaccurate results when direct radiative heating occurs (which can be a serious problem in concentrated solar beams). For optical pyrometry to be useful, two well-known problems have to be overcome: (1) all radiation not emitted by the sample of interest must be excluded from the pyrometer detector and (2) the in situ emissivity (which may be changing as the sample is heated) must be known.

The first problem (i.e. detection of non-emitted radiation) is frequently revealed by a sensitivity of the pyrometer to the incident solar spectrum. Of course, the indicated temperature is incorrect. In the extreme case found with a high concentrated solar beam, the reflected solar radiation can, in fact, saturate the pyrometer electronics. With the Barnes series of pyrometers, this saturation is exhibited by the pyrometer outputting a fixed signal of -0.4 volts. To achieve solar blindness one needs a pyrometer which is sensitive only to wavelengths not present in the incident spectrum. One could use an atmospheric absorption band to "filter" the incident radiation and observe the emitted radiation at that wavelength. However, the detected signal would then be sensitive to differences in signal path length and to variations in atmospheric conditions. We chose instead to make use of the absorption band of the glass in the heliostats used to concentrated the solar beam. Figure 1 shows an infrared transmission

spectrum for one thickness (3 mm) of the glass used in the heliostats at the Advanced Components Test Facility (ACTF). Starting at 4.5μm and extending to at least 14μm the transmission is essentially zero. We chose a wavelength of 4.7μm since it is above the 4.5μm cut-off of the glass and avoids the CO_2 and H_2O absorption bands of the atmosphere (see Figure 2). The shorter wavelength was chosen rather than some longer wavelength such a 8μm to enhance the sensitivity of the pyrometer. The bandwidth of the filter is 0.1μm. In Figure 3 (an expanded view of Figure 2) we can more clearly see the relative position of the detector response band at 4.7μm to the H_2O and CO_2 absorption.

This 4.7μm pyrometer has proven to be effectively "solar blind" to the presence of solar concentrations up to 2400. Objects in the concentrated solar beam known to be cool (e.g. water cooled shields, etc.) are measured as cold within the lower limit of this instrument ($\sim 200^{o}$ C).

While the above narrow band single-wavelength instrument addressed the problem of solar blind optical pyrometry it still can only give accurate results if the emissivity is known (and known at temperature and as the surface conditions change). The second optical pyrometer we have designed (construction is now nearing completion) addresses this problem of needing to know the ε in real-time to obtain accurate measures of the temperature. This pyrometer design is based on a broad-band response pyrometer (1μm to 5μm) with computer-controlled narrow-band interference filters to allow the selection of one of four different narrow spectral bands.

The idea is to make more use of the information contained in the emit spectrum to simultaneously determine the temperature and emissivity of the sample. A similar approach is taken with the commercial two-color pyrometers, where one measures the emitted radiances in two bands. One ends up with two equations and three unknowns (the temperature and the ε at eac

wavelength). By introducing a constraint on the permissable values of the emissivities, one can then solve the two equations for the temperature and emissivities. The usual assumption is that $\varepsilon(\lambda_1) = \varepsilon(\lambda_2)$; that is, the body is assumed to be grey. This is by no means the only constraint that could be used with the two color radiance information. In fact, with our four-color pyrometer we will relax the constraint and allow conditions other than grey body.

In what follows, I will present some of the theory of extracting emissivity and temperature from multi-band radiance measurements, for more details one should read the papers of Svet (e.g. Svet, D. Ya, Sayapina, V. I., Levchuk, V. V., Ezhova, T. N. and Parfinovich, A. F.; High Temperatures-High Pressures, 1979, Vol. II, pp. 117-118.). Let us define the radiance at a given λ and T as:

$$R(\lambda,T) = \varepsilon(\lambda,T)R_B(\lambda,T) \qquad (1)$$

where R_B is the Planck distribution. And let us form a function I defined as:

$$I = \frac{R_1R_2}{R_3R_4} = \frac{\varepsilon_1\varepsilon_2}{\varepsilon_3\varepsilon_4}\frac{R_{B1}R_{B2}}{R_{B3}R_{B4}} \qquad (2)$$

We shall show that for certain assumptions about the emissivities that

$$\frac{\varepsilon_1\varepsilon_2}{\varepsilon_3\varepsilon_4} = 1 \qquad (3)$$

If equation (3) is valid it then becomes straight forward to solve equation (2) for the temperature, and once the temperature is known one can solve eq. (1) to obtain an emissitivity at each of the observed wavelengths and at the observed temperature.

Let us assume a series expansion for the natural log of the emissivity

$$\ln\varepsilon = \sum_{i=0}^{m} a_i\lambda^i \qquad (4)$$

One should note that no assumption has been made that the a_i's are independent of temperature. We will in fact, assume that the a_i's are changing with

temperature at a rate which is slow compared to the time it will take to measure the radiances at all four wavelengths ($\sim$2 to 5 seconds). If we restrict the series expansion (4) to only the first two terms

$$\ln\varepsilon = a_o + a_1\lambda \tag{5}$$

we have an emissivity model which incorporates both the black-body and grey body cases as well as giving us an additional degree of freedom. For the black-body case $a_o = a_1 = 0$ and for the grey-body case a_o = constant and $a_1 = 0$.

Substituting equation (5) into equation (2) we obtain for the emissivity factor

$$\frac{\varepsilon_1\varepsilon_2}{\varepsilon_2\varepsilon_3} = \frac{e^{a_1\lambda_1}e^{a_2\lambda_2}}{e^{a_3\lambda_3}e^{a_4\lambda_4}} \tag{6}$$

Equation (6) can be simplified to:

$$\frac{\varepsilon_1\varepsilon_2}{\varepsilon_2\varepsilon_3} = e^{a_1(\lambda_1 + \lambda_2 - \lambda_3 - \lambda_4)} \tag{7}$$

Now if one is careful to select the wavelengths such that $\lambda_1 + \lambda_2 = \lambda_3 + \lambda$ than equation (3) is obtained and the emissivity factor becomes an invaria of the measurement process.

The selection of wavelengths to obtain an invariant emissivity factor must be made with the solar blindness requirements satisfied as well (i.e. the selected λ's must fall within either the glass or atmospheric absorpti bands). For our current four-color pyrometer two of the wavelengths fall above the glass cut-off while the other two occur in atmospheric CO_2 band Construction of the four-color pyrometer should be completed by November and initial measurements taken not long after.

Figure 1

ra-red Transmission of
F Heliostat Glass.

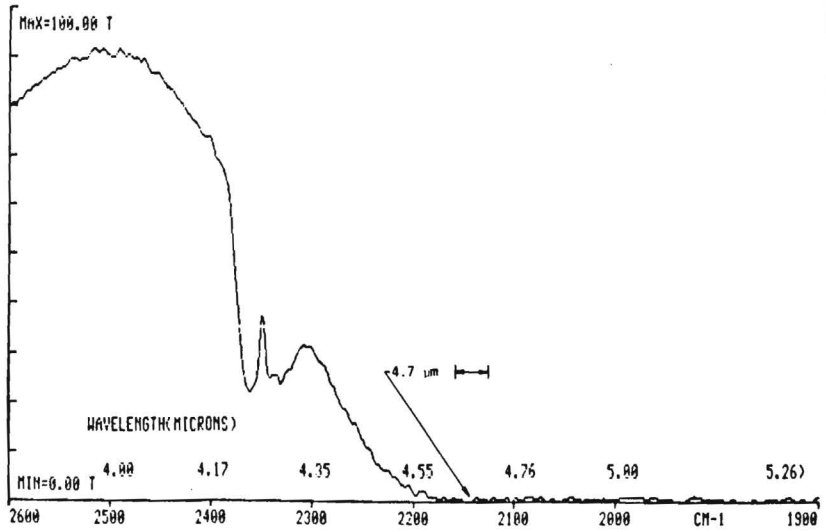

Figure 2

spheric Absorption Bands.

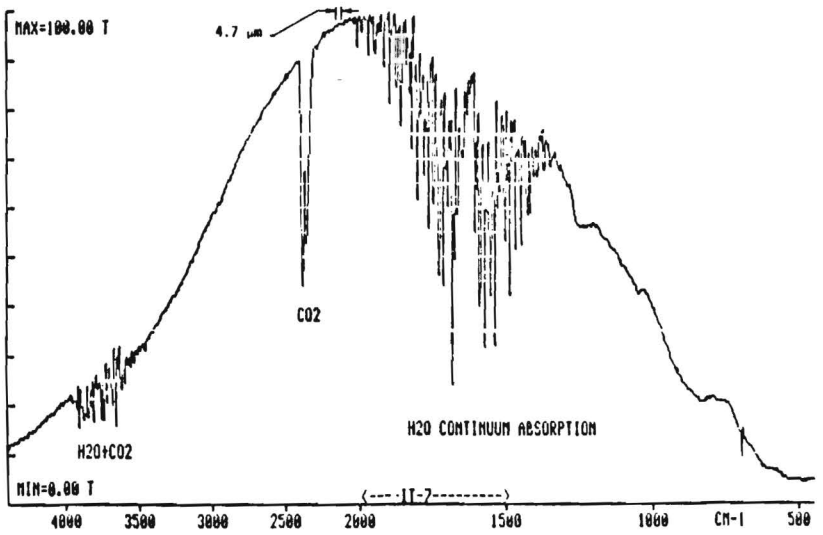

Figure 3

pheric Absorption Bands
ded View of Figure 2.

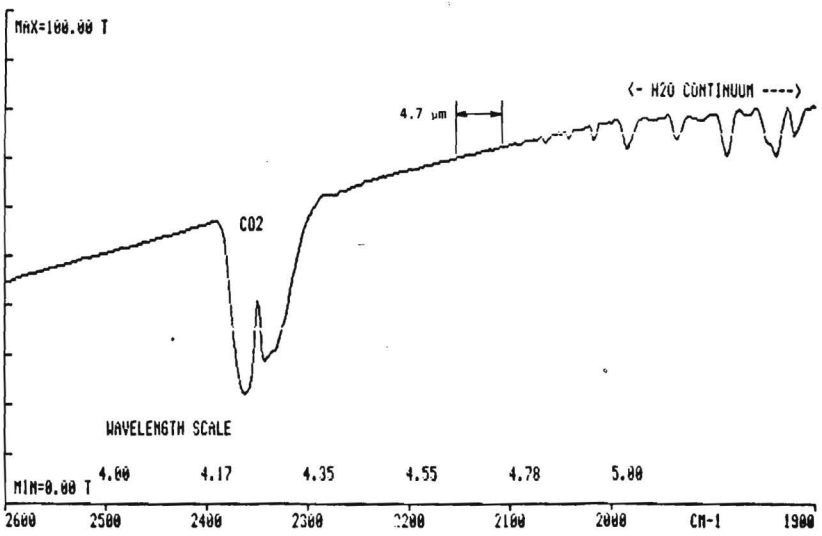

ACTIVITIES AT THE CENTRAL RECEIVER TEST FACILITY 1982 - 1983

John T. Holmes and Cheryl Maxwell*

Division 6222
Sandia National Laboratories
Albuquerque, NM 87185

Solar Thermal Research Workshop

Georgia Institute of Technology

September 7, 8, 1983

INTRODUCTION

Over the past two years, the Central Receiver Test Facility (CRTF) has assembled a major solar central receiver test program called the Molten Salt Electric Experiment (MSEE). In addition to this program, the CRTF has conducted a variety of facility development tests and has simulated chemical and nuclear thermal effects on materials and components.

MOLTEN SALT ELECTRIC EXPERIMENT

Construction of the solar Molten Salt Electric Experiment (MSEE) was completed in August 1983 at the Central Receiver Test Facility (CRTF) near Albuquerque, NM. The MSEE uses a molten salt as its solar receiver and thermal storage working fluid and uses water/steam as its electric power generating working fluid.

The molten sodium nitrate (60 percent) and potassium nitrate (40 percent) salt melts at about 430°F (220°C). Because it is chemically stable in air and has a low vapor pressure at high temperatures, it is an ideal medium for storing heat for use in cloudy weather or at night. The MSEE integrates the existing CRTF heliostat field, 5 MWt solar receiver, 7 MWH thermal storage system, a new 3 MWt steam generator, a used 0.75 MWe turbogenerator, and a digital process control system. Figure 1 is a photo of the CRTF indicating the location of the major MSEE subsystems. The amount of electricity that will be produced by the MSEE is sufficient for about 250 homes.

The MSEE design effort was started in late 1982. In order to meet a timely start up schedule, construction was performed as design details were completed. A previously operated solar receiver and a thermal storage subsystem were both

---

*Cheryl Maxwell is an employee of Technadyne, on contract to Sandia National Laboratories.

refurbished after having been stored for over one year. A new steam generator was designed, built, and installed by one of the industrial participants. A surplus turbogenerator was located, refurbished and installed. The existing CRTF heliostats and distributed, digital process control system are being used for the MSEE.

The organization and funding of the MSEE is unique. This program is a cooperative venture that combines government, utility and industrial funding, material design efforts, and operational expertise. The participants are:

U.S. Department of Energy and Sandia National Laboratories
Electric Power Research Institute with
- *Arizona Public Service*
- *Southern California Edison*
- *Pacific Gas and Electric*
- *Olin Chemical*
- *Arizona Energy Commission*

Black and Veatch
Martin Marietta
McDonnell Douglas
Babcock and Wilcox
Public Service Company of New Mexico
Foster Wheeler

The government (Department of Energy) is providing the use of the CRTF, through Sandia National Laboratories. In late 1983 and 1984, commercial utilities will receive hands-on training for teams of operations engineers and technicians. The Department of Energy will support the operation and maintenance of the MSEE through its characterization and training programs.

An overall functional schematic of the MSEE is given on Figure 2.

Solar Receiver - The solar receiver was designed by the Martin Marietta Company and underwent over 500 hours of testing at the CRTF in 1980 and 1981. The receiver is a flat vertical panel that has 288, 0.75 in OD Incoloy 800 tubes. The overall size is 13 ft by 18 ft. It uses the molten salt working fluid. The flow of salt enters one side of the panel and flows across the panel in an up and down serpentine pattern. Its thermal capacity is 17×10^6 BTU/hr (5 MW). The inlet and outlet salt temperatures of 550 F (288 C) and 1050 F (566 C) and the salt flow rate is about 1380 lb/min (630 kg/min). The receiver is located atop the 200 ft (61 m) tall CRTF tower. The cold, inlet salt is pumped from ground level to the receiver by a 40 hp cantalevered centrifugal pump.

Thermal Storage - The thermal storage system was also designed by the Martin Marietta Company. It underwent about 100 hours of operation in 1981 and 1982. The thermal storage system has a 7 MWH capacity. The hot salt tank (1050 F) is a unique design that has a pleated Inconel liner that was developed for liquid natural gas storage and transportation tanks. The system also includes a carbon steel lined cold salt storage tank (550 F) and associated pumps, piping, and valves. A hot salt pump provides salt from the hot tank to the steam generator and back to the cold tank.

Steam Generator - *The steam generator is a new component, not previously tested. It was designed by the Babcock and Wilcox Company. It supplies steam to the turbogenerator using a forced circulation evaporator, steam drum, and superheater. The steam to the turbine is at 940 F (504 C) and 1100 psi ($7.6x10^6$ Pa). The steam generator has a 3 MWt capacity and can operate about two hours on hot salt from the thermal storage system or as long as the solar receiver is in operation.*

Electric Power Generating System - *A surplus, General Electric turbogenerator that was used aboard the USS Norfolk from 1951 to 1974 will produce the electrical output of the MSEE. It has a 0.75 MWe capacity. The condenser is cooled by a dry cooling tower, using a mixed water - ethylene glycol cooling fluid. The electrical output is fed into the local grid and is sufficient to power about 250 households.*

Master Control System - *The MSEE is controlled by a distributed digital process control system manufactured by the EMC Company. This process controller integrates all of the thermal and electrical processes. Heliostat control is not integrated into the overall process control scheme at this time. The MSEE controls are supported by a hard-wired, relay-logic system that automatically provides for safe shutdown in the event that the control computers, critical hardware components, or operating electrical power fails.*

System Characterization - *During the fall of 1983, the MSEE components and subsystems will be operated separately and eventually integrated into the full MSEE operating system. This part of the program is being coordinated by the Martin Marietta Company using CRTF engineers and technicians as support. At the end of this phase of MSEE operations, the system will have been characterized regarding its operating capabilities and all anticipated faulted conditions will have been demonstrated.*

Utility Training - *As soon as the characterization phase is completed, electric utility teams will reside at the CRTF for hands on experience with this new technology. To date, nine utility companies have shown interest in this phase of the MSEE. Training and coordination of this work will be provided by the McDonnell Douglas Company with support from the CRTF operations and maintenance engineers and technicians. This program will provide the utilities with information and experience useful in evaluating the technology.*

MSEE Summary - *For the first time, the molten salt heat transfer working fluid will be used in an integrated system that converts sunlight to electricity via a thermodynamic cycle. The power produced will be fed into the local utility grid. Industry and utility participants will gain first hand experience with this technology so they can evaluate it for future commercial application.*

NON-MSEE OPERATIONS AT THE CRTF

The CRTF has recently initiated an experimental evaluation of the HELIOS optical model. This involves comparison of calirometric and flux gage array measurements with the HELIOS predictions at two locations on the CRTF tower. The goal of this work is to either confirm the HELIOS model or develop appropriate modifications so it will accurately predict the power and flux density contours for experiments located anywhere on the CRTF tower.

Preliminary data has been taken and the experiment is being refined to provide improved measuring accuracy.

A program to evaluate high temperature materials for long term use in central receiver or other solar thermal systems has been initiated. Over 100 candidate materials have been selected. During 1983, ranking of the materials, based on their failure thresholds and cost, will be done at the 16 KW Solar Furnace located at the CRTF. Preliminary results indicate that cost effective materials are available. Previous testing has shown that most materials fail at lower flux levels, when exposed to the solar beam on the tower, therefore, additional full scale materials tests will be conducted on the CRTF tower in 1984.

Loss of coolant in a nuclear reactor may lead to a major fuel melt down. This must be limited by the reactor containment building structure. Magnesium oxide bricks, for possible use in the building foundation, have been exposed to a high flux density solar beam to determine the effect on these bricks in this simulated melt down thermal environment.

A fuel melt down in a water cooled nuclear reactor can be accompanied by the release of hydrogen (metal/water reaction) to the reactor containment vessel. The CRTF beam has been used to simulate the thermal effect of the hydrogen/air burn on critical control systems and instrumentation that are located inside the reactor containment.

The CRTF one meter square shutter (0.7 sec. time constant) has been used to simulate the thermal effects of a nuclear weapon explosion on a variety of paints and coatings used by the Navy and on a chemical detector that is used by ground troops.

FUTURE TESTS AT THE CRTF

Future tests to be conducted at the CRTF include additional thermal effects as well as new solar receiver tests. A falling, solid particle receiver designed by Sandia National Laboratories in Livermore, California is being developed fo testing at the CRTF. Thermal effects experiments include testing of a full scale nose cone of a reentry vehicle. The test will include the nose cone material, radar window material, and radar transmission studies. An ambitious schedule of testing ceramic bricks for nuclear reactor containment building foundations is also planned.

The solar furnace will be used for high temperature material evaluations, flux gage calibrations, and for simulation of thermal effects from a nuclear blast on about 300 paints and coatings for the US Army.

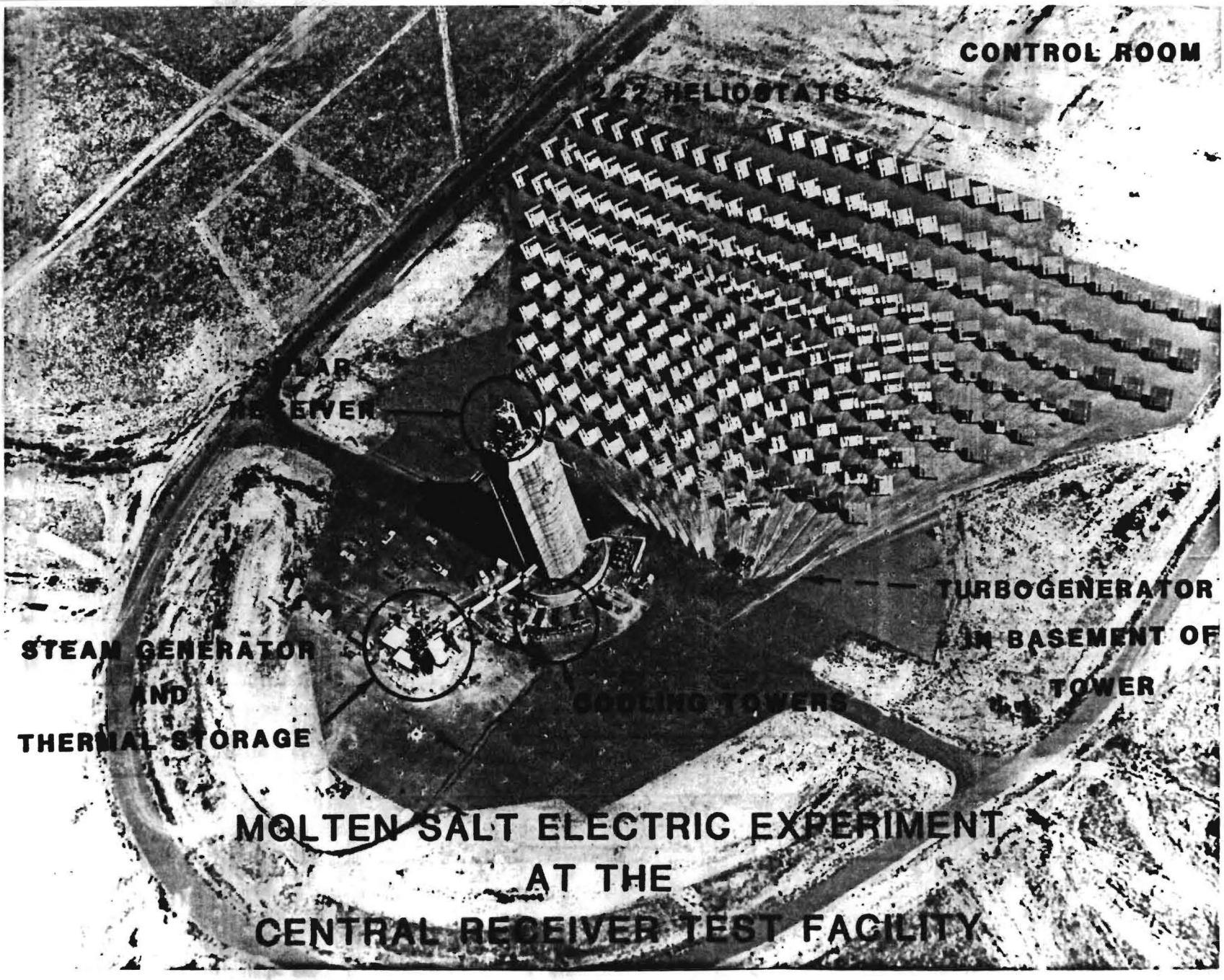
CONTROL ROOM
HELIOSTATS
TURBOGENERATOR
IN BASEMENT OF
TOWER
STEAM GENERATOR
AND
THERMAL STORAGE
COOLING TOWERS
MOLTEN SALT ELECTRIC EXPERIMENT
AT THE
CENTRAL RECEIVER TEST FACILITY

MOLTEN SALT ELECTRIC EXPERIMENT

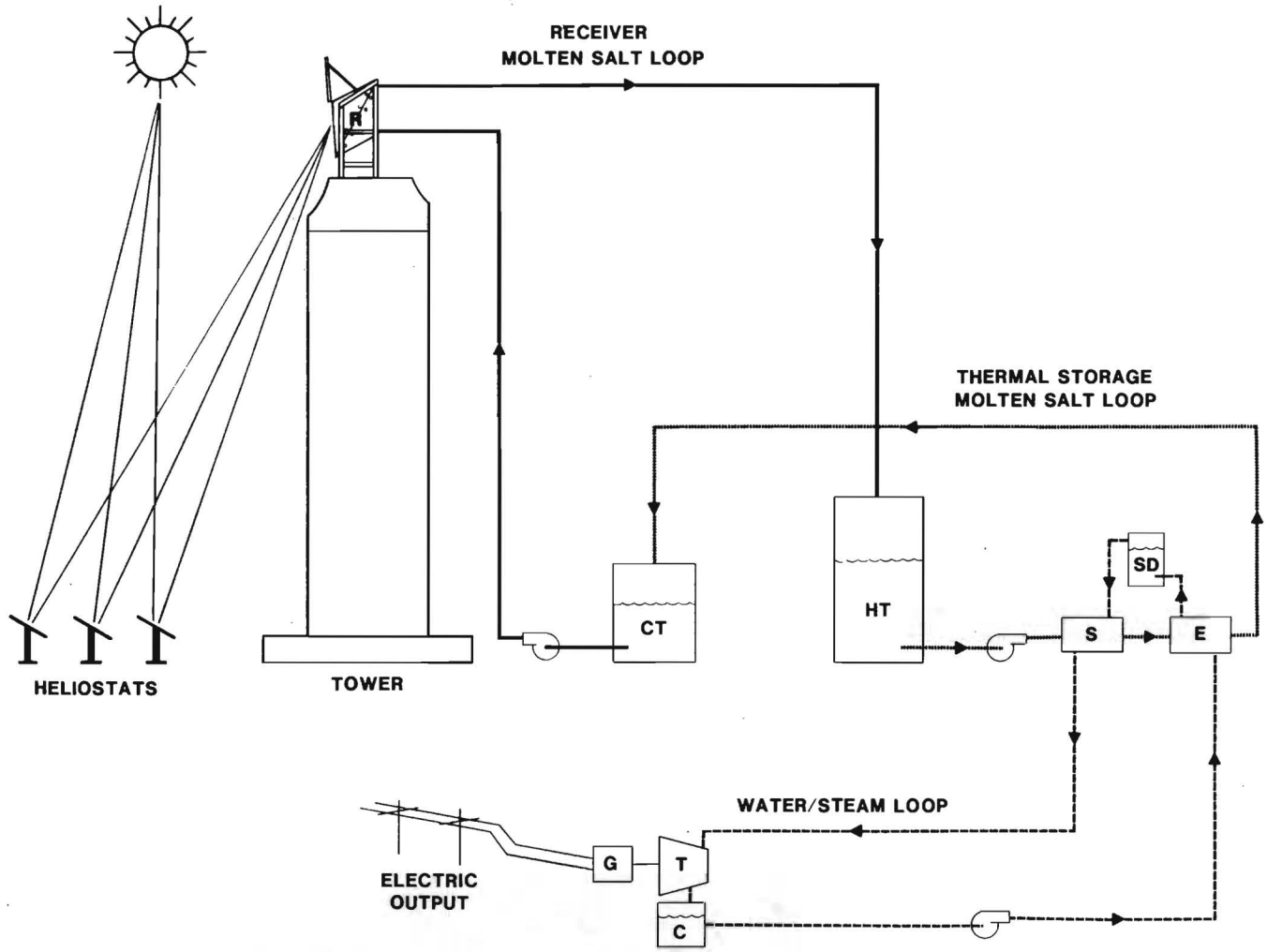

C -- CONDENSER
CT - COLD TANK
E -- EVAPORATOR
G -- GENERATOR
HT - HOT TANK
R -- SOLAR RECEIVER
S -- SUPERHEATER
SD - STEAM DRUM
T -- TURBINE

AN OVERVIEW OF RECENT DEVELOPMENTS AT THE PARABOLIC DISH TEST SITE*

Darrell L. Ross
Jet Propulsion Laboratory
California Institute of Technology
Pasadena, California

INTRODUCTION

The Parabolic Dish Test Site (PDTS) was established in 1978 for the Department of Energy by the Jet Propulsion Laboratory (JPL), a part of Caltech. It was established for the purpose of testing and evaluating parabolic dishes at the component, subsystem and system (or module) level. The PDTS is located on Edwards Test Station (A JPL facility), which in turn is located on Edwards Air Force Base. The test site is situated approximately a hundred miles north of Los Angeles. Figure 1 shows two identical Test Bed concentrators, 11 meters in diameter (on the right) and a single 12 meter diameter concentrator (on the left) designated Parabolic Dish concentrator Number One.

This paper reports on the results of investigations into three different problems: (1) developing a method of rapidly aligning the mirror facets on a Test Bed Concentrator, (2) effects on insolation levels at the PDTS because of the El Chichon Volcanic eruption, and (3) developing a receiver aperture material that will withstand a sun walk-off.

TBC Rapid Alignment Method

There are 220 mirror facets on each Test Bed concentrator, which must be individually aligned. This is a process that has required one to two weeks of nightime work in the past. While this alignment is in process, no testing can be accomplished during the day, thus it is very desirable to minimize alignment time which tends to maximize testing time. For this reason, a much more rapid method of aligning the facets was sought.

The approach used to solve this problem was to develop a computer program that will calculate and outline the aim point on a target for each mirror facet (the computer program used was developed by T. B. Elfe of Georgia Tech). Two targets were created - one for the center mirrors and a second one for the outer mirrors. The target for the center mirrors was placed thirty inches in front of the nominal focal plane and the target for the outer mirrors was placed thirty inches behind the nominal focal plane, both on axis. Figure 2 shows the two targets mounted near the focal plane of Test Bed concentrator Number one (TBC-1). The technique used then is to adjust each mirror to overlay the aim point with its own discrete image. This was accomplished with all mirrors exposed, instead of (as previously done) covering all mirrors except the one that is being aligned.

* The work described in this paper was carried out or coordinated by the Jet Propulsion Laboratory, California Institue of Technology, and was sponsored by the U.S. Department of Energy through an agreement with the National Aeronautics and Space Administration.

This eliminates the usage of a cherry picker in covering and uncovering mirrors, thus significantly reducing the time involved and enhancing the safety aspects of the operation, since the cherry picker is being operated at night right next to the mirror facets. TBC-1 was realigned using this technique.

The conclusions reached after the alignment was completed are the following (1) the technique was proven to work very well by realigning TBC-1 mirror facets in two nights instead of the usual one to two weeks previously required, (2) aligning the center mirrors proved to be more difficult than anticipated because of overlapping images. This simply meant being very careful in the alignment process which translated to more time required than planned on, and (3) the first alignment was a significant learning process that will make subsequent alignments much easier and faster. Future alignment of a TBC can be accomplishe in one night with trained personnel. Information for this section was gathered with the help of M. J. Argoud, Member of the Technical Staff at JPL.

El Chichon Volcanic Eruption and PDTS Insolation

Since the El Chichon volanic eruption in Mexico on March 28, April 3, and 4, 1982, there have been reports from various solar sites in the United States of its effect. It was decided to determine the effect (if any) of these eruptio on insolation levels at the PDTS. Having this data would then enable a comparis to be made of volcanic effects at solar sites throughout the United States.

The approach employed to make this comparison was to compare the direct normal energy at the PDTS for the summers of 1981, 1982 and 1983, or in other words compare data for a year before the explosion, the summer shortly after the explosion and a year after the explosion. Secondly, determine the effect on peak insolation levels for the same period of time. This information is compiled in Tables 1 and 2 below.

TABLE 1

COMPARISON OF DIRECT NORMAL ENERGY AT
ETS FOR THE SUMMERS OF 1981, 1982 and 1983

	1981 kW-HR/SQ-METER/DAY	1982 kW-HR/SQ-METER/DAY	1983 kW-HR/SQ-METER/DAY
June	10.93	8.78	9.62
July	10.09	9.21	10.05
August	9.44	7.71	7.68

TABLE 2

COMPARISON OF PEAK DIRECT NORMAL INSOLATION LEVELS AT ETS FOR THE SUMMERS OF 1981, 1982, 1983

	1981 AVG. FOR TOP 3-DAYS W/SQ-METER	1982 AVG. FOR TOP 3-DAYS W/SQ-METER	1983 AVG. FOR TOP 3-DAYS W/SQ-METER
June	1025	984	956
July	1026	967	995
August	1040	960	967

The conclusions reached after studying the data were the following: (1) there was a greater decrease in direct normal energy at the PDTS for June, July and August of 1982 vs. 1981 as compared to the decrease in peak insolation for the same period: 8.7% to 19.7% vs. 4.0% to 7.7%, (2) there was a smaller decrease in direct normal energy at the PDTS for 1983 vs. 1981 for June, July and August as compared to the decrease in peak insolation for the same period: 0.4% to 18.6% vs. 3% to 7%, and (3) another significant difference between 1982 and 1981 (also between 1983 and 1981) was the decrease in the number of days 1,000 w/sq-meter or greater in 1982 and 1983. There were 29 days in June through August of 1981 that equaled or exceeded 1,000 w/sq-meter. For the same months in 1982 and 1983, there were zero days in 1982 and one day in 1983 where the insolation level was greater than or equal to 1,000 w/sq-meter. Further, there was a hiatus of thirteen months (from end of May 1982 until July 1983) during which time there were zero days of 1,000 w/sq-meter or greater. Material for this section was acquired with the aid of C. K. Miyazono, Member of the Technical Staff at JPL.

Aperture Plate Materials for Solar Thermal Dish Collectors

When a parabolic concentrator is tracking the sun, a malfunction may cause the concentrator to stop following the sun. In this event, the use of protective materials that can withstand exposure to walk-off conditions, without active cooling provides significant advantages. The problem then is to find an existing material that can be used in making a receiver aperture plate that will withstand a walk-off of the spot of concentrated sunlight at the focal plane. Secondly, this material must be able to withstand a large number of cycles of solar acquisition and de-acquisition, as well as solar spillage. The approach used was to conduct a series of tests (at the focal plane of a TBC) on a wide range of materials that are likely to survive under high temperature and high flux level conditions. The top materials or the best material would then be selected to use in eventually building an aperture plate for existing and future concentrators.

Materials tested as possible candidates for walk-off protection were each subjected to an exposure of concentrated sunlight at the focal plane at a flux

density of 7,000 kW/sq-meter for fifteen minutes or until the sample failed, whichever was less. The types of materials tested under simulated walk-off conditions included: graphite, silicon carbide, silica, various silicates, alumina, zirconia, aluminum, copper, steel and polytetrafluoroethylene. The only material tested under simulated solar acquisition, de-acquisition and solar spillage conditions was grade CS graphite. It was tested for up to 2,000 cycles simulating 1 second periods of acquisition at the same flux density as the walk-off test. Grade CS graphite was also tested at solar spillage levels of 1 to 2%.

The test results were as follows: (1) of all the materials tested, the only material that neither cracked nor melted was grade G-90 graphite, a premium grade. See Table 3 for a summary of materials tested. Grade CS graphite, a lower cost commercial grade, cracked halfway across, but did not fall apart. With proper design, this grade should probably perform satisfactorily as a receiver aperture plate, (2) for the simulated sun acqusition test on the grade CS graphite sample, the loss in 2,000 cycles at moderate to high winds was about 5 mm in thickness or 3% of the sample mass; this appears to be tolerable, and (3) at solar spillage levels of 1 to 2%, the lip temperature of grade CS graphite was 150 to 300°C (300 to 570°F), low enough to provide adequate lifetim of this material with respect to oxidation. For more detailed information as well as additional data see the reference.

RERERENCE

1. L. D. Jaffe, "Solar Tests of Aperture Plate Materials for Solar Thermal Dish Collectors," JPL Document 5105-121, June 30, 1983.

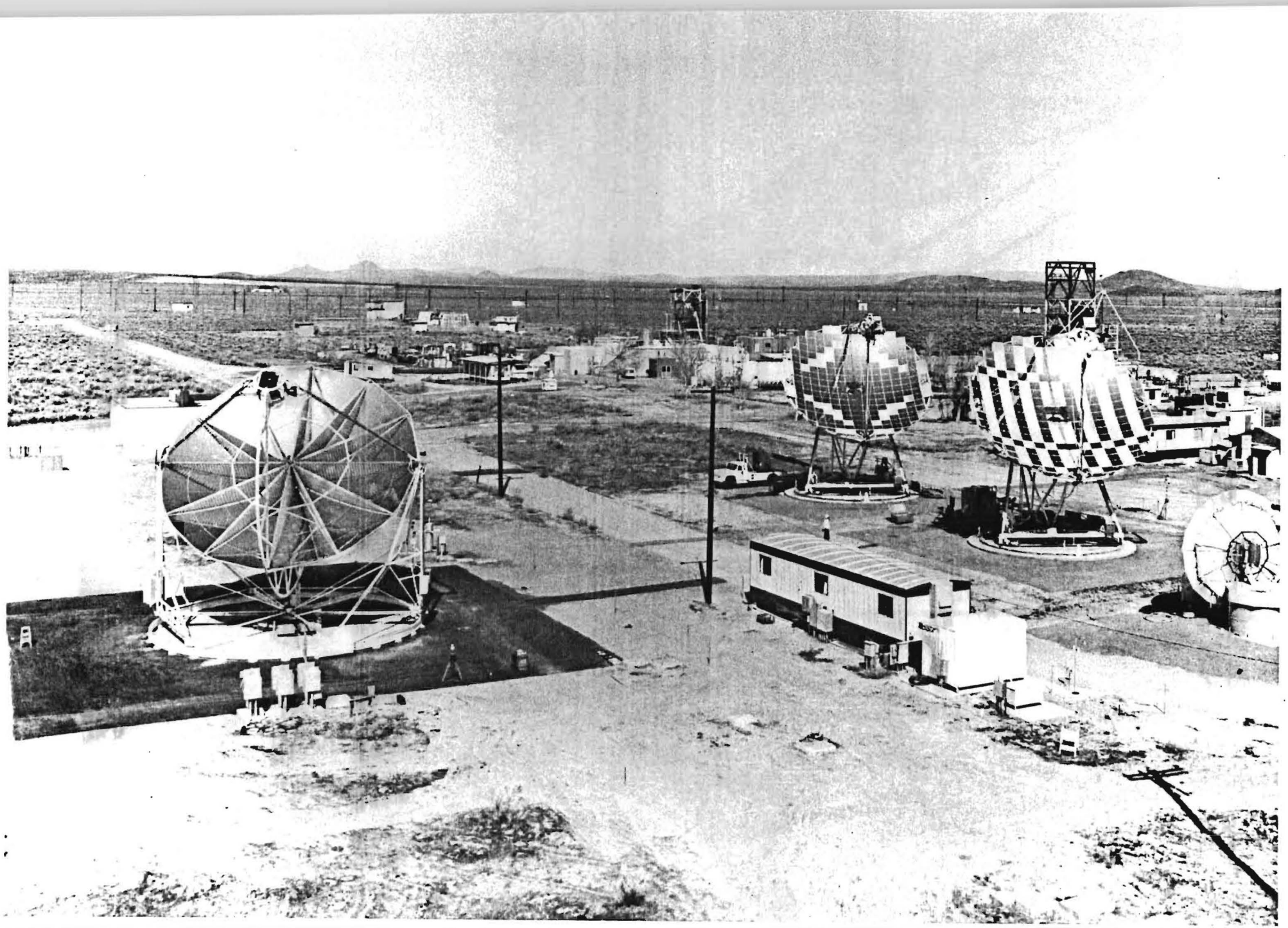

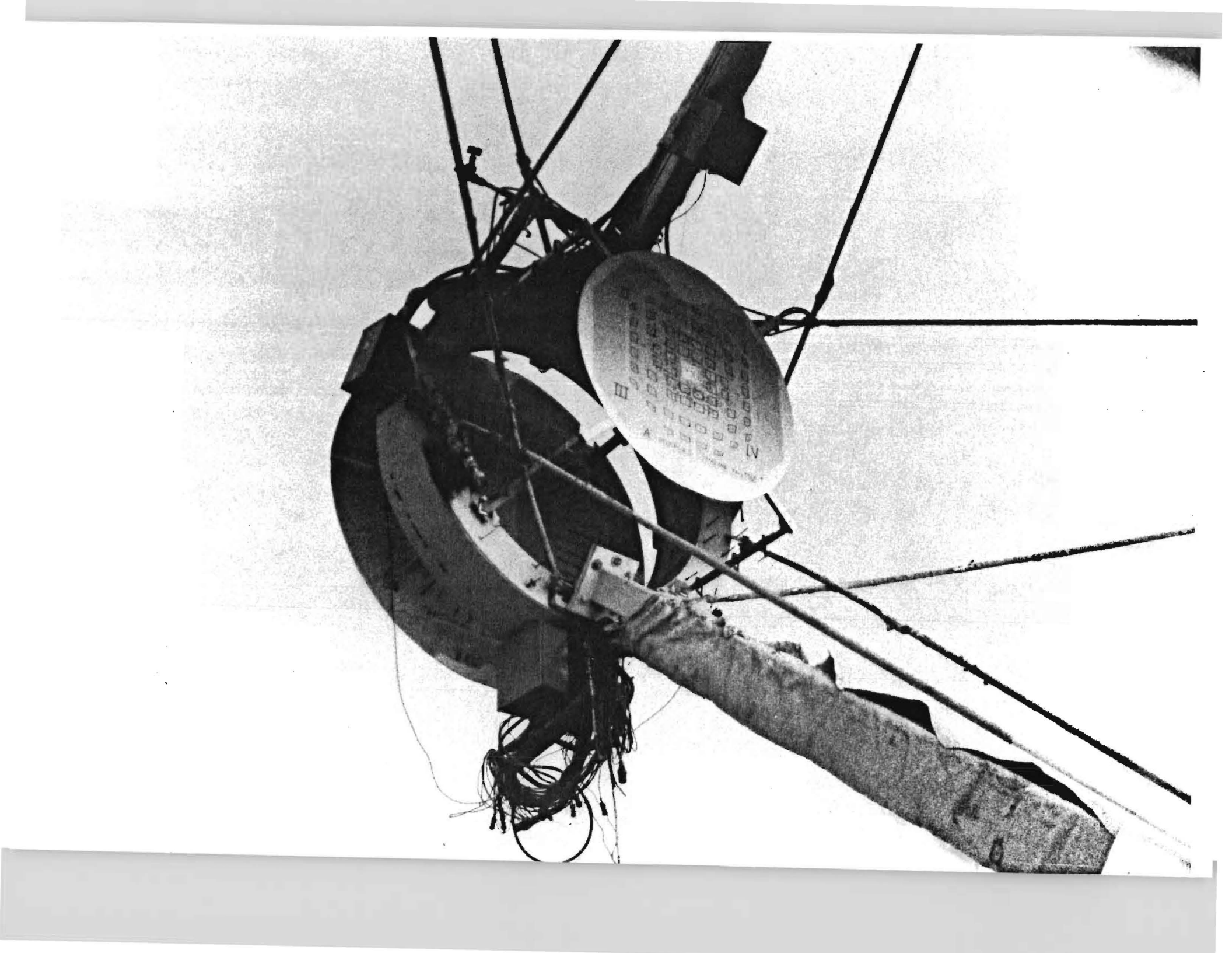

Table 3

Summary of Results of Walk-off Tests

Material Type		Thickness (mm)	Failure Mode	Time
Graphite	3499	26	Shattered	1 to 8 min
	8826	26	Shattered	1 to 1-1/2 min
	CS	14-50	Cracked halfway (1 of 10 survived)	10 s to 14 min
	HLM-85	24-26	Shattered	1 to 1-1/2 min
	G-90	24-25	(Survived)	30 min
	Cloth	0.4	Holed	30 s
SiC		6-32	Shattered	1 s
SiO_2	Slipcast, high purity	18-21	Slumped	1-1/2 to 4 min
	Slipcast, commercial	20-26	Dripped	10 s
	Fibrous, glazed	41	Dripped	7 s
Silicates	Mullite	32-38	Melted	1 to 4 s
	Processed kaolin	27	Melted	3 s
	Cordierite	25	Melted	2 s
	Alumina-boria-silica	0.5-0.7	Melted	1 s
Al_2O_3	Paper	0.4-1.4	Melted	2 to 6 s
ZrO_2	Cast & sintered	29	Melted	20 s
	Fibrous board	25	Melted	1 min
	Cloth	0.5	Melted	8 s
Copper		26	Melted	1 to 3 min
Aluminum		1.8	Melted	1 s
Steel		2	Melted	2 s
Polytetrafluoroethylene		38	Melted	2 min

HIGH TEMPERATURE LARGE SCALE SOLAR THERMAL ENERGY UTILIZATION AT THE CNRS 1 MW SOLAR FURNACE

C.Royère
Engineer
1 MW Solar Furnace Scientific and Technical Manager
Solar Energy Laboratory
CNRS - Odeillo - France

I - Introduction and Summary

II - Historical and technical Background of the 1 MW Solar Furnace :

1 - main milestones of Félix TROMBE activities with CNRS support in the field of direct solar radiation point focussing for achieving high temperatures

1-1- Meudon searchlights (1946)

1-2- Montlouis 2 and 50 kw heliostat type facilities (1949)

2 - Useful outcomes and utilizations of the Montlouis 50 kw facility (until 1967)

2-1- Benchmodel for developping design criteria and construction techniques of large scale point focussing facilities

2-2- Designs and experiments of specific techniques for the use of solar radiant heat :

- materials processing : high temperature inorganic chemistry (refractory materials) and metallurgy (refractory alloys)
- materials evaluation : thermal shocks resistance and ignition tests

3 - Other facilities in the world designed and built after Montlouis furnace in the range of 50 kW :

3-1- Natick/White Sands US Army facility (1958),(1973)

3-2- Sendaï Tohoku University,Japan (1963)

3-3- Odeillo French Army (1971)

4 - Typical features of point focussed solar radiant heat

4-1- achievement of high temperatures up to 3000°C under the presence of air

4-2- large scale units feasible (industrial process heat)

4-3- in comparison with arc furnace,high frequency furnace, electron,beam,laser heating and arc image furnace

4-3- direct and local heat inputs (direct heating)

4-4- possibility of flux shaping (thermal shocks)

4-5- clean and free environment around the focal spot (high purity materials processing, electro magnetic windows evaluation)

4-6- no special constraint from the heat source concerning the use of a protective gaseous atmosphere (air or any gas behind a proper window)

4-7- wavelength range of the radiant heat spectrum

III - The Odeillo 1 MW Solar Furnace Facility

A - Description

1 - flat heliostat unit

1-1- dimensions and design

1-2- facetted reflector

1-3- hydraulic actuators

1-4- closed loop tracking (sun rays sensors)

2 - 63 héliostats field

2-1- field design (illsided terraces, quincunces display, shadowing and blocking)

2-2- stow position

2-3- land use and accessibility

3 - parabolic concentrator

3-1- dimensions

3-2- facetted reflector (mirrors material and bending mechanism)

4 - focal building
  4-1- heliostat field control room
  4-2- focal room

B - Operation
1 - acquisition and tracking (steady or transcient : clear or partly clouded sky)
2 - all field or part field operation (flux and flux distribution control)
3 - typical solar direct radiation data at the site (hours of insolation above different levels yearly and monthly available, expectable continuous operation capabilities for different timelength durations)
4 - typical performances
  4-1- flux
  4-2- flux densities
  4-3- circumsolar radiation
5 - maintenance related topics
  5-1- minor concern :
    - general maintenance : mechanics, hydraulics, optics, electronics
    - environment effects : wind, hail, snow, lightning
    - mirror facets breakage
  5-2- special concern
    - mirrors soiling frequency has been increasing in the recent past years (North African soil dust particles wind carried and deposited by short showers : red showers)
    - clearness of the sky affected by unusually prevailing south wind
    - mirrors back coatings aging

C - Testing equipments
1 - data acquisition system and storage
2 - data processing : graphic terminal computer and plotter
3 - flux and flux density and temperatures measurements
4 - flux shaping (under air or specific gases)
5 - dummy cavities for flux mapping

6 - different types of furnaces for materials processing
7 - flux gages calibration capabilities
8 - computer code for flux predictions

IV - Typical and recent utilizations of the 1 MW facility

A - Testing activity under contracts with customers charged on a cost sharing basis .

1 - General background

1-1- financial return aspect of the facility

1-2- scientific and technical benefit aspect

2 - Inorganic materials clean processing

2-1- temperature and quantities ranges

2-2- materials : glassy and refractory compounds

2-3- processes : liquid phase synthesis, purification, roasting, volatilization, quenching, spheroïdization

2-4- examples

- stabilized zirconia (calcia, magnesia or yttria doped) for refractory ceramics industry: solid particles spheroïdized from the melt at 2700°C
- aqueous gels of vanadium pentoxide from the liquid phase at 800°C

2-5- processes temperatures and rates control

3 - Metallurgy

3-1- windowed processing techniques

3-2- large ceramic crucibles making

3-3- refractory alloys metallurgy

3-4- casting oxygen free compounds : the boron example

4 - Materials evaluation under radiant heat

4-1- radiant thermal energy effects related problems

4-2- fields of applications concerned : defence (nuclear weapons, rockets, lasers) space and astronautics (thermal shields), steelplants, energy (nuclear reactors and solar thermal energy)

4-3- flux shaping capabilities (from 50ms up to several hours)

4-4- electromagnetic windows evaluation

- nose cones

- Ariane's payload thermal protection
- Starprobe thermal shield
- multilayer composite materials behaviour
- shielding materials for solar thermal power plants components

B - Benchscale solar thermal receivers testing activity

1 - Background

1-1 Facility capabilities : power level, items sizes, test duration

1-2 Accomplishments in this field :
ERDA water steam cavity receiver 1976
CNRS benchscale solar power plant (oil cooled receiver, thermocline storage and grid connected electric power plant)

2 - Ongoing receivers testing

2-1 air cooled receiver : CNRS SIROCCO project

2-2 high temperature solar heat loop : particulate solid heat carrier (receiver and storage) for industrial heat and ore processing)

V - High temperature solar heat related research activites in progress .

1 - General rationale

1-1 medium and high temperature solar heat : large scale solar thermal facilities specific capabilities

1-2 specific uses of solar heat : competition with other heat sources ; the high temperature field challenge

1-3 prime concern topics : receivers and storage ; how to overcome the variable inputs to master this heat source

1-4 thermal energy cost optimization versus solar facility design selection and source temperature target

2 - Solar concentrators related research

2-1 solar furnace type double reflection facilities vs central receiver type single reflection facilities
- specific temperature range capabilities
- optimized temperature range capabilities
- optimized efficiencies

2-2 heliostats-concentrator facilities performances modeling : flux prediction

2-3 evaluation and design of methods for aligning facetted reflectors : minimized cost for upgrading or designing facilities

2-4 mirrors materials evaluation : effects on facilities performances

3 - High radiant heat resistant materials

3-1 fundamentals of materials behaviour under radiative heat transfer condition

3-2 selection criteria : mechanical failure and thermal shock resistance prediction vs thermal radiative properties

3-3 materials evaluation for specific applications (solar or non-solar sources)

3-4 associated fluxes and temperatures measurements, real time absorbed solar flux at the surface of materials under test

4 - High temperature conversion of radiant energy into heat and sensible heat storage

4-1 general survey of the particulate solid thermal loop : high temperature solar heat

4-2 direct absorption "sand" receiver

4-3 high temperature sensible heat storage

4-4 modeling for design criteria and performances prediction : effects of radiative heat transfert

4-5 evaluation of loop and components performances under real variable inputs

5 - Interfacing chemical reactors receivers for solar fuels and chemical storage of solar thermal energy

5-1 windowed direct absorption falling particles reactor experiment for flash pyrolysis of biomass materials : cold wall clamshell reradiating cavity

5-2 cyclone reactor for low residence time flash pyrolysis of biomass particles : uniform heating of an opaque reactor inside a medium hot reradiating ceramic cavity receiver

5-3 moving bed reactor modeling for coal or biomass steam or CO_2 gasification : temperature profiles, solid consumption rates, gas phase composition, conversion efficiency, operating parameters optimization

5-4 direct absorption windowed cavity gazifier derived from "sand" receiver

5-5 gasification in a multi-stage fluidized bed with a solar heated particulate solid heat transfer medium

VI - Other high temperature solar heat related research activities in progress

1 - At the Odeillo Solar Energy Laboratory or in cooperation with other CNRS laboratories

1-1 porous media (for high temperature gas heating or chemical reactors)

1-2 thin wall fluidized beds

1-3 hydrogen production (water direct thermal splitting , high temperature thermo chemical cycles)

1-4 biomass flash pyrolysis and coal gasification

1-5 lime calcination : 50 KW solar loop experiment

2 - At other sites and CNRS laboratories

2-1 Poitiers : SIROCCO air cooled receiver

2-2 Vignola (Corsica) : linear collectors

2-3 Marseille : PERICLES bowl concentrator

2-4 Saint Chamas : THEK dish collectors

2-5 Targasonne : THEMIS central receiver and THEK dish collectors

REFERENCES

(1) H.Connel PSL, Large Scale Solar Energy Test facilities, Proceedings, National Science Foundation International Seminar, New Mexico State University, (november 18-19,1974)

(2) P.Lebeau, F.Trombe, Les hautes températures et leurs utilisations en chimie, Masson et Cie, Paris 1950

(3) Colloques Internationaux du CNRS, Applications thermiques de l'énergie solaire dans le domaine de la recherche et de l'industrie, Montlouis, 23-28 Juin 1958,CNRS,Paris ,1961.

(4) G.Chaudron, F.Trombe, Les Hautes températures et leurs utilisations en physique et en chimie, Masson et Cie, Paris, 1973

(5) Journées d'Etudes d'Odeillo Font-Romeu, Les Fours Solaires et les Fours à images, 1-2 Octobre 1971, Revue Internationale des Hautes Températures et des Réfractaires,1973, t.10, N°4

(6) F.Trombe, A.Le Phat Vinh, C.Royère, The French CNRS 1000 KW Solar Furnace : description, performance characteristics, present utilizations and perspectives in (1) op.cit.

(7) F.Trombe,L.Gion,C.Royère,J.F.Robert, Traitement d'oxydes réfractaires au Four Solaire de 1000 KW du CNRS,C.R.Acad. Sc. Paris,T 272,pages 1971-1973, 14 Juin 1972

(8) F.Trombe,L.Gion,C.Royère,J.F.ROBERT, First Results obtained with the 1000 KW Solar Furnace, Solar Energy, Vol.15, pages 63-66, 1973

(9) F.Trombe,L.Gion,C.Royère, Perfectionnement aux procédés et dispositifs de granulation et de sphéroïdisation de matières notamment de matières réfractaires,Brevet ANVAR, 2.098.951 du 14 Février 1972

(10)C.Royère,Solar Chemical Engineering research and test activities using the 1 MWth Solar Furnace at CNRS, Solar Thermal Test Facilities Users Association,Facility operators and Experimenters Workshop,May 3-4 1979,Albuquerque NM, Proceedings pp. 24-29

(11)C.Royère,F.Trombe,Etude au four solaire de la cinétique de réduction par l'hydrogène du sesquioxyde de chrome pur ou dopé,C.R.Acad.Sc.Paris,T 267, pages 1275-1278, 13 Novembre 1968

(12)C.Royère,Péduction des oxydes par l'hydrogène à Hautes températures,Application au sesquioxyde de chrome,Rev.int.Htes Temp.et Réfrac.T.10,pages 241-249, 1973

(13)M.J.Antal JR,Princeton University,C.Royère and A.Vialaron, CNPS Odeillo,France,ACS Symposium séries n° 130 thermal conversion of solid wastes and biomass,pp.237-255

(14) J.D.Walton,C.Royère,Evaluating the thermal shock resistance of ceramics in a radiant thermal energy environment, Sciences of Ceramics, 1973, p.219-236

(15) E.Bilgen,C.Royère,Transient Heat transfer at the Focal Plane of Solar Furnaces, Fredericton, 26-30 Mai, 1975, Proceedings CANCAM, 1975

(16) D.Balageas,A.Sarremejean,C.Royère,High temperature electrical evaluation of slipcast fused silica radome Using Solar Energy,Office National d'Etudes et de Recherches Aérospatiales, 21-23 Septembre 1976

(17) B.A.Gordon,T.M.Knasel,M.D.Mr Donnel,R.Sievers,SAI S.H Bomar GIT,C.Royère CNRS,Design of a flux diverter and containment tube with results of tests at ACTF and CNRS, Presented at AS/SES 1980, Annual Meeting

(18) J.P.Carrie et H.Le Doussal (SFC),M.Chastant,L.Halm et M.Jon (IRSID),C.Royère et JL.Tuhault (CNRS) Comportement des produits réfractaires soumis à des sollicitations thermomécaniques sévères, Bull.Soc.Fr.Ceram, N°124, Juillet-Septembre 1979

(19) T.R.Tracey,F.A.Blake,C.Royère,C.T.Brown,1 MWth Solar steam generator.Solar test program,ISES Journal,30 Avril 1977

(20) Martin Marietta,Engineering experiment station,Georgia Institute of Technology,CNRS,1 MWth Bench Model Cavity receiver Steam Generator Build and Test,Phase 3 summary report june 1977

(21) A.Hassan,C.Royère,JL.Tuhault,LES CNRS/C.Laguerie,M.Peyman IGC Toulouse,Evaluation of multistage fluidized bed heat exchanger to transfer thermal energy at high temperature to a gas from a granular solid storage heated by concentrated solar radiation,Proceedings of annual meeting STTFUA, april 15-17, 1980, Las Cruces NM, pp.145-156

(22) C.Royère,Température limitations of solar point focussing facilities; optimization of cavity receivers, Solar Thermal Test Facilities Users Association,april 11-12,1978, Golden Co,Proceedings of annual meeting p.79-90

(23) Thèse de 3ème cycle (énergétique solaire)
Contribution à l'étude de la répartition de la densité de flux énergétique dans l'espace focal d'un système concentrateur de rayonnement solaire, Novembre 1977, Université de Poitiers, Orlayer ALCAYAGA

(24) Thèse de Docteur Ingénieur
Contribution à l'étude théorique et expérimentale d'un système de captation, stockage et restitution d'énergie thermique à haute température à l'aide d'un caloporteur solide divisé pour l'utilisation du rayonnement solaire concentré, Octobre 1981, Université Paul Sabatier de Toulouse, Ahmed Hassan Mohamed HOOD

(25) Thèse de Docteur Ingénieur
Contribution à la modélisation d'un gazogène à front chaud solaire en lit mobile poreux appliqué à la gazéification de produits carbonés, Septembre 1983, Institut National Polytechnique de Toulouse, Marie Claire QUELARD

NOVEL COMPOSITE TES SUBSYSTEMS FOR HIGH TEMPERATURE SOLAR THERMAL APPLICATIONS

Randy J. Petri
Institute of Gas Technology

ABSTRACT

An advanced, thermal energy storage (TES) media concept based on composite metallic phase change materials (PCM's)/ceramic (or higher melting point metals) materials is being developed for high temperature applications in solar TES power and chemical/fuels systems. This composite sensible/latent concept permits direct contact heat exchange with high-temperature, inert or reducing, gaseous working fluids; thus offering significant potential TES system performance and cost advantages over previous molten PCM-based storage systems or passive sensible heat systems.

INTRODUCTION

Many TES technologies are under development to provide continuous operation of solar power systems during nonsolar hours and during periods of variable insolation.[1] First-generation TES subsystems included dual media oil/rocks and oil thermoclines. Second-generation TES technology development focused on storage subsystems for solar receivers cooled by water/steam, molten salts, liquid metals, organic fluids, or gases.

Some latent-heat based programs, including IGT's system under ERDA and DOE sponsorship, have shown that heat transfer rates from molten salt TES are limited by heat transfer through the solidified salt. IGT improved heat transfer rates from 25% to 45% by using "passive" means such as finned tubes and metallic conductivity promoters. Honeywell has significantly increased heat transfer rates by an "active" method that uses mechanical scrapers to remove the solidified salt during the discharge cycle. But this system has many shortcomings: the frequent maintenance requirements and limited lifetime of the mechanical system; scraper freeze-up, which prevents complete system discharge (solidification); and long-term stability and composition control of the salt necessary to maintain the needed "slush" conditions. In addition, this mechanical scraper system is only usable on the discharge cycle (when the salt is molten); a separate finned-tube heat transfer is only possible for one-half of the operating cycle — the discharge cycle. Another drawback of

tube-intensive latent heat designs is that systems for very high-temperature (1300°F) applications require superalloy materials for adequate strength and corrosion resistance, which significantly increases capital costs.

Because of these limitations in the mechanical scraper system and other tube-intensive configurations, IGT is targeting its research to study alternative means of promoting heat transfer in TES systems with molten alloy phase-change material (PCM).* This method uses a heat exchange concept in which the working fluid is in direct contact with composite sensible/latent thermal storage media. This eliminates costly heat exchanger tubes and permits the composite pellets, bricks, or other shapes to be in direct contact with compatible fluids. Thus, signifcantly higher heat transfer rates are expected by control and minimization of solidified layers by elimination of thermal resistance from heat exchanger tubing and by the high thermal conductivity of the metallic composite media.

This innovative TES concept specifically addresses the "extreme temperature" (over 950°C) concerns of efficient thermal storage in the materials research section of DOE's Solar Thermal Energy Systems Program. The incentives for development of higher temperature materials include: a) increased cost-effectiveness of the total system; b) increased efficiency by higher operating temperatures of heat engines (predicted efficiency for a fully regenerative open-cycle Brayton engine increases from 26.8% at an inlet temperature of 1850°F to 48.3% at an inlet temperature of 2500°F with the same outlet[2]); and c) the long-term oxidation resistance and mechanical properties of conventional alloys at over 1600°F.[3]

TECHNICAL DISCUSSION

Composite Latent/Sensible Media Concept

Recently, work performed on an IGT-funded program resulted in an innovative approach to containment of molten salts that offers significant potentia for cost reduction and performance improvement of latent-heat TES systems.** This advanced concept involves utilization of a composite latent/sensible hea

---

* IGT retains a patent disclosure for this concept.

** IGT retains a patent for this concept, effective September, 1983.

medium in which the molten salt (latent-heat phase) is retained and immobilized within the microstructure of a highly porous ceramic (sensible-heat phase) by capillary surface tension forces. Figure 1 is a schematic microstructure of such a composite (latent/sensible) material. The volume fraction of molten PCM that can be retained is determined by the characteristics of the support material (e.g. particle size and shape distributions and specific surface area), salt (PCM) properties (e.g. surface tension and viscosity), and wetting behavior between molten PCM and sensible support phases.

More recent R&D efforts at IGT have demonstrated the feasibility of an attractive approach to containing molten carbonate salts that offers the potential for elimination of HX tube configurations and operation in direct contact with compatible working fluids (e.g. a stacked array of bricks, or packed "pebble-bed"). The good thermal stability of such pellets (50 wt % Na_2CO_3-$BaCO_3$/50 wt % MgO) has been successfully demonstrated during 1790 hours of testing of 3 lbs of media in air with 180 thermal cycles (from 1472°F to 1100°F) and 1600 hours of testing of 47 lbs of media (packed bed) in a computer controlled test facility with 50 charge/discharge thermal cycles in an air working fluid (0.3% gross weight loss). Also, retention of carbonates, other salts, or metallic PCM's within chemically compatible porous ceramics or refractories will lead to composite latent/sensible media in which heat is available over a wider temperature range. Molten PCM's with different melting points can then be easily installed at different locations within a solar TES system. Both these characteristics make the system flexible and thermally tailorable to meet storage requirements of a variety of duty cycles.

The technical feasibility of the extension of this original scheme to the potentially higher storage density/higher melting point metallic PCM/ceramic (or metallic) sensible heat composite systems is dependent on a number of key factors:

- Wetting capability of metallic PCM on sensible heat phase
- Ability of porous shape to retain the molten metals by capillary action above their melting point, with minimal chemical interaction between metal and support matrix (ceramic or metal). Creepage of molten PCM metal from the porous shape must be minimal.
- Availability of ceramic in sub-micron sizes to maximize capillary retention force.

- Ability of the PCM alloy/sensible support composite to be repeatedly thermal cycled (melting/solidification of the PCM metal phase) with minimal cracking, spalling, or other structural damage.

- Chemical compatibility of the molten metals with charge/discharge fluid to minimize changes in chemistry, melting behavior, and other physical properties (heat effects, thermal conductivity, viscosity, surface tension, etc.).

- Sufficient strength to maintain physical integrity under the stresses imposed by the system design.

Composite Media Develpment and Testing

Review of High Temperature Storage Components and Concepts

We are currently conducting a literature review of past and present work in high-temperature materials prepartions, treatment, and long-term compatibilities. Evaluations will be based on the potential impact on the ultimate composite composition/processing and anticipated system storage characteristics.

Materials Selection

Birchenall *et al.*[4,5] found that Al, Si, Zn, P, Na, Cu, Mg, and Ca were preferred starting elements for metal heat storage applications. After further investigation, at least eight binary and ternary alloys were identified with melting points from 172°C (343°F), Mg/Mg_2Zn, to 946°C (1735°F), Mg_2Si/Si (Table 1).

Candidate metals are being selected primarily on the basis of melting point, heat-of-fusion, wetting angle (strong wetting behavior of metal on ceramic), surface tension, viscosity, vapor pressure, volume change on fusion, thermal expansion, and compatibility with support matrix and working fluid environments.

Materials are being selected to demonstrate the metallic-based composite media concept initially using a low-melting metal composite, thus simplifying the experimental test procedures. The sensible support materials will be selected from commercially available products based on carbides, nitrides, borides (oxides or aluminates), high melting silicides and other high melting (refractory) metals. The suitability of these media is expected to be controlled significantly by their compatibility with molten metals and alloys (e.g., corrosion, solubility of ceramic, loss of surface area, etc.). Overal

compatibility will depend on compositions of the metal and ceramic phases, temperature, gas environment, and impurities.

Media Processing, Fabrication and Behavior

Composite metal/ceramic powders are initially being prepared by dry-mixing. These materials are being characterized with respect to critical properties such as chemical composition, specific surface area of support, particle size and shape distributions, and forming characteristics.

For laboratory testing purposes, composite powders are cold-pressed into cylindrical pellets at pressures of 10,000 to 50,000 psi and sintered to densities of 50% to 90% of theoretical. The feasibility of forming composite pellets by more cost-effective methods (e.g. automatic dry pressing, extrusion, molten metal impregnation of porous sintered ceramic shapes) will be investigated.

The composite media are being evaluated in experiments designed to address and quantify the above mentioned key technical issues, which are expected to significantly influence their functionality under actual solar thermal storage conditions. These tests include thermogravimetric analysis to evaluate metal decomposition and vaporization loss effects in proposed solar Brayton working fluids; and thermal aging and thermal cycling tests for measuring support particle stability, metallic retention, and media thermal shock resistance and shape dimensional/stability.

Solar Thermal Storage Application

Techno/Economic Benefits

To illustrate the potential cost/performance benefits of a composite system relative to current reference systems, a preliminary estimate of the comparative media mass, volume, cost, and resultant system volume requirements for a very high temperature TES system for a solar Brayton power system was conducted.

The TES subsystem costed by Stearns-Roger[6] for this Brayton application was based on the conceptual design proposed by Boeing. The alternative TES system investigated involves an advanced composite containing 50 wt % silicon PCM and 50 wt % MgO ceramic support material. The melting point of Si is reported as 2579°F, with a latent heat of fusion of 776 Btu/lb. To compare

sensible media with composite media, the system was assumed to be in a packed-bed configuration. Three baseline sensible media were assessed:

1. Al_2O_3 Brick (95.1% purity): Data were supplied from a Stearns-Roger[6] TES study that screened a number of conceptual sensible-media TES designs.

2. MgO Brick (95.1% purity): Data were also from a Stearns-Roger report[6].

3. "Lofero" MgO Brick: Data were supplied from Kaiser Refractories Co. for high-temperature regenerator-quality brick.

Comparative media mass, volume, cost, and resultant system volume requirements were calculated on the following consistent bases: storage of 1,055 MJ (million Btu) of heat (293 kWh); packed-bed void fraction = 0.4; temperature swing of media (ΔT) = 450°F ($\Delta T/2$ above and below metal melting point, 2354° to 2804°F); appropriate physical properties of sensible and composite media (such as density, heat capacity, heat-of-fusion, composition); projected fabricated cost of composite media = $/kg ($/lb) unit cost of powders + 0.22 $/kg ($0.10/lb) for spray drying/mixing + 0.11 $/kg ($0.05/lb) for briquetting (obtained from discussions with industrial producers of ceramic powders and shapes); and technical-grade materials are acceptable.

One direct conclusion from these calculations is that use of the 50 wt % Si/50 wt % MgO composite in a 450°F temperature swing process results in: a 20% (versus Lofero MgO Brick) to 72% (versus Al_2O_3 bricks) reduction in fabricated media costs; an average 75% reduction in media mass; and an 82% decrease in system volume requirements per million Btu stored at 2354° to 2804°F; this translates to an additional 64% savings in the TES unit containment costs (by the 0.6 "rule").

CONCLUSION

The composite metal/ceramic (or metallic) TES media under development offer the potential for a cost effective and direct-contact approach to utilization of phase change storage materials. By proper selection of metal and ceramic materials, these media can be designed for storage systems covering a broad range of use temperatures (648°F to 2579°F) and working fluids. However, further efforts in the areas of composite materials development, long-term stability testing in representative working fluids, and TES system performance evaluation and scale-up are required before the technology can be practically implemented.

REFERENCES

1. U.S. Department of Energy, Division of Energy Storage Systems and Division of Central Solar Technology, "Thermal Energy Storage Technology Development for Solar Thermal Power Systems: Multiyear Program Plan," Draft. Washington, D.C., March 13, 1979.

2. Ewing, J., Zwissler, J., "Performance Prediction Evaluation of Ceramic Materials in Point Focusing Solar Receivers," Report prepared under Contract DOE/JPL-1060-23 for U.S. Department of Energy. Pasadena, Ca: Jet Propulsion Laboratory. June, 1979.

3. Lyman, Taylor, ed., Metals Handbook, 8th edition, Vol. 1, American Society for Metals, 1972.

4. Birchenall, C. E., "Heat Storage Materials." Report prepared under Contract No. EY-76-S-02-4042 for the U.S. Dept. of Energy. Newark, Delaware: University of Delaware, December 1977.

5. Birchenall, C. E., et al, "Heat Storage in Alloy Transformations." Report prepared under Grant NSG-3184 for the National Aeronautics and Space Administration. Newark, Delaware: University of Delaware, March, 1981.

6. Stearns-Roger Services, Inc., "Cost and Performance of Thermal Storage Concepts in Solar Thermal Systems — Conceptual Design Review." Work performed for SERI, Denver, September 1980.

Table 1. CANDIDATE ALLOYS FOR THERMAL ENERGY STORAGE[4,5]

No.	Alloy System	Composition (wt %)	Melting Point °C	Melting Point °F	ΔH_f Btu/lb	Heat Capacity Btu/lb-°F Solid	Thermal Conductivity Btu/lb-°F-ft	Density lb/ft^3	Cost,* $/lb	Btu/$**
1	Al-Mg-Zn	35mg-6Zn	443	829	133	0.39	—	149	0.93	145
2	Al-CU-Mg-Zn	22Cu-18Mg-6Zn	520	968	131	0.36	—	196	0.84	156
3	Al-Cu-Si	30Cu-5Si	571	1060	182	0.31	—	170	0.82	220
4	Mg-Cu-Zn	45Cu-6Mg	705	1300	76	0.10	—	541	0.61	125
5	P-Cu-Zn	17Zn-14P	720	1328	158	0.13	—	437	0.72	220
6	Cu-Mg-Si	27Si-17Mg	770	1418	182	0.18	—	260	0.98	185
7	Cu-Si	20Si	803	1477	85	0.12	—	412	0.86	100
8	Mg_2Si/Si	56Si	946	1735	326	0.19	13.3	119	1.23	265
9	Si		1415	2519	776	0.25	—	145	1.20	645

* Costs from Chemical Marketing Report, August 29, 1983.

** Based on heat-of-fusion only; sensible heats neglected.

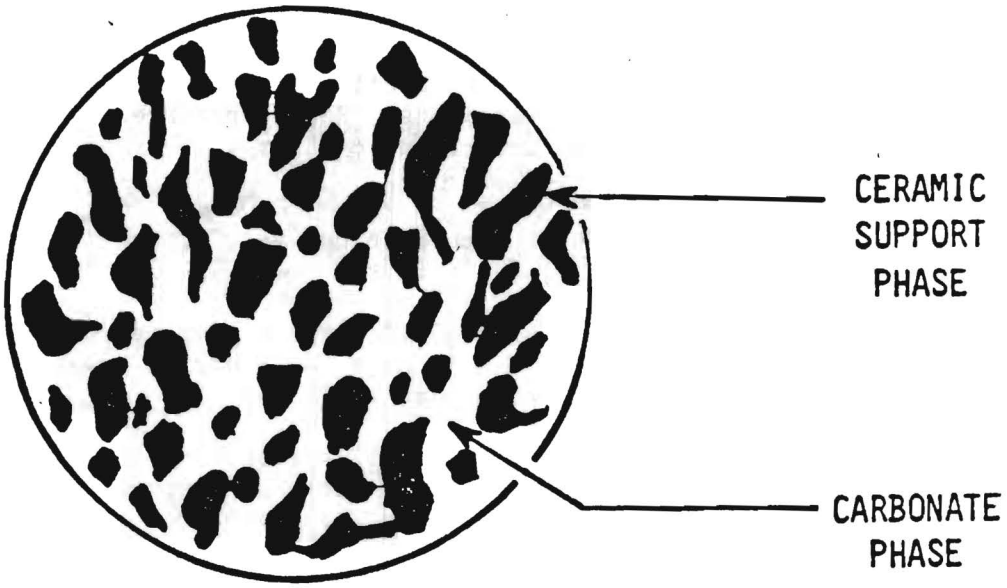

Figure 1. MICROSTRUCTURE OF COMPOSITE TES MEDIA — MOLTEN PCM SUPPORTED BY CERAMIC MATRIX

INNOVATIVE RECEIVER DESIGN FOR PARABOLIC TROUGH AND PARABOLOIDAL DISH SOLAR COLLECTORS

Dr. T. H. Kuehn
Department of Mechanical Engineering
University of Minnesota
111 Church Street Southeast
Minneapolis, MN 55455-0111

ABSTRACT

A feasibility study is outlined for a receiver that can be used to provide high temperature liquid or vapor from a parabolic trough or paraboloidal dish solar collector. The receiver design utilizes principles of optics, radiation heat transfer and convection heat transfer to maximize the absorption of incident solar energy on the absorber and minimize the thermal losses from the heated fluid. It is anticipated that the present receiver design will have better thermal performance and cost effectiveness than any existing design when both are operated under the same conditions.

INTRODUCTION

Thermal losses from the receiver of a concentrating solar collector often dominate the performance of the collector system under high temperature operation. Conventional receiver designs incorporate transparent enclosures, selective surfaces, or cavities to reduce convection and radiation losses. A need exists to develop innovative receiver designs that operate with reduced losses at elevated temperatures and are more cost effective to construct and operate.

Two liquid-heating porous absorber receiver designs that show promise of operating with better thermal performance than conventional receivers at high exit fluid temperatures are illustrated in Figure 1. The configuration shown in Figure 1(a) is a cylindrical receiver with a porous inner cylinder used for heating liquids to high temperatures in a parabolic trough collector. Figure 1(b) shows a cross section of a circular receiver in which high pressure liquids could be heated or

vaporized in a paraboloidal concentrator. Both receivers are shown with the concentrated solar energy entering from below. The liquid used as the heat transfer fluid is assumed to be transparent to radiation in the solar spectrum but opaque to infrared radiation such as water. The cool fluid enters between the transparent enclosure and the heated porous absorber. The fluid is heated as it passes through the porous wall and exits on the other side of the absorber. The receiver design shown in Figure 1(a) could be constructed from black screen or mesh, a glass tube and rigid high temperature insulation. The entire receiver can be built with low cost, commercially available materials and requires no special skill in construction.

The following section explains the advantages of the proposed design over conventional receivers in terms of enhanced optical and thermal performance. The cost effectiveness of the present system is expected to equal or surpass any presently available high temperature receiver.

BACKGROUND

A porous absorber solar collector is not a new concept as studies by Shoemaker (1), Chiou et al. (2), and Hamid and Beckman (3) have previously considered air heating collectors with a porous screen absorber. However, the present receiver design is quite different in that it is used to heat liquids and operates best in a concentrating collector with a large heat flux. The improvements in performance of the proposed receiver design over conventional designs can be classified as either optical or thermal.

The optical efficiency of the porous absorber receiver is better than a conventional evacuated tube receiver with a selective surface on the absorber tube. The reflection loss from a transparent enclosure such as glass is a function of the indices of refraction of the glass, the air on the exterior, and the fluid on the inside. If the interior fluid is a gas or a partial vacuum, significant reflection losses occur on both sides of the glass enclosure. The reflection loss on the second surface of the glass is greatly reduced if a liquid such as water is used inside the glass rather than air. The indices of refraction at the second interface are more equal which improves the transmittance of the

glass by 3% at normal incidence and by 6% at 60° incidence. The reflection loss on the second surface can be eliminated entirely if one chooses a transparent enclosure with the same index of refraction as the internal fluid. For example, polyfluorinated ethylene propylene has a refractive index nearly equal to that of water. Using this as the transparent enclosure increases the transmissivity 6% at normal incidence and 10% at 60° incidence over the original glass-in-air enclosure. This transmissivity increase does not depend on surface coatings which can be expensive and short lived.

The amount of solar radiation captured by the receiver depends on the apparent absorptivity of the absorber surface in the solar spectrum. The porous absorber has large scale roughness and numerous cavities. This provides multiple reflections and results in an effective absorptivity that is larger than when the same material is smooth. This concept has been used previously in vee-groove solar collectors and in cavity receivers (4,5). Therefore, the absorptivity of the absorber material is not as critical as when the receiver is fabricated as a smooth surface.

The greatest advantage of the present design is the small thermal loss from the absorber to the aperture. The liquid flow rate within the channels of a porous receiver is very low when large temperatures are desired so the flow is laminar. This usually creates difficulties because of the correspondingly low heat transfer coefficients. However, in the present case, this is an advantage because the fluid mixing caused by turbulence is avoided. The orientation shown in Figure 1 with the heated absorber above the inlet liquid channel also minimizes mixing by natural convection as the hot fluid is always above the cold fluid. Therefore, the flow and heat transfer within the liquid channel can be readily analyzed by solving the governing laminar forced convection momentum and energy equations. A simple analytical solution has been developed for flow between two parallel plates which predicts the temperature distribution in the liquid as a function of velocity through the porous wall (6). When the flow rate is zero, heat is transferred from the heated absorber through the liquid by conduction to the opposing transparent cover. Therefore all the heat absorbed by the

absorber is lost out the cover resulting in a thermal efficiency of zero, $\eta_T = 0$. However when the liquid is passed through the absorber, the energy conducted to the fluid below the absorber is convected back toward the absorber reducing the loss at the cover. The faster the flow toward the porous absorber, the smaller the loss at the cover. This has been quantified by the following equation

$$\eta_T = 1.0 - \exp(-0.4468\ Pe_w) \qquad (1)$$

where η_T is the overall ratio of energy gained by the liquid to energy captured by the absorber and the Peclet number $Pe_w = VH/\alpha$ where V is the liquid velocity toward the porous absorber at its surface, H the spacing between the absorber and transparent cover and α is the liquid thermal diffusivity. This simple correlation indicates that when $Pe_w \geq 10$, more than 99% of the energy absorbed in the porous absorber is captured by the liquid passing into the exit liquid channel; less than 1% of the energy is lost out the transparent cover. This remarkable result indicates that at a large enough flow rate the convective heat loss through the receiver aperture is nearly zero and therefore independent of the absorber temperature and exit liquid temperature. As most liquids are opaque to infrared radiation, the only other possible means of heat loss from the absorber or heated liquid is through the insulating cavity which can be designed to reduce the heat loss to any level desired. Therefore extremely high temperatures can be achieved with practically no change in receiver thermal loss. This is one of the main advantages of the present design. In addition, the porous absorber has a very large surface area which improves the heat transfer to the liquid so tha low flow rates do not significantly impart its heat transfer capabilities. The pressure drop through the absorber is not anticipated to be very significant as the porosity can be very high and the velocities are less than 1 inch/sec.

The porous receiver could also be used to boil liquids in addition to its use for liquid heating. A design such as the one shown in Figure 1(b) could be constructed for use in a paraboloidal concentrating collector with large concentration ratios (10,000). All the advantages

mentioned before for liquid heating are still valid in the boiling application. The only differences are that the heat fluxes are much larger, the liquid flow rate is higher per unit area of aperture and the absorber and exit channel operate in a two-phase flow condition. The transparent aperture cover could be made small enough to withstand the pressures required in a steam generator application. A possible absorber configuration would be an array of vertical tubes or honeycomb structure with an aspect ratio greater than 10 so the incident radiation would be scattered and absorbed within the absorber. The boiling mechanism would be basically nucleate-pool-boiling as the velocities are very small.

PROJECT OBJECTIVES

A. Conduct a detailed optical and thermal simulation study of the cylindrical porous receiver design (Figure 1(a)) to determine the influence of design parameters on its thermal performance.

B. Compare the thermal efficiency of the cylindrical porous receiver with existing receiver designs operating with a parabolic trough reflector under identical conditions to determine the relative advantages or disadvantages of the proposed design.

C. Determine the feasibility of using the porous absorber as a steam generator (Figure 1(b)) by evaluating previous studies of boiling in porous media and in a vertical tube or honeycomb matrix.

D. List and rank for acceptability various fluids and materials to be used in constructing a porous receiver. Identify possible problems in construction and operation and suggest solutions to these problems.

REFERENCES

1. Shoemaker, M. J., "Notes on a Solar Collector with a Unique Air-Permeable Media," Solar Energy, Vol. 5, pp. 138-140, 1961.

2. Chiou, J. P., El-Wakil, M. M. and Duffie, J. A., "A Slit-and-Expanded Aluminum-Foil Matrix Solar Collector," Solar Energy, Vol. 9, pp. 73-79, 1965.

3. Hamid, Y. H. and Beckman, W. A., "Performance of Air-Cooled Radiatively Heated Screen Matrices," Journal of Engineering for Power, Vol. 93, pp. 221-224, 1971.

4. Hollands, K. G. T., "Directional Selectivity, Emittance and Absorptance Properties of Vee Corrugated Specular Surfaces," Solar Energy, Vol. 7, pp. 108-115, 1963.

5. Barra, O. A. and Franceschi, L., "The Parabolic Trough Plants Using Black Body Receivers: Experimental and Theoretical Analyses," Solar Energy, Vol. 28, No. 2, pp. 163-171, 1982.

6. Balvanz, J. L. and Kuehn, T. H., "Experimental and Theoretical Investigation of Laminar Flow and Heat Transfer in Rectangular Ducts with One Heated Porous Wall," Final Report, NSF-78-05562, July, 1980.

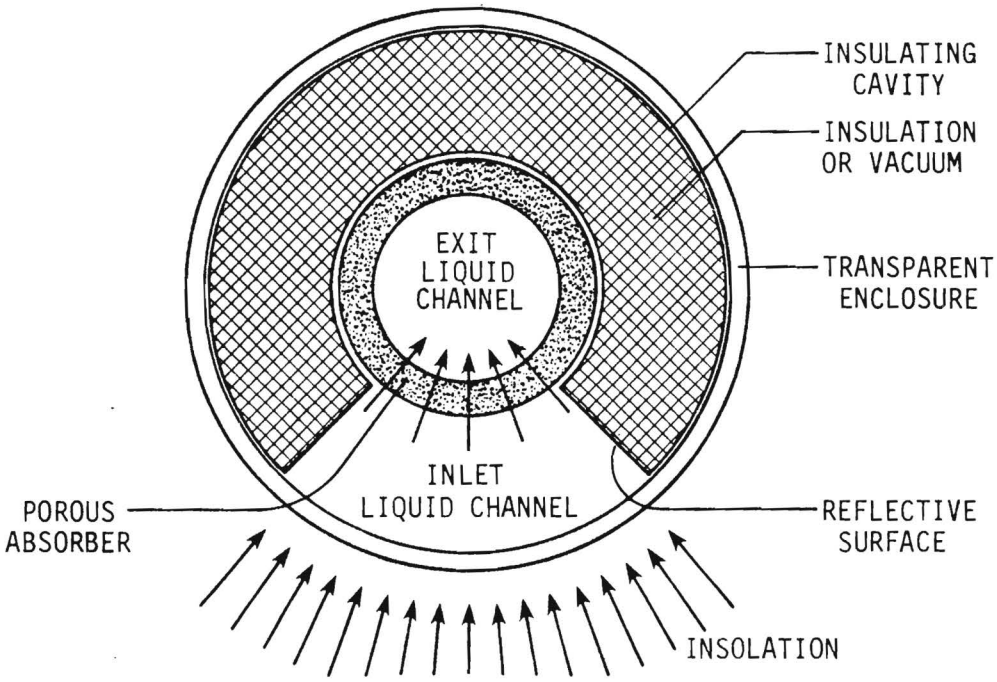

a) Annular Duct with Heated Porous Inner Cylinder Used for Heating Low Pressure Liquids in Parabolic Trough Collectors.

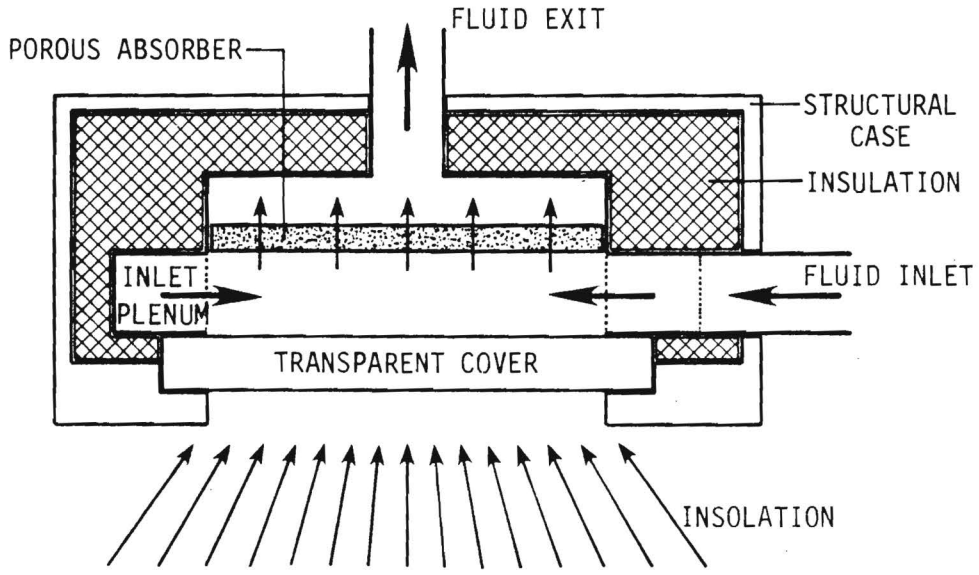

b) Circular Porous Absorber Used for Heating High Pressure Liquids or for Vapor Generation in a Paraboloidal Concentrator.

Figure 1. Cross Sections of Two Possible Porous Absorber Receiver Designs.

Project Title: Photosynthesis of Ammonia Using Open-Celled Silica Foam as Catalyst Substrate and Cocatalyst

Sponsored by: Department of Energy

Project Managers: W. A. Mallow and D. M. Deffenbaugh

ABSTRACT

An open-celled foam of inorganic, solidified silicon oxide polymer is doped with catalyst which produces ammonia from air and water when exposed to sunlight or other appropriate electromagnetic energy. The catalyst/dopant is selected from the family of titanium oxides and iron oxides of varied crystalline form.

BACKGROUND

The commercial synthesis of ammonia by the Haber, Bosch, Casale, Fauser, Claude, and Mont Cenis processes require a considerable input of energy despite the fact that the reaction is exothermic. The yield of ammonia per cycle and the number of cycles required to effect a commercially practical conversion as the gases are cycled through the reactor further complicates and enhances the cost of energy and equipment. Ammonia is derived from the reaction of high purity nitrogen and hydrogen, the latter extracted from methane gas or similar hydrocarbon sources. The extraction of nitrogen and hydrogen for this synthesis is also fuel intensive and requires considerable handling, storage, transport, etc., costs. The gases are mixed, heated and conducted through various catalyst beds generally comprising iron oxides (II or III) and zeolites with complex recycle loops to enrich the yield before recovery. Fuel demand for the most energy effective process exceeds 30,000 cubic feet per ton by the present commercial methods.

Photolysis or photochemical dissociation has been shown to occur naturally in many chemical processes, including the synthesis of ammonia from nitrogen and water. Such synthesis occurs both on earth and in extraterrestrial sources, most often catalyzed by silicon oxide containing trace amounts of iron and titania. While photosynthesis is most often regarded as an organic chemistry phenomenon, it does occur in certain inorganic materials as well. We propose to study the optimization of such synthesis by application of conventional principles of photosynthesis to an already demonstrated process observed when SwRI silica foam was shown to catalyze ammonia products from moist air in the presence of light, including fluorescent light and sunlight. The proposed study will explore the rate dependency of such synthesis on both light intensity (using sunlight with parabolic collectors to concentrate the solar energy) and wavelength (from IR to UV) to establish quantum yields and the most effective region of the frequency spectrum for bond cleavage. As with all photochemical reactions, the mechanism and kinetics are expected to be both frequency and intensity dependent.

In photochemical polymer synthesis the rate of polymerization is proportional to the light intensity (I_o), the monomer concentration, and the light absorption I_{abs} or

$$R_p = k_p (f\varepsilon I_o/k_t)^{1/2} \cdot [M]^{3/2}$$

where $I_{abs} = \varepsilon I_o[M]$ and ε is the molar absorption coefficient for the active radiation which relates to the quantum yield of the energy source, f represents the fraction of the free radicals which initiate chain growth in polymers or in our proposed study, the molecular interaction by nitrogen radica with water molecules, ions, or radicals.

If the radiation is absorbed by a photosensitizer (Fe, Ti, Si in the case of doped foam) which generates radicals, ion radicals or ions on photoactivation, or which induce initiation of reactions by some other mann then $I_{abs} = \varepsilon C_s I_o$ for sufficiently small concentrations (C_s) of the sensitizer. Thus the rate R_p is proportional to $C_s^{1/2}$ and to $I_o^{1/2}$.

The effluent gases will be collected and analyzed by various means such as neutralization in phosphoric or sulfuric acids, gas sampling for VP analysis, and collection of effluent gases in Nessler reagent using calorimetric methods to quantify yield. These simple procedures will provide the basis of computing optimum parameters for more efficient utilization of solar energy and input feedstock (air, nitrogen, water and heat).

The life of the catalyst bed will also be semi-quantified by noting changes in ammonia and by-product yield with time.

This process introduces a single, inexpensive and low energy method of generating ammonia and derivatives thereof using sunlight to stimulate the liberation of hydrogen on an iron-doped titania catalyst which is distributed over a bed of open-celled, amorphous silica foam. The silica foam provides a high surface area substrate, transparent to the visible and IR spectra and appears to enhance the activity and durability of the cataly This method requires only water and air as reagents, though nitrogen and hydrogen may also be used if convenient. The air is saturated with water vapor by any convenient means, such as passage through a water trough prior to the solar reactor. In practice, the water laden air is conducted throug a bed of silica foam, specially formulated and treated to provide the optimum distribution of catalyst and the highest amount of surface contact per unit of exposure time, while the reaction can be induced to occur over a bed of iron-doped titania imbedded on alumina or on clay, zeolite, molecular sieves, activated silica, etc.; the optimum yields are achieved with the high surface area, light transmitting silica foam bed of this process.

OBJECTIVES OF PROJECT

It is a general object of this technology to provide a process for mak ing ammonia and its by-products without direct application of fossil fuels except to manufacture the catalyst and equipment employed in the process.

The goal of this project therefore is to optimize a SwRI developed method for making ammonia using only sunlight as the source of energy and an open-celled, amorphous silica foam catalyst substrate whose surface is doped or treated to contain varied concentrations of selected catalysts such as iron oxide dissolved in titania with and without added light absorbing agents to enhance the efficiency of light energy transfer to the catalyst. These agents may be dyes of organic or organo-metallic nature which broadens the spectrum of light energy absorbed by the catalyst, enhancing the quantum yield. The preferred reagents for the production of ammonia of useful quality and quantity at minimal costs and energy requirements are the combination of air and water. Since air is over 80% nitrogen the remaining gases must not poison or limit the activity of these catalysts which are reportedly altered by oxygen and carbon dioxide. In a parabolic, solar energy intensifier, however, the catalyst does not appear to be irreversibly poisoned by these agents probably due to the localized heating induced by the incident light in the focal plane of the parabolic mirror. At any rate, the reaction is continuous and undiminished with time and exposure.

Air is pre-moistened by passage through a tank of water, conducted through the bed of foam, suspended in a glass tube at the focal point of a parabolic solar collector where intensified sunlight (or UV light in lab experiments) is focussed on the reaction bed (see illustration). The water is converted to hydrogen and oxygen by titania induced photolysis and the hydrogen so released combines with nitrogen to form ammonia and derivatives thereof (hydrazine, hydroxides, etc.). The products of this gas phase reaction are swept from the reactor and collected by scrubbing through aqueous solutions of phosphoric, sulfuric and nitric acids, if it is to be used as fertilizer or absorbed in untreated water, condensed in vapor traps or otherwise accumulated as preferred.

The novelty of this approach lies not in the application of sunlight to synthesis of ammonia; this is a well defined phenomenon, but in the surprising high levels of ammonia produced at SwRI with the introduction of the foamed amorphous silica substrate which enhances residence time and surface interaction to increase the yields from micromoles per hour to millimoles per hour--many orders of magnitude enhancement compared to prior art.

The photochemical properties of rutile and anatase forms of titanium dioxide have been often reported. The photo-oxidation and photo-reduction reactions have been described as well. G. N. Schrauzer and T. D. Guth of the University of California at San Diego, USA, and V. Augugliaro, et al, of the Institute of Chemical Engineering of the University of Palermo, Italy, have published papers covering the science of photochemical conversion of nitrogen to ammonia using doped titania on alumina and other substrates. Yields of micromoles per hour were reported by all authors to date. The SwRI process provides a durable, non-deteriorating, low-pressure resistance matrix and activated substrate for the titania based catalyst enabling the generation of significant quantities of ammonia at ambient temperatures using only wet air and sunlight.

A further object of this project is to develop a prototype of a portable, low cost source of fertilizer which can be produced and utilized by farmers and ranchers especially in developing countries where the cost and availability of fertilizer is limiting to its use.

Another object of this project is to reduce the demand and consumption of exhaustible fossil fuels while utilizing and harvesting solar energy in the conversion of solar energy to a food source through the generation of water soluble and soil compatible supplies of nitrogen compounds.

The silica foam used as a catalyst support and surface area enhancing substrate is produced in accordance with U.S. patent 3,741,898 (SwRI, Mallow, Baker, Owen). The foam may be prepared with active catalyst dopants introduced during the foaming process or the dopants may be added to the cured foam.

To generate ammonia, air is bubbled through a water bath and conducted through the catalyst bed at ambient temperature with the catalyst charged into a glass tube or pipe positioned at the focal point of the parabolic solar collector. The rate of air delivered through the system is adjusted to prevent excessive carryover of water from the bubbler-saturator into the photolyzer tube. The air pump used in the SwRI study delivers about 4 cubic feet/hour of air or about 5 moles of nitrogen per hour. In the present state of the art of SwRI, yields of ammonia as high as 0.5 moles per day or a yield of 0.35% per cycle or pass are typical. This compares to 7-8 micromoles per hour in the prior art. A tenfold or greater enhancement will be a goal of this project.

SILICATE FOAM PROCESSING

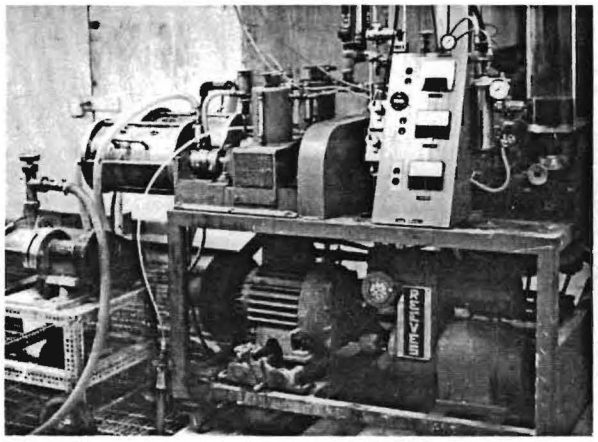

Silicate Foam Generating Machine

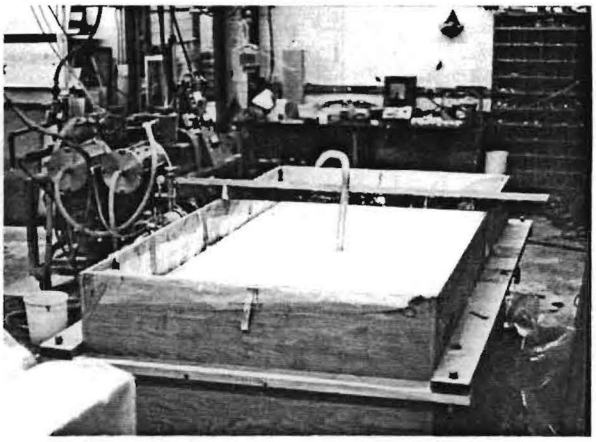

Molding and Curing Silicate Foam

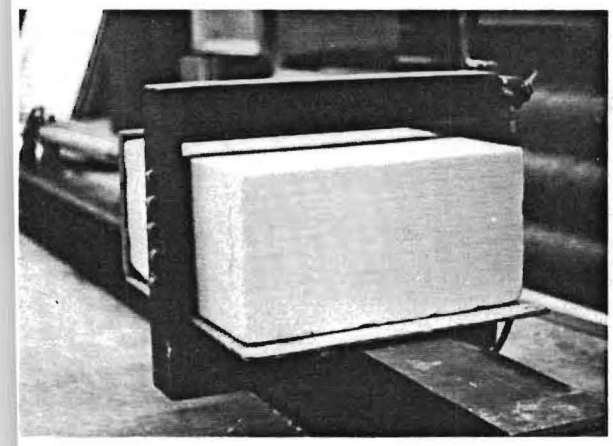

Slicing of Silicate Foam

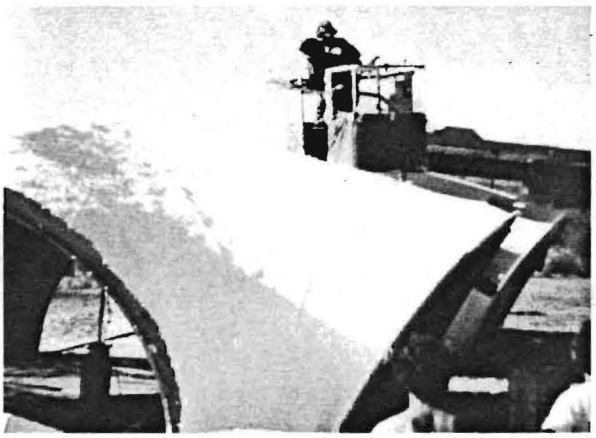

Spray Coating Tent with Silicate Foam Insulation

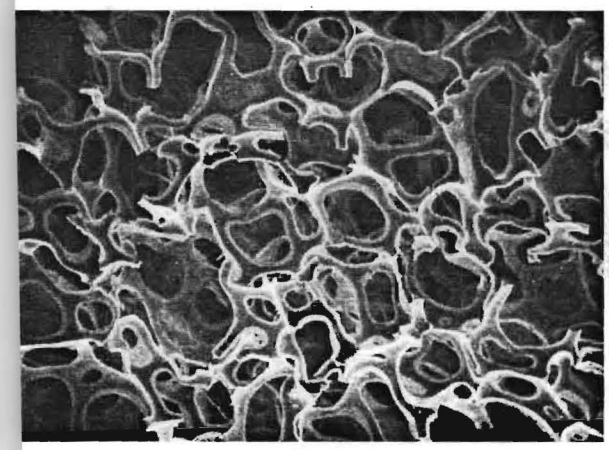

SEM of Silicate Foam (150X)

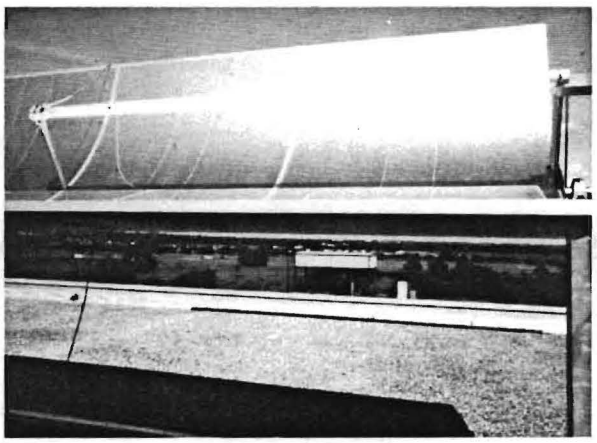

Solar Conversion of Air and Water to Ammonia via Doped Silicate Foam Catalyst Bed

INVESTIGATION OF PHOTOCURING MECHANISMS OF ULTRAVIOLET ABSORBING CLEAN POLYMERIC COATINGS AND FILMS FOR SOLAR THERMAL APPLICATIONS

Vincent McKoy
California Institute of Technology
Pasadena, CA

Ranty H. Liang
Jet Propulsion Laboratory
California Institute of Technology
Pasadena, CA

ABSTRACT

A novel photocuring process followed by "insitu" creation of ultraviolet absorbing chromophore is proposed as an integral processing and forming technique for inexpensive polymeric domes (enclosures) and mirrors. An acrylic formulation containing a benzophenone or a benzotriazole derivative will be photocured at a wavelength not absorbed by the aromatic chromophore. The photocuring process will yield a preformed dome or a mirror. The photocured films will then be irradiated at another wavelength to generate stable ultraviolet absorbers *via* photodissociation or photorearrangement of the aromatic derivatives. This concept, if proved feasible, will permit for the first time, use of photocuring technique to form ultraviolet absorbing, stabilized acrylic or polyester films.

Large scale collection and concentration of solar energy to generate heat at temperatures up to 1300°C has been proved to be feasible. However, adoption and utilization of this technology by industry cannot occur until the cost of energy conversion is reduced to $70.00 or less per square meter of collector area of a deployed large scale energy conversion unit.[1] Key to cost reduction is the replacement of conventional second surface glass mirrors and heliostats with inexpensive, light weight, polymeric mirrors and heliostats as solar energy collectors. Use of light weight mirrors would then allow the use of light weight polymeric support structures, which may be constructed of low-cost filled polyethylene or polypropylene. This substitution would also substantially reduce transportation and erection costs which together constitute a major fraction of the total cost of the energy conversion system.[2]

Fabrication of collectors and support structures out of inexpensive, light weight polymers would cause both immediate and long term problems adversely affecting the efficiency of energy conversion and life cycle costs. It is encouraging that a preliminary analysis indicates that for low to medium temperature applications (up to 800°C), polymeric components can meet all of the initial performance specifications, in other words, the only problem

expected to be encountered are environmental in origin. Some of these are detailed below.

Mirror corrosion and hence loss of collection efficiency has been identified as an important failure mechanism which limits the life of the energy conversion system, and hence increases its life cycle cost.[3] It occurs when the metallic layer comes in contact with condensed moisture. Corrosion is controlled in second surface mirrors by providing a layer of water impermeable paint at the back of the metallic coating, and an edge seal. Corrosion would be expected to be an even worse problem in inexpensive polymeric mirrors. Light weight polymeric mirrors would also be subject to wind stresses. The effect of the wind load would be to change the mirror configuration and curvature, serving to decrease the collection efficiency. Cyclic wind stresses, applied over long periods could also cause fatigue and failure. Lastly, polymeric materials deployed outdoors would undergo photo-oxidative degradation unless they are protected from solar ultraviolet radiation (300-400 nm). Photooxidative degradation leads to chain scission in plastics, while both chain scission and crosslinking processes occur in elastomers such as natural rubber and polyethylene. Photooxidation ultimately leads to a catastrophic loss of mechanical properties, including modulus and toughness. Hence, lacking protection from solar ultraviolet, polymeric collectors and supports would become embrittled. The adhesion between the metallic layer and the polymer may also be lost, causing delamination.

To conclude, conventional collectors and collector supports may be substituted by inexpensive polymeric components only if protection is provided against condensed moisture, wind stresses and solar ultraviolet.

Protection against these environmental hazards may be provided by enclosing the collector assembly in a transport plastic bubble or dome. The feasibility of utilization of protective domes in this manner is being evaluated by several laboratories.[4] A series of performance, cost and service life criteria have emerged from these studies. The performance of the dome may be measured in terms of the fraction of solar radiation which is collected and directed towards the absorber. In order to maintain the efficiency of collection and conversion within acceptable limits, the dome is required to have specular transmission greater than 0.92 in the wavelength range 400-2000 nm. The dome should absorb solar ultraviolet radiation in the wavelength range 300-400 nm and thus screen out solar UV in order to protect the enclosed solar collector assembly against photodegradation. Installed cost of the dome should not exceed $7.00 per square meter of the enclosed area, and it should have a service life of five years or more.

In this paper we discuss a novel polymerization and curing process which combines into one operation the polymer manufacturing process with the process of forming the polymeric film into a dome or a mirror blank. This process involves use of UV radiation to drive the polymerization reaction, and is known in industry as photocuring. Photocuring of acrylics and polyesters is well known, and is considered to have great potential in developing fast, automated fabrication procedures for polymeric devices, e.g., microelectronic components using polymers for substrate and encapsulation. However, addition of UV absorbing chromophores such as I and II in the curing mixture inhibits the photoinitiation step and prevents photocuring from proceeding at a proper rate. We are developing a concept which will allow photocuring of polymeric

films incorporating specific molecules or pendant groups which may be considered to be precursors of stable UV absorbing chromophores. Subsequent to curing, these precursors are made to undergo photorearrangement at a different wavelength in order to form "in-situ" the desired UV absorbing derivatives.

The use of photopolymerization and photoinitiated curing reactions has grown considerably, especially with the commercialization of ultraviolet curable inks and wood coatings.[5] Photoinitiated radical polymerization of vinyl monomers have been studied extensively using aromatic ketones as initiators.[6,7] More recently, photoinitiators have been reported for cationic polymerization. For example, $TiCl_3$ and VCl_3 have been shown to be effective photoinitiators for isobutylene,[8] while bis(cyclopentadienyl) titanium dichloride sensitizes the cationic polymerization of 2-chloroethyl vinyl ether.[9] Crivello and Lam[10] reported a series of diaryl onium salts which serve as photoinitiators of cationic polymerization of a wide variety of monomers, including olefins, epoxides, cyclic sulfides, acetates and lactones. Photopolymerization of methyl methacrylate as well as mixtures of methyl methacrylate with other acrylates have been demonstrated by several groups.[11] In our investigation we propose to adapt one of these several well known photopolymerization procedures for our formulation containing an aromatic chromophore which would subsequently undergo a photorearrangement reaction on irradiation at a different wavelength to form a UV absorber derivative.

The principal photorearrangement reaction which will be evaluated falls within the general class of photoreactions known as photo-Fries rearrangement. Several reviews have been published.[12,13] The scope of the reaction has been extended from phenyl esters and carbonates to phenoxyacetic acid, acetamilides, phenyl ethers and hydroxyphenyl cinnamates. It was observed that the photo-Fries rearrangement reaction may be utilized to generate internal UV stabilizers in bulk polymers.[14] It has also been shown that in certain polymers such as bisphenol A polycarbonate, occurrence of the photo-Fries reaction inhibits further photodegradation. In these polymers, the photo-Fries products were shown to act as both UV absorbers and also as excited state quenchers.[15]

Recently, we have demonstrated in our laboratory that by acetylating a commercially available UV absorber (eq. 1) 2,2'-hydroxyphenyl benzotriazole (K), resulted in a shift of the absorption spectrum significantly to the blue wavelength region as illustrated in Fig. 1 and Fig. 2. Compound (I) can be regenerated by irradiating (II) with short UV light. This reaction is demonstrated in polymethylmethacrylate (PMMA) matrix and is shown in Fig. 3.

Mechanistic studies will be carried out in order to determine if the acetoxy precursor interferes with the photopolymerization process in any way. If interference is observed, a different photoinitiator will be used in an attempt to eliminate this interference.

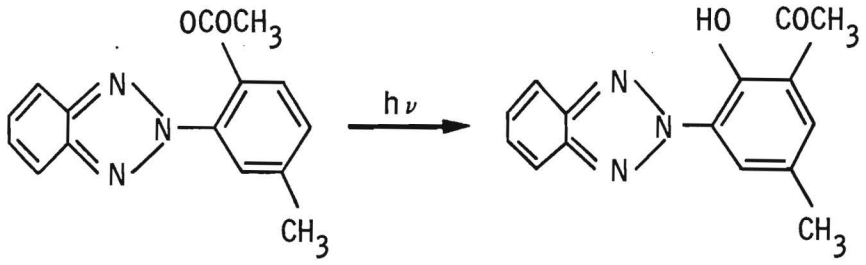

(I) (II)

Equation 1

BIBLIOGRAPHY

1. A. Gupta, Light Stabilization of Plastics for Solar Applications, Proceedings of the Intl. Symp. on 3rd Polymer Degradation and Stabilization, New Paltz, NY, June 1981.

2. B. L. Butler, et.al. in Proceedings of the Workshop on Basic Research Needs and Opportunities on Interfaces in Solar Materials, April 1981, pp. 183.

3. Solar Thermal Energy Systems, Ann. Tech. Progr. Rep. 1980, DOE/CS/4042-2, July 1981, p. 97.

4. W. F. Carroll and P. Schissel, Polymers in Solar Technologies, SERI/TR-334-601, July 1980.

5. V. D. McGinniss, T. Provder, C. Kuo and A. Gullopo, Macromol., 11(2), 393 (1978).

6. J. F. Ackerman, U.S.P. 3,673,140 (1972).

7. S. P. Pappas and A. Chattopadhay, J. Amer. Chem. Soc., 95, 6484 (1973).

8. M. Marck and L. Toman, J. Polym. Sci., Polym. Symp., 42,339 (1973).

9. K. Kaeriyama and Y. Shimura, J. Polym. Sci., Polym. Chem. Ed., 10, 2833 (192).

10. J. V. Crivello and J. L. Lee, Macromol. 14(5), 1141 (1981); idid 10(6), 1314 (1977).

11. R. S. Davidson and J. W. goodie, Europ. Polym. J. 181, 597 (1982).

12. V. I. Stenberg, "Organic Photochemistry," O. L. Chapman, ed., Volume 1, Marcel Dekker, New York, N.Y. 1967, 127.

13. D. BELLUS, ADV. PHOTOCHEM., 8, 109 (1971).

14. S. M. Cohen, R. H. Young and A. H. Markhart, J. Polym. Sci., Part A-1, 9, 3263 (1971).

15. A. Gupta, et. al, Macromol, 11, 1285 (1978); ibid, 13, 262 (1980).

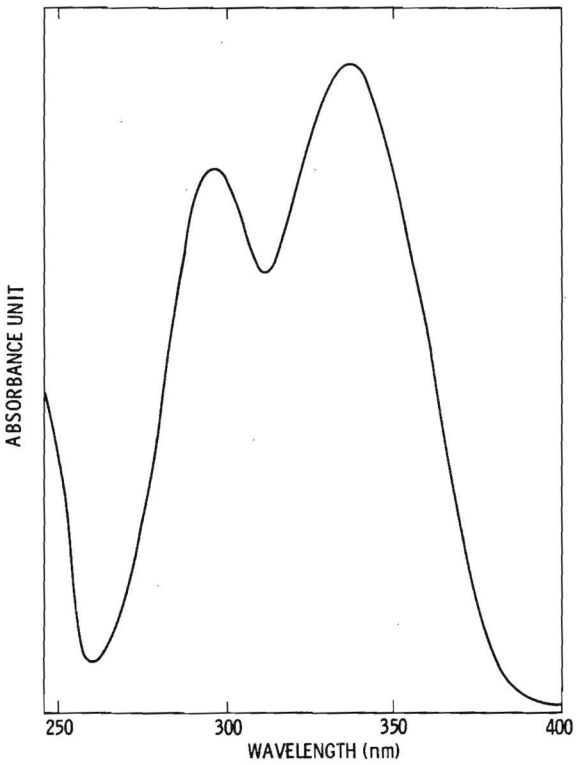

Figure 1. Absorption Spectrum of (I)

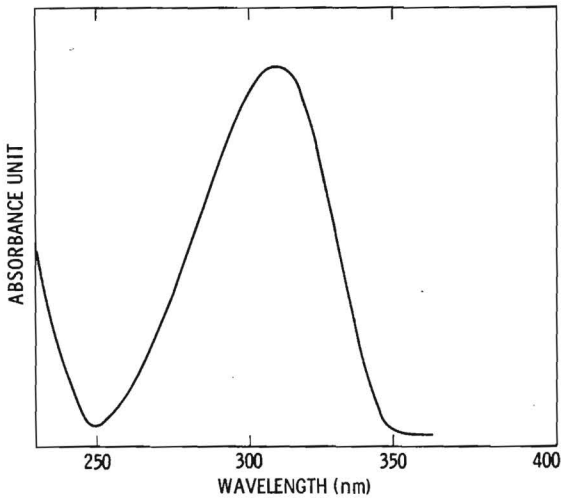

Figure 2. Absorption Spectrum of (II)

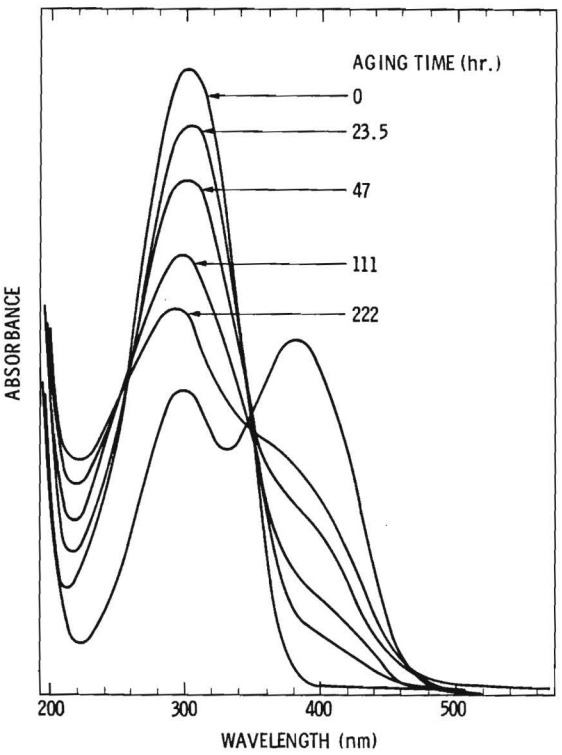

Figure 3. Absorption Spectra of II as a Function of Photoirradiation

INNOVATIVE RESEARCH PROGRAM SUMMARY

Keith A. Rose
U.S. Department of Energy
San Francisco Operations Office
Oakland, CA 94612

The Solar Thermal Research Program was initiated in December 1982 with the release of a Program Research and Development Announcement. Proposals were received and evaluation initiated in February 1983. The evaluation criteria used to select proposals were:

1) Evidence of a potential "quantum" improvement in performance or cost over existing solar thermal technology or novel application

2) Demonstration of an understanding of the scientific and engineering fundametals required to perform analyses to define the feasibility of the proposed concept

3) Demonstation of adequate experimental techniques to verify concept performance

Twelve proposals were selected for award and work was intitiated in September 1983. Phase I of the program, concept verification, will involve conceptual design, modeling, and preliminary experiments. Phase II, concept development, will focus on construction of prototypes, prototype testing, and optimization of designs.

I will present an overview of objectives, approach, and potential benefits of eight of the twelve projects in this program.

I. Acurex Corporation

Objective: Determine feasibility of using holographic optical elements as line and point focus solar concetrators

Approach: Experimentally determine the effects on holographic optical efficiency due to type of photsensitive emulsion, antireflective glass cover, and material differential thermal expansion. Determine the effects of thermal cycling, ultraviolet radiation and weathering on lifetime of holographic collectors

Benefit: Light-weight, low-cost solar collectors for line and point focus applications

II. Babcock and Wilcox Company

Objective: Study feasibility of using a direct flux solar incinerator for destruction of hazardous industrial wastes

Approach: Design a laboratory scale direct flux solar incinerator, establish gas dynamics and optical requirements. Prepare detailed plans for construction, installation, and testing of a prototype at a solar test facility. Select candidate PCB materials for initial testing

Benefit: Unique process for photolytic/thermal destruction of hazardous waste materials

III. HMJ Consulting Associates, Inc.

Objective: Assess feasibility of liquid metal magnetohydrodynamics (LMMHD) for solar central receiver technology

Approach: Identify key performance criteria, perform sensitivity analyses on key criterial, and define system characteristics

Benefit: Higher solar thermal electric power conversion efficiency

IV. Hughes Aircraft Company

Objective: Experimentally demonstrate a new themal electrochemical converter for production of electricity

Approach: Design and construct a thermogalvanic cell and an isothermal concentration cell. Measure cell voltage, current, heat input and efficiency as function of several variables

Benefit: High efficiency solar thermal combined cycle when coupled with topping cycle such as a sodium heat engine

V. Nielsen Engineering and Research, Inc.

Objective: Investigate feasibility of using a swirling-air curtain to reduce convective losses from central receiver cavities

Approach: Fabricate a model cylindrical cavity and a radial inflow jet with tangential velocity to create a swirling air curtain. Define jet parameters and other independent variables necessary to prove the concept. Define requirements for scaling model to a full-scale central receiver

Benefit: Increased thermal performance of central receivers due

to reduction of convective losses

VI. Martin Marietta Aerospace

Objective: Analytically demonstrate the feasibility of a ceramic tube receiver based on a translucent ceramic tube concept using a unique porous matrix absorber

Approach: Develop a conceptual design of commercial size ceramic tube receiver to determine requirements of tube thermal stress, fluid flow distribution and receiver mechanical support. Use TRASYS and DELSOL II computer codes to optimize absorbing surface size, shape, flux levels, arrangement of ceramic tubes, and cavity configuration

Benefit: Higher efficiency Brayton cycle receiver operating up to 2000 F

VII. Mathematical Sciences Northwest, Inc.

Objective: Investigate feasibility of using an air jet window to improve performance of solar receivers for fuels and chemical production

Approach: Conceptual design and analysis of types of air jet windows applicable to solar receivers. Evaluate performance relative to windowed receivers and identify potential fuels and chemical processes compatible with air jet window concepts

Benefit: Improved receiver/reactor thermal performance for fuels and chemical processes

VIII. Pacific Sun, Inc.

Objective: Identify the cost and performance advantages of in-situ steam generation for line focus solar collectors

Approach: Experimentally study flow stability problems under different operating conditions typical of high temperature industrial process heat PH)systems

Benefit: Potential for higher performance line focus solar systems for steam production for IPH applications

PANEL DISCUSSION SUMMARY

Directly following the last workshop session a panel of six solar thermal experts was convened to summarize views of the workshop and the solar thermal research program. Following this, workshop attendees participated in an open floor discussion with the panel in which specific and general aspects of the solar thermal program were addressed.

The summary which follows is a compilation of both the panel comments as well as the floor participation:

- a general sense of continuity and direction in the program is evolving including a positve thrust even though budgets are diminishing - probably partially due to large demonstration projects coming on line

- direction of research program should be for new markets and new technology rather than solving problems in a retrospective mode

- general perception is that industrial view of research and development is very near term

- engineering design problems have in some instances become confused with research

- recommend a more open approach to selection and performance of research topics rather than establiment of artificial criteria

- this workshop is based on peer review - this type of review process should continue on an annual basis

- there is a danger in looking at too many diverse studies and trying to define future needs too far in future
- recognize important work being done in materials and heat and mass transfer but sharp focus lacking in both
- recommend getting industry acceptance of R&D approach then work to commonly accepted goal with all resources available
- recommend focus on controls, storage, materials, heat and mass transfer as research topics
- recommend narrowing field of view and concentrating effort to show industry real progress
- emphasis of research program should be to reduce cost of current systems by introducing innovative ideas, improve performance to reduce cost and widen application potential
- recommend a fixed 25-30 percent level of solar thermal budget for research
- research cannot be effectively focussed on industrial needs
- it is important to understand and make transition from research to engineering development
- some activities even if not strictly defined as research are as important as research in the end result
- a diminishing budget has caused introspective questioning of relevancy of heretofore reasonable research thrusts

- industry has to make known their concerns through better communications with research community
- critical to amassing large amounts of capital for energy research is national energy policy including tax credit policies - high focus in this area now
- must strive towards strengthened co-operative link between research community and industry
- more industry participation is needed directly with universities and national laboratories
- recommend diminishing the programmatic issues in favor of the philosophical and directional issues
- need to publish more in refereed journals
- need to be more quantitative as our efforts reach maturity
- recommend smaller research group meetings/reviews to scope out receivers and reactors in fuels/chemicals area since this technology will be critical to success
- better liason between industry/universities/labs can be achieved through workshops and jury or advisory board activities with overview functions for solar thermal program
- need for a clear-cut goal is evident as opposed to extended option sorting activities

- appears that there is a missing emphasis of solar thermal research for fossil fuel displacement in favor of solar uniqueness - while displacement is not as attractive as uniqueness, goal of program should be to convert solar energy into a more useful form of available resource to which displacement addresses.
- need to set a common goal or define a large project to strive toward (and one which is attainable) similar to Barstow project since so many diverse interests abound.

SOLAR THERMAL RESEARCH WORKSHOP
September 7-8, 1983
ROSTER

Brian I. Ashkenazi
Sales Engineer
1737 South Date Avenue
Torrance, CA 90503

John M. Berry
Georgia Power Company
7 Solar Circle
Shenandoah, GA 30265

Charles N. Bolton
Manager, Solar Thermal
Applications
Martin Marietta
Box 179
Denver, CO 80201

Raymond Cedillo
Senior Research Engineer
Southern California Edison
P.O. Box 800
Rosemead, CA 91770

Duane G. Chadwick
Associate Professor,
Electrical Engineering
Utah State University
Logan, UT 84322

Robert J. Copeland
Principal Engineer
SERI
1617 Cole Boulevard
Golden, CO 80401

Cynthia L. Dalton
Marketing Specialist
Babcock & Wilcox, Contract
Research Division
1562 Beeson Street
Alliance, OH 44601

Daniel B. Dawson
Sandia National Laboratories
Division 8454, Box 969
Livermore, CA 94550

Donald R. Duffy
Engineering Manager
Acurex Solar Corporation
555 Clyde Avenue
Mountain View, CA 94042

Joe H. Evans
Materials Laboratory Manager
Ramada Energy Systems Limited
1421 South McClintock
Tempe, AZ 85281

Gordon E. Gross
Chief, Materials Branch
SERI
1617 Cole Boulevard
Golden, CO 80401

Bimleshwar P. Gupta
Program Manager
Solar Energy Research Institute
1617 Cole Boulevard
Golden, CO 80401

Richard A. Hays
Engineer
White Sands Missle Range
STEWS-TE-N
White Sands, NM 88005

Alvin F. Hildebrandt
Director, Energy Laboratory
University of Houston
4800 Calhoun
Houston, TX 77004

Arlon J. Hunt
Staff Physicist
Lawrence Berkely Laboratory
90-2024
Berkeley, CA 94720

William A. Hunt
TPI Office
SERI/SNLL
Sandia National Laboratory
Division 8454
Livermore, CA 94550

E. Neville Hunter
Vice President, Business Development
VEDA Incorporated
1225 Jefferson Davis Highway
Suite 300
Arlington, VA 22202

Alex Ignatiev
Professor
University of Houston
Department of Physics
Houston, TX 77004

John H. Norman
Senior Staff
Georgia Technologies
P.O. Box 85608
San Diego, CA 92138

David H. Johnson
Group Manager
SERI
1617 Cole Boulevard
Golden, CO 80401

Steven D. Johnson
Engineer
Babcock & Wilcox
91 Stirling Avenue
MS BB3A
Barberton, OH 44203

Michael A. Kast
President
Research Engineering Associates, Incorporated
420 Addsion
Palo Alto, CA 94301

Gerald Katz
Engineer
US DOE
1333 Bway
Oakland, CA 94612

Thomas H. Kuehn
Associate Professor, Mechanical Engineering
University of Minnesota
111 Church Street, SE
Minneapolis, MN 55455-0111

Carlo LaPorta
Director, Marketing Research Technology
Solar Energy Industries Association
US 6 15th Street NW
Washington, D.C. 20036

Gerold Lemperle
DFVLR
PFAFFENWALDRING 38-40
7000 STUTTGART 80
West Germany

Ranty H. Liang
Technical Group Leader
Jet Propulsion Laboratory
4800 Oak Grove Drive
Pasadena, CA 91109

Andrew V. Logie
Manager, Facilities Engineering
DSMA Engineering Corporation
6220 South Orange Blossom Trail
Suite 186
Orlando, FL 32809

Frank A. Ludwig
Senior Scientist
Hughs Aircraft
P.O. Box 902
El Segundo, CA 90245

William A. Mallow
Staff Scientist
Southwest Research Institute
6220 Culebra Road
San Antonio, TX 78284

Ram Manvi
Member, Technical Staff
Jet Propulsion Laboratory
4800 Oak Grove Drive
Pasadena, CA 91109

J.I. Martinez
Member, Technical Staff
Sandia National Laboratories
Division 6227, P.O. Box 5800
Albuquerque, NM 87185

Cheryl R. Maxwell
Engineer
Sandia National Laboratory
Division 6222
Albuquerque, NM 87185

Oden J. McMillan
Research Engineer
Nielsen Engineering and
Research, Incorporated
510 Clyde Avenue
Mountain View, CA 94043

Robert K. McMordie
Departmental Staff Engineer
Martin Marietta
P.O. Box 179
Denver, CO 80201

Charles L. Pitman
Graduate Student
University of Houston
4800 Calhoun, 115 SPA
Houston, TX 77004

H. William Prengle, Jr.
Professor
Univeristy of Houston
Chemical Engineering Department
4800 Calhoun
Houston, TX 77004

James T. Richardson
Professor
University of Houston
Department of Chemical
Engineering
Houston, TX 77521

Darrell L. Ross
Technical Group Supervisor
Jet Propulsion Laboratory
4800 Oak Grove Drive
MS 507-228
Pasadena, CA 91109

Claude Royere
Engineer
CNRS LES INW Solar Furnace
P.O. Box 5 Odeillo 66120
Fontromeu, France

Paul O. Schissel
Principal Scientist
Solar Energy Research Institute
1617 Cole Boulevard
Golden, CO 80401

Robert T. Taussig
Director, Energy Technology
Mathematical Sciences Northwest,
Incorporated
2755 Northup Way
Bettevue, WA 98004

Ali T-Raissi
Assistant Researcher
University of Hawaii
Renewable Resources Research
Laboratory
2540 Dole Street
Honolulu, HI 94720

Lawrence E. VanBibber
Manager, Systems Design and
Integration
Westinghouse Advanced Energy
Systems Division
P.O. Box 10864
Pittsburg, PA 15236

Lorin L. Vant-Hull
Solar Thermal Division Head
University of Houston
4800 Calhoun, 115 SPA
Houston, TX 77004

Frank W. Wilkins
Program Manager
U.S. Department of Energy
Washington, D.C. 20036

Tom Williams
Battelle/PNL/SNLL
Sandia National Laboratory,
Division 8454
Livermore, CA 94550

James B. Wright
Manager, Solar Central Receivers
Sandia National Laboratories
Livermore, CA 94550

Bernard D. Yudow
Chemical Engineer
Institute of Gas Technology
3424 South State
Chicago, IL 60616

GEORGIA TECH PARTICIPANTS

Steve H. Bomar, Jr.
Principal Research Engineer
Engineering Experiment Station
Georgia Tech
Atlanta, GA 30332

Charles T. Brown
Principal Research Scientist
and Branch Head
Engineering Experiment Station
Georgia Tech
Atlanta, GA 30332

Robert A. Cassanova
Engineering Experiment Station
Georgia Tech
Atlanta, GA 30332

Thomas B. Elfe
Senior Research Scientist
Georgia Tech
Atlanta, GA 30332

Joe N. Harris
Senior Research Engineer
Engineering Experiment Station
Georgia Tech
Atlanta, GA 30332

Joseph P. Hoppe
Research Engineer I
Engineering Experiment Station
Georgia Tech
Atlanta, GA 30332

Prasanna V. Kadaba
Associate Professor
Mechanical Engineering
Georgia Tech
Atlanta, GA 30332

James M. Lefferdo
Head, Thermal Sciences Branch
Engineering Experiment Station
Georgia Tech
Atlanta, GA 30332

Walter S. Lewis
Research Scientist
Engineering Experiment Station
Georgia Tech
Atlanta, GA 30332

Paul Mackie
Senior Research Scientist
Georgia Tech
Atlanta, GA 30332

Douglas H. Neale
Senior Research Engineer
Engineering Experiment Station
Georgia Tech
Atlanta, GA 30332

Osamu Shinoura
Visiting Researcher
Engineering Experiment Station
Georgia Tech
Atlanta, GA 30332

Richard S. Zabor
Research Engineer
Engineering Experiment Station
Georgia Tech
Atlanta, GA 30332

SOLAR THERMAL RESEARCH WORKSHOP
September 7-8, 1983
ADDENDUM

Randy J. Petri
Project Manager
Institute of Gas Technology
3424 South State Street
Chicago, IL 60616

Barry Butler
Division Manager
Solar Energy Research Institute
1617 Cole Boulevard
Golden, CO 80401

L. M. Murphy
Group Manager
Solar Energy Research Institute
1617 Cole Boulevard
Golden, CO 80401

Keith A. Rose
U. S. Department of Energy
San Francisco Operations Office
Oakland, CA 94612